EFFECTS OF VAPOR GROWN CARBON NANOFIBERS ON ELECTRICAL AND MECHANICAL PROPERTIES OF A THERMOPLASTIC ELASTOMER

A Thesis

by

DANIEL THOMAS BASALDUA

Submitted to the Graduate School of
The University of Texas-Pan American
In partial fulfillment of the requirements for the degree of

MASTER OF SCIENCE

December 2014

Major Subject: Mechanical Engineering

EFFECTS OF VAPOR GROWN CARBON NANOFIBERS ON ELECTRICAL AND MECHANICAL PROPERTIES OF A THERMOPLASTIC ELASTOMER

A Thesis
by
DANIEL THOMAS BASALDUA

COMMITTEE MEMBERS

Dr. Robert Jones
Co-Chair of Committee

Dr. Constantine Tarawneh
Co-Chair of Committee

Dr. Karen Lozano
Committee Member

December 2014

ABSTRACT

Basaldua, Daniel T., Effects of Vapor Grown Carbon Nanofibers on Electrical and Mechanical Properties of a Thermoplastic Elastomer. Master of Science (MS). December, 2014, 120 pp., 4 tables, 80 figures, 53 references, 60 titles.

Carbon nanofiber (CNF) reinforced composites are exceptional materials that exhibit superior properties compared to conventional composites. This paper presents the development of a vapor grown carbon nanofiber (VGCNF) thermoplastic polyurethane (TPU) composite by a melt mixing process. Dispersion and distribution of CNFs inside the TPU matrix were examined through scanning electron microscopy to determine homogeneity. The composite material underwent durometer, thermal gravimetric analysis, differential scanning calorimetry, heat transfer, hysteresis, dynamic modulus, creep, tensile, abrasion, and electrical conductivity testing to characterize its properties and predict behavior. The motivation for this research is to develop an elastomer pad that is an electrically conductive alternative to the elastomer pads currently used in railroad service. The material had to be a completely homogenous electrically conductive CNF composite that could withstand a harsh dynamically loaded environment. The new material meets mechanical and conductive requirements for use as an elastomer pad in a rail suspension.

DEDICATION

It is my greatest honor and joy to dedicate this thesis to my mom and dad. Thank you all so much for pushing me to put education first. Dad this is the culmination of your lifelong dream for all your children to graduate from college. Thank you for financially providing for me in this time. Mom you put your career on hold for my sisters and I to receive a great education. Thank you so much mom! It has made a world of difference to all of us.

ACKNOWLEDGMENTS

I will forever be grateful to my two thesis co-chairs, Dr. Robert Jones and Dr. Constantine Tarawneh, my thesis committee member Dr. Karen Lozano, and my undergraduate research assistant Anthony Villarreal. Dr. Jones, you have provided extensive advise, guidance, and mentorship in this project. Thank you for constantly asking me to draw more results out of the data. Dr. Tarawneh, your hard work and management of the University Transportation Center for Railway Safety at the University of Texas-Pan American has provided the funds to sponsor this project. Thank you for directing our center. Dr. Lozano, you have always made yourself available to answer all of my questions and provide expert advise in the field of nanotechnology. Thank you for being so understanding willing to work with me.

Lastly, I would like to thank Anthony Villarreal. He has worked timelessly beside me on this project. Without his help this project would not see its completion until a much later date. Thank you so much.

TABLE OF CONTENTS

LIST OF TABLES

LIST OF EQUATIONS

LIST OF FIGURES

CHAPTER I

INTRODUCTION

Material science has evolved beyond using pure materials to design structures or components. Currently scientists and engineers are working to create novel materials, which can perform previously unimagined tasks to simplify the design process. No alloy or additive will make a greater contribution to material design than carbon nanofibers (CNF) and carbon nanotubes (CNT). Since their discovery in the 1990s CNF/CNTs have been the subject of a significant amount of research. The time and money dedicated to their research has proven to be very beneficial. CNT/CNFs are now impacting the semiconductor, medical, chemical, textile, electronic, and many other important industries. This thesis will focus on using CNFs in one of their most promising application: CNT/CNF reinforced polymer composites.

CNF – polymer composites are potentially useful because CNFs can enhance polymers in unique ways. The properties CNFs exhibit are attributed to their physical attributes. CNFs have extremely high length to diameter and surface area to volume aspect ratios. Some CNF diameters can be less than 50 nm across creating extremely high surface areas in comparison to their volumes. Because the space a CNF occupies is extremely small they can be compounded into a polymer matrix and not drastically weaken the polymer's backbone. CNFs do this by fitting inside the available spaces between polymer chains. Enhancing a polymer without dramatically disrupting its physical makeup allows an engineer to selectively add properties to a material, thereby custom designing it for his/her application.

The University of Texas-Pan American is one of the premier institutions for CNF research. One professor, Dr. Lozano has done extensive research concerning the development and mass-production of CNFs. Mass producing CNFs is currently the one of the limiting steps toward developing CNF-polymer composites because conventional production methods are slow and costly. Dr. Lozano discovered a new method – force spinning, which produces CNFs at an exponentially faster and cheaper rate than previous techniques. As the cost to manufacture CNFs decreases, the attractiveness of their properties will increase, and CNF composite materials will showcase a more prominent place in the science of material engineering. The success of Dr. Lozano's research has prompted UTPA to allocate funds toward nano research, and encouraged Dr. Jones and Dr. Tarawneh to view CNFs as a viable option to solve problems within their own research.

Dr. Tarawneh leads a large research initiative sponsored by the United States Department of Transportation. His research specializes in solving load, vibration, and other bearing related issued within the railroad industry. Dr. Jones is a materials expert who works along side Dr. Tarawneh researching novel solutions to improve transportation safety. One area of interest is to create conductive composites. Some applications within the railway industry utilize conductive materials under high stress environments. Traditionally metals are used to make components in stress environments, however a conductive polymer composite is beneficial because it can reduce wear on adjacent components. Conventional composites have nominal to poor mechanical properties at high fiber loadings due to matrix disruptions. Because CNFs do not drastically disrupt the polymer matrix they can be used in high load environments such as the railroad industry.

CNFs are known for their electrical capabilities and compound well with thermoplastic polyurethane (TPU). After a literature review revealed a shortage of research studies in the area of CNF elastomer composites under dynamic loading a formal study was outlined. Although the outlined study was conceived as a solution to a problem in the transportation industry, a conductive composite material maybe used in many other industries as well. The material testing extended beyond electrical conductivity testing and included thermal and mechanical tests as well.

This thesis details how CNFs were used in conjunction with TPU to create a fully conductive elastomer composite suitable for dynamic loading. The following chapters outline how CNFs were used to create a homogenous elastomer composite. These chapters include a literature review of the current research being conducted on CNF polymer composites, the materials and methods used to create an effective composite elastomer, the results from mechanical, thermal, and electrical testing, and future investigations that can be built off of the results of this thesis's research.

CHAPTER 2

LITERATURE REVIEW OF CONDUCTIVE NANOCOMPOSITES

The primary goals of this project were to create a reinforced CNF-TPU polymer material with optimized mechanical, thermal, and electrical properties. To minimize the amount of guesswork spent on creating an effective CNF-TPU composite, a thorough literature review was completed. The review included studying journal publications about CNFs and TPU, as well as their respective uses. The review provided a sufficient understanding of these materials' respective properties, their applications and the novel research being done on them. The purpose of this chapter is to offer the reader a concise yet detailed understanding of, conductive CNF reinforced composites and describe previous conductive polymer work performed at the Transportation Center for Railway Safety with other additives.

CNFs can form composite materials that exhibit exceptional characteristics. CNFs, due to their properties, allow material engineers to design composite materials with unique electrical, mechanical, and thermal properties. As a result CNFs have been the focus of much institutional and industry research. CNFs are a subcategory of CNTs called stacked cup carbon nanotubes. Carbon nanotubes come a couple different varieties including multi-walled carbon nanotubes (MWCNTs), single walled carbon nanotubes (SWCNTs), and stacked cup carbon nanotubes (CSCNTs). CNFs or stacked cup carbon nanotubes, have graphene planes that are canted about the fiber axis exposing the interior and exterior surfaces of the fiber. The graphene sheets in CNTs assemble in concentric cylinders providing a true tube like appearance [1]. Because of this morphology difference stacked cup CNTs are referred to as CNFs. Vapor grown CNFs (VGCNFs) refer to CNFs grown by plasma vapor deposition. Each class its own advantages and disadvantages, but the main differentiating factors revolve around purity and cost. CNTs have fewer microstructural defects, therefore increasing their structural integrity. This leads CNTs to have better mechanical properties and smaller more uniform diameters compared to VGCNFs [2]. However, VGCNFs are often chosen over CNT in industry due to their lower cost. VGCNFs can range from $100 to $500 per pound and can be manufactured in large quantities, up to 70,000 pounds per year in some cases. Their counterpart, CNTs are significantly more costly ranging from $100 per gram up to $750 per gram [1]! These values do not include functionalization or compounding. However, CNTs' price is modest when compared to MWCTs and SWCNTs, which are astronomically more expensive. VGCNFs' price has decreased since their initial development and it is expected that CNTs, MWCNTs, and SWCNTs will as well. Cost is the driving factor in choosing VGCNFs over CNTs.

2.1 VGCNF Production

VGCNFs are produced through catalytic chemical vapor deposition (CCVD). The process entails the decomposition of gas phase molecules at temperatures between 500 and 1500 ℃. When gases such as methane, propane, acetylene, benzene, ethylene, and carbon monoxide are decomposed, volatile components such as hydrogen and oxygen burn off, leaving carbon to be deposited on to a substrate with a catalyst [3]. The nano fiber's diameter is dictated by the catalyst's size, while fiber length is controlled by the resonance time. Typical fibers are less than 0.1 mm long, which produces an extremely high aspect ratio with respect to the diameter [4].

A team led by Lee Woo and Kim performed studies to determine the effect different catalysts and gases had on VGCNFs. They found that CNF morphologies are sensitive to the type of hydrocarbon gas they are deposited from. CNFs prepared from propane contained linear conformations, fibers from ethylene gas had mainly twisted conformations, and fibers from acetylene were both twisted and helical in shape. It was also found that CNFs produced from propane and a nickel-copper catalyst had the highest surface area to length ratio, while fibers made from ethylene and a pure nickel catalyst had the highest electrical conductivities [5]. The Pyrograf PR-19-XL-LHT VGCNFs used in this project were heat-treated at 1500 ℃ converting any surface carbon molecules into short chain ordered structures and increasing the electrical conductivity of each fiber[1]. The ability to control fiber morphology and functionality opens the door to broader CNF applications.

2.2 Applications

The major applications for conductive polymer composites are electromagnetic interference (EMI) shielding and electrostatic discharge (ESD) protections [6]. Both applications work to inhibit interference but EMI works to shield electronic components from outside electromagnetic fields while ESD works to ground objects keeping them from developing a charge which can be damaging to nearby electronic devices. EMI shielding materials surround components, acting as barriers, which absorb and conduct any interfering electromagnetic radiation away from the devise. Almost all electronic devices including laptops, cell phones, aircraft, etc. emit electromagnetic radiation because in most common cases their main material coating, plastic, has no intrinsic shielding capability [5]. Carbon nano materials produce greater shielding capabilities at lower concentration than traditional conductive additives.

Current conductive fillers include carbon black (CB) and metal fibers. These composite modifiers have many limitations. Metal fiber composites for example, are not easily recycled, generally suffer from poor mechanical properties, and have significantly higher densitys. CB composites require very high CB concentrations to provide effective EMI shielding. Increasing the CB concentration not only raises cost but also reduces toughness, wear resistance, and general mechanical durability. The University Transportation Center (UTC) at UTPA researched CB as a conductive additive in TPU. Ruben Suarez developed a formulation for use in a steering pad. The formulation required that two competing demands be balanced. The CB loading needed to be large enough to guarantee the required level of conductivity while too high a level increased the stiffness and reduced the durability of the pad.

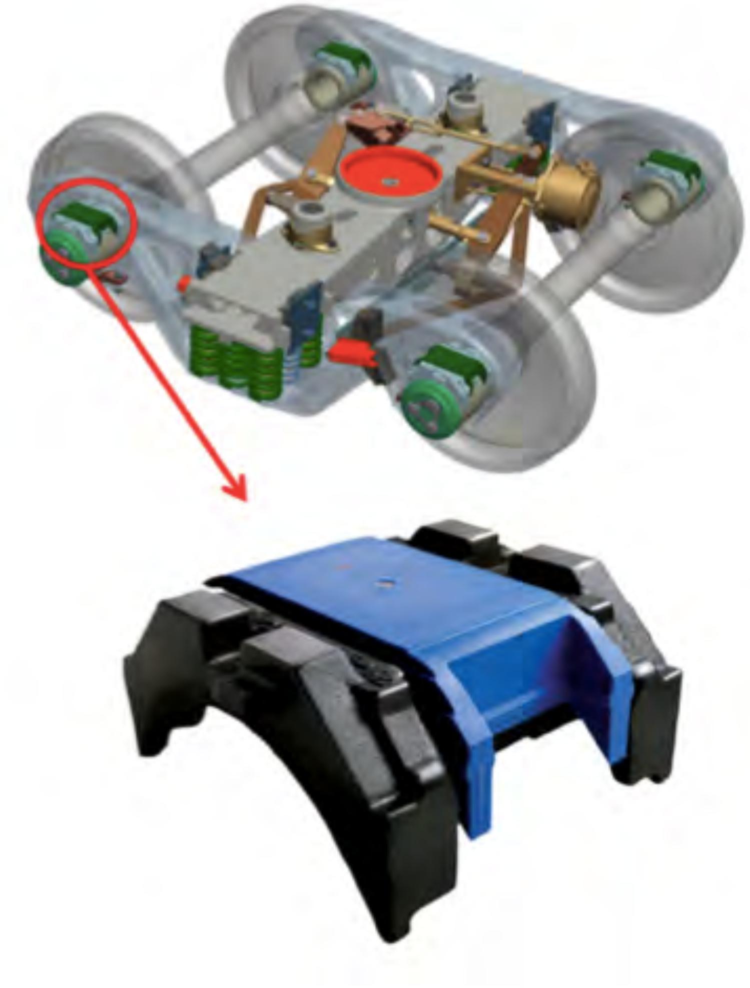

Figure 2.1: Railway steering pad (blue) and chassis [7]

The railway steering pad, Figure 2.1 used underneath the railcar experiences a dynamically loaded environment in service. The American Association of Railroads (AAR) placed constrains on the minimum mechanical properties the pad must exhibit. These mechanical requirements were kept in mind as the TPU was modified with CB to produce electrical conductivity. In order to satisfy customer requests for electrically actuated gate automation the pad material needed to conduct at least 260 milliamps of current under both empty and full car loads. It was found that this required a CB loading 17 to 21 weight percent [7]. While these CB percentages satisfied the conductivity requirements for gate automation CB-TPU composites suffered a significant reduction in mechanical properties. The CB-TPU composite prototypes lost their conductivity in the high shear process used to manufacture and barely failed a simulated service test. A review of commercially available conductive CB/TPU systems indicated that all of those systems relied on much higher CB loadings to guarantee adequate conductivity after processing.   Addition of more CB was not an option due to the mechanical requirements of the application. Producing conductivity at the cost of mechanical properties is not a new phenomenon. Feng and Chan found similar results in their research of CB-polypropylene/polyethylene composites [8].

The reason CB composites require high loadings is because CB's primary mechanism of conductive is through chain formation [9]. A small number of highly conducive chains can run through a matrix and render it conductive. Forming chains however, is a delicate process. Short mixing times leave more CB chains inside composites, but they also increase the percentage of agglomerates, which dramatically reduce mechanical properties. Increasing the mixing time applies more sheer history to the polymer breaking up more CB chains. Finding the appropriate mixing time was one of the most difficult challenges. CNFs do not have such stringent mixing constraints allowing them to be more easily compounded. This prompted the UTC to sponsor research toward developing a CNF reinforced conductive composite.

Outside of the railway application and EMI shielding, CNFs are changing many other industries. Batteries are expected to realize great improvements from CNF research. Carbon materials are ideal for battery systems because of their high electrical conductivity and corrosion resistance [10]. The ability to order the morphology and grow fibers off of different catalysts makes VGCNFs prime candidates for anodes in lithium ion batteries. They can also be used as an environmentally friendly alternative material that is cheaper than conventional metal oxides and sulfides. Biomedical researchers indicate that CNFs will foster tissue growth and may be used to manufacture artificial organs such as kidneys in the future [11]. IBM is creating a new computer chip with CNFs at its core. This microchip will have higher processing speeds and require less energy. The applications mentioned in this section only begin to scratch the surface of the possibilities for applications of CNFs.

2.3 CNF Properties

VGCNFs have larger diameters compared to CNTs, SWCNTs, and MWCNT. Generally VGCNF exhibit diameters between 50 and 200 nm. The VGCNFs purchased from Pyrograf had an average listed diameter of 150 nm. Nonetheless fiber diameters were measured under an SEM to verify this claim, see Figure 2.2. SWCNT and MWCNT can have diameters ranging from 1 to 50 nm [12]. VGCNFs have a high aspect ratio and hollow core. The core can be single or double layered with cupped or stacked conformations, Figure 2.4. Endo researched a cup-stacked morphology conformation, Figure 2.4. This morphology had large reactive edges on the inside and outside increasing surface area of the fiber and available space for chemical functional groups. The transmission electron micrograph shown in Figure 2.3 displays fibers used in this research [1]. The micrograph allows an inner hollow core to be clearly seen and a thick layer of carbon vapor deposited on the outside. Depending on the application demands, a CNF can be created with different diameters and morphology.

The primary benefit CNFs hold over conventional additives is that they can be modified and tailored to have specific dimension, structure, electrical, mechanical, and thermal properties in the manufacturing and post production processes [13]. The VGCNF used in this research were heat treated and functionalized with short range ordered structures to increase the fiber electrical conductivity [1]. One example of postproduction modification of CNFs is heat treatment. Heat treatment increased crystallinity, and removed layers of amorphous carbon that degraded conductivity characteristics [6]. Endo led a research team that analyzed electrical conductivity values before and after heat treatment. He found that the volumetric resistivity of CNF decreased by several orders of magnitude after heat treatment. Heat treatment at 1200 ℃ yielded a 10^{-3} Ω cm decrease and treatment at 2800 ℃ yielded 10^{-4} Ω cm decrease when compared to untreated fibers. The Pyrograf fibers purchased for this project underwent a heat treatment process at 1500 ℃. Therefore, in accordance with Endo's research, it was assumed that heat treatment enhanced their intrinsic volumetric resistivity by a factor of at least 10^{-3} Ω cm.

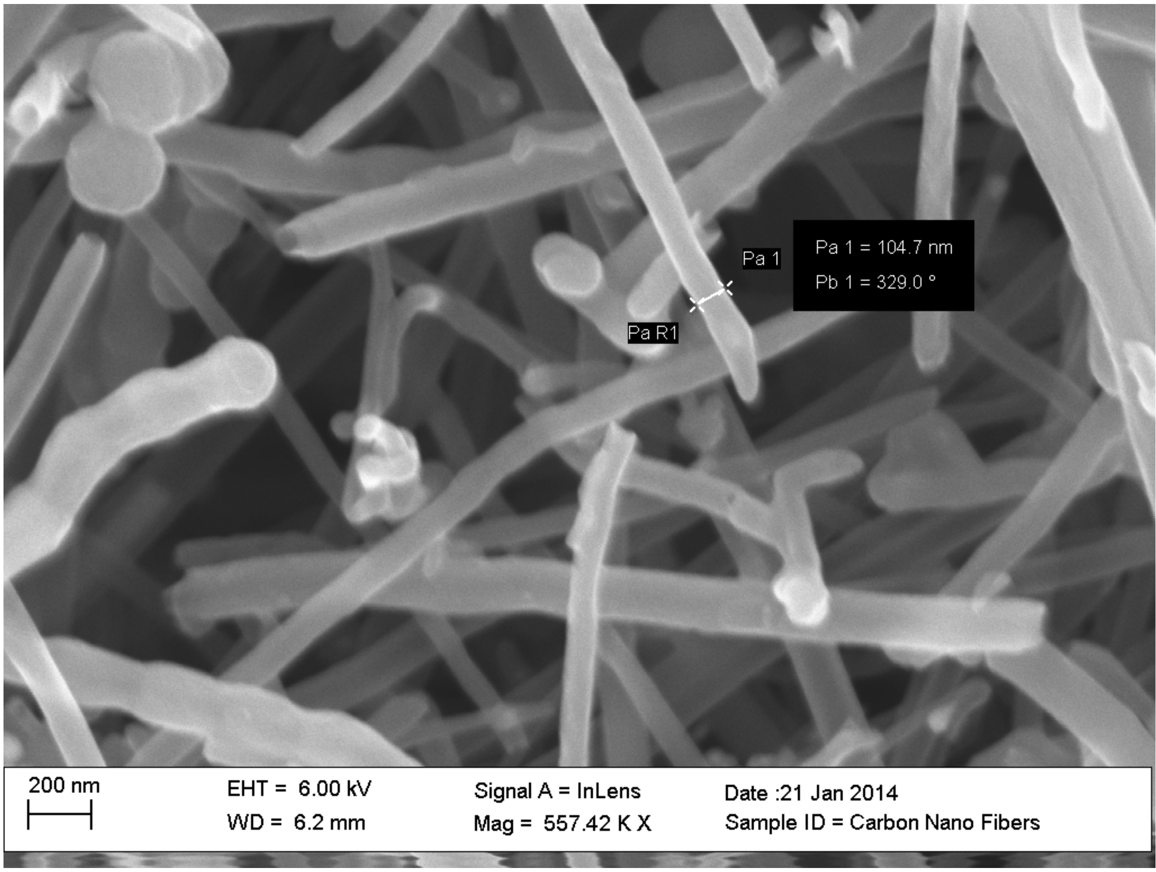

Figure 2.2: SEM measurement of Pyrograf CNF

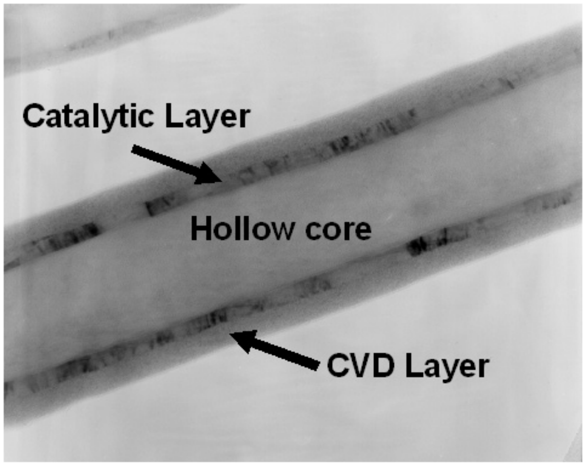

Figure 2.3: TEM Pyrograf CNF [1]

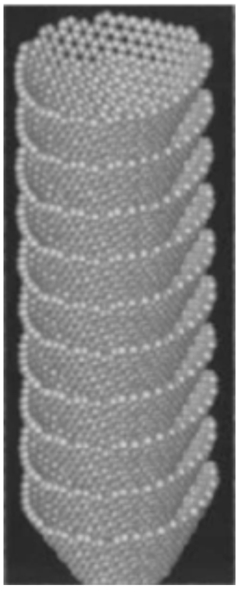

Figure 2.4: Cup stacked formation [1]

2.4 Electrical Conductivity in Composites

Creating an electrically conductive composite requires the percolation threshold to be met and a tunneling or direct contact network made inside the polymer matrix. The percolation threshold is the critical concentration when a composite transforms from an insulator to a conductor in nature. Percolation is characterized by a decrease in resistivity of an order of several magnitudes, Figure 2.5. The required concentration for percolation can vary based on the polymer and type of CNF used. After reaching the percolation threshold adding additional CNFs will not greatly influence conductivity.

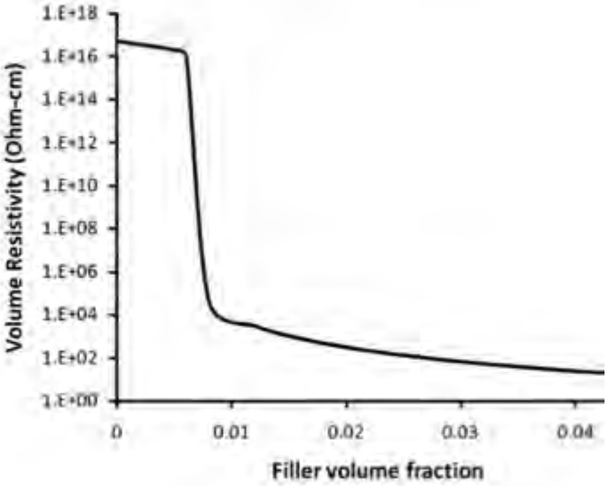

Figure 2.5: Percent Concentration Resistivity relationship [6]

CNFs provide conductivity by means of direct contact and/or tunneling. Direct contact consists of CNFs physically touching end-to-end forming chains throughout the matrix. Tunneling consists of a CNF network with fibers spaced an average of 10 nm or less from each other. When spaced within this proximity of each other electrons can jump from fiber to fiber [14]. Deciding whether to produce a conductive composite through tunneling or direct contact is dependent on the user's application. In tunneling, CNFs are more spread out in a matrix, requiring a higher overall concentration. Higher concentrations translate to higher costs, but composites with a tunneling CNF network also have superior mechanical properties. Direct contact produces conductivity at lower concentrations because the matrix does not need to be saturated, however it unfortunately also causes pockets of CNFs to which act as stress concentrators and fracture initiation sites in the composite. If the component is not in a high stress environment, direct contact maybe the preferred method of conductivity to keep production costs down.

Existing steering pads sustain loads between 27,000 to 39,000 lbs depending on the bearing's class [15]. See Table 2.1 for respective bearing class weights. Loadings at the levels listed in Table 2.1 apply high amounts of compressive stress & strain to the pad; hence optimal mechanical properties are required. Due to these constraints, tunneling is the mechanism of producing conductivity which is appropriate in this application.   One may determine the mechanism of conductivity by examining the current voltage relationship [16]. A linear current voltage relationship indicates that direct content between CNFs is the dominant mechanism of generating conductivity. Tunneling is the dominant form of conductivity when the current voltage relationship is characterized by the power law [17]. Also if conductivity increases greatly when CNFs are added after the percolation threshold has been reached then direct contact is the dominant mechanism for conductivity [6].

Table 2.1: Max Bearing Loading [15]

Loadings by Bearing class	
Bearing class	Load Per Bearing [lb_f]
Class E	27,000
Class F	35,750
Class G	39,375
Class K	35,750

Because CNFs are considerably more expensive than the matrix materials they are compounded in it is critical to reduce the percolation threshold as low as possible. The percolations threshold depends on many factors including CNF functionality, aspect ratio, distribution, dispersion, fiber conductivity, polymer surface tension, and polymer crystallinity. CNT's high aspect ratio enables them to percolate system at low volume fractions [18]. Researchers have sought out different techniques to reduce percolation thresholds; many of which center around manipulation of the polymer type and processing conditions.

2.5 Heat Transfer

Thermally conductive polymer composites can be created with CNFs. Heat dissipation is an attractive and sometimes necessary characteristic in electronic and industrial applications. Within electronics, polymers play a major role of scaffolding for devices. Polymers do not conduct thermal energy efficiently and therefore act as insulators trapping heat in and overheating components. This forces researchers to place heat sinks and fins in their designs to absorb and dissipate heat from electrical devices. Using a cost effective thermally conductive polymer would eliminate fins and shrink component boards. For the steering pad system a thermally conductive polymer composite would improve heat dissipation from the bearing into the side frame and thus decrease bearing temperatures and increase bearing life if utilized in the steering pad.

Currently researchers are looking to CNFs to create thermally conductive polymer composites because of their high aspect ratios, thermal conductivity coefficients, and small coefficients of thermal expansion. CNFs have thermal conductivities as high as 1950 W/m·K which is much higher than aluminum, 190 W/m·K [19]. The over all conductivity of a CNF-polymer composite is not merely based off of CNF conductivity but also dependent upon filler concentration, aspect ratio, CNF orientation, dispersion, and interfacial thermal resistance between the CNF and the polymer [20]. Chen performed studies creating CNF-epoxy composites and reported that there was no percolation threshold with regard to thermal conductivity. The thermal conductivity of the composite continued to increase with CNF loading. At 56% CNF loading their epoxy composite exhibited a conductivity of 291 W/m·K. This is a dramatic increase over virgin epoxy's 0.1 W/m·K thermal conductivity coefficient. Thermoplastics exhibited this same relationship of a gradual increase in conductivity with increasing CNF content [21].

CNTs are known to have higher thermal coefficients than CNFs because they contain higher surface area to volume ratios [22]. In studies by Biercuk researchers found that equivalent thermal conductivity coefficients could be achieved with CNT at half the concentration of CNF. Perhaps with future production cost decreases CNT can be seen as viable conductive additives for polymer composites.

2.6 Polymer Type

Polymer type has a profound impact on the electrical properties of a CNF composite. Polymer surface tension, polarity, and crystallinity are the major contributing factors to CNF dispersion and percolation [23]. With regards to surface tension a direct relationship exists between the polymer and CNF percolation thresholds. The reason for this is because higher polymer surface tensions lead to lower CNF-polymer interfacial tensions. At low CNF-polymer interfacial tension CNFs can be easily wetted by the polymer matrix facilitating even distribution throughout the polymer. Well-distributed CNF networks yield higher percolation thresholds, because conductivity is generated through tunneling. Comparatively high CNF-polymer interfacial tension tends to inhibit fiber distribution and produce agglomerates. By utilizing these relationships researchers are able to effectively choose the best polymer for their application. Choosing a polymer with high surface tension will produce a well-distributed CNF conductive tunneling network with optimal mechanical properties at higher concentrations. However, choosing a polymer with low surface tension will produce conductivity at lower concentration due to agglomerates and thereby reduce costs.

Polarity has a similar effect to surface tension. Highly polar polymer chains exhibit higher percolation thresholds due to better interactions between the CNF and the polymer [24]. Enhanced CNF-polymer interactions wet fibers promoting dispersion in to and distribution throughout the polymer matrix. Researchers have found that semi-crystalline polymers like TPU provide better conductivity at lower percolation thresholds compared to amorphous polymers [23]. TPU is a block co-polymer made of soft nonpolar and hard polar segments, Figure 2.6. During compounding, fibers are easily spread throughout the matrix due to TPU’s polarity, surface tension, and semi-crystalline nature, but as the polymer cools and recrystallization takes place fibers are ejected from the crystalline region increasing the concentration in the amorphous region. There is a lack of studies in literature on the effects of molecular weight and percolation threshold.

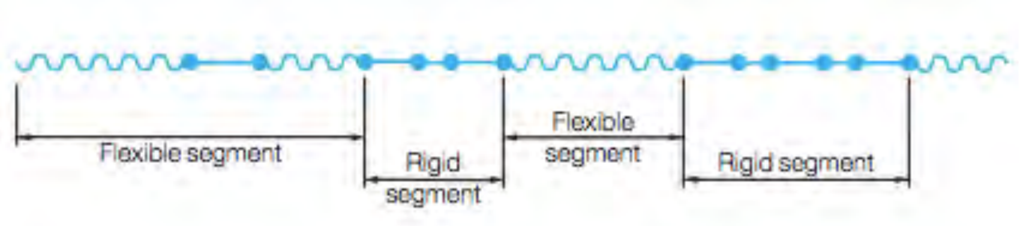

Figure 2.6: TPU morphology [25]

2.7 Overview

The background research conducted on CNF production, properties, polymer effect, and electrically and thermally conductive composites assisted in creating a conductive CNF composite. After examining different CNF options from Pyrograf Products, PR-19-XL-LHT VGCNFs were chosen due to their conductive characteristics after heat treatment. Understanding TPU's semicrystalline, polar, block copolymer nature helped predict CNF reactions during compounding. Reviewing conductive composite research helped determined the necessary loadings to meet percolation thresholds. Since creating an electrically conductive composite was the primary goal of this research any thermal heat transfer though the material was viewed as a secondary benefit. The following sections will outline how CNFs were compounded on a HAAKE Polylab reomixer and pressed using compression and transfer mold. All samples underwent an array of tests following creation.

CHAPTER III

MATIALS AND PREPARATION

Based off of the literature review it is clear that CNFs and CNTs can enhance electrical, thermal, and mechanical properties when compounded into materials. Theoretically CNTs have better mechanical, thermal, and electrical properties compared CNFs, but CNT form agglomerates and entangle more easily than CNFs complicating the compounding process and limiting their dispersion throughout the polymer matrix [26]. CNFs have weaker Van der Waals forces and disperse more uniformly throughout the matrix, and cheaper to manufacture. After taking into account all these considerations Pyrograf III carbon nanofibers PR-19-XT-LHT, Figures 3.1 and 3.2 were chosen as the additive because they exhibited high electrical conductivity characteristics after heat treatment.

In addition to increasing conductivity, CNFs raise the overall hardness of the material. Hardness can be controlled by the percentage of CNFs added and by polymer they are compounded with. The hardness was preset to a durometer of 52 Shore D, because this research was initially for a specific railway application. Trains operate in a mechanically demanding environment; therefore a lower durometer would lead to creep under stress and raising the durometer would lead to excessive abrasion on adjacent parts. CNFs are extremely hard and increase the hardness of a material they are compounded with. Keeping this in mind BASF Elastollan 1195A55 was chosen as the TPU because its durometer reading was slightly lower than the target 52 D, Figure 3.3. Various weight percentages of CNF-TPU compounds were made by melt mixing to produce a composite suitable for molding and testing.

Figure 3.1: Pyrograf III PR-19-XT-LHT

Figure 3.2: Carbon Nanofiber

Figure 3.3: Elastollan 1195A55

3.1 Mixing

Melt mixing CNF into TPU demands a vigorous process. CNFs have an extremely high surface area to volume ratio, which leads to a high degree of hydrogen bonding though Van der

Waals forces. Hydrogen bonding promotes agglomeration and low dispersion into the polymer. In order to produce a true composite material with optimum electrical and mechanical properties a uniformly dispersed and distributed matrix is necessary. Incomplete dispersion and distribution produces agglomerates – brittle pockets of CNFs in the composite matrix. CNF agglomerates yield unrealistic material properties during testing. For example, CNF agglomerates act as corridors for electrical current creating the illusion of a homogenous conductive composite material. In a true homogenous composite, electrons jump from CNF to another CNF. This phenomenon is called tunneling. Tunneling occurs when CNFs are evenly spaced apart maximum distance 10 nanometers from each other. The presence of a few CNF agglomerates in a matrix produces a couple current pathways making a composite seem as if it were electrically conductive; however, the material is only conductive where the agglomerates are.

Assuming a composite material is conductive when conductivity is only due to a few agglomerates is extremely detrimental if the composite material is scaled up and put into production. Because an equal distribution of agglomerates is impossible, some parts will receive an excessive amount of CNF agglomerates and exhibit hyper conductivity, while other parts will lack agglomerates all together and be non-conductive. Although CNF agglomerates enhance conductivity, they crash mechanical properties due to their brittle characteristics. For example, strain to failure will sharply decrease due to brittle agglomerate concentrations embedded in the matrix. To bypass these difficulties a Haake Polylab Reomixer was used because it offered a controlled mixing environment where temperature, mixing time, and extruder RPM could be monitored.

The Haake Polylab Reomixer compounded materials by melt mixing. This machine provided the best avenue for compounding due to its precise, real time feedback of the mixing chambers. Two mixing screws rotated inside a heated mixing chamber compounding the CNFs into the polymer. To limit the mixing time needed to create a dispersed CNF composite, TPU pellets were mixed inside the machine until they became a viscous melt before adding any CNFs. If the CNFs had been added into the Haake PolyLab mixer simultaneously with the TPU pellets the CNFs would be pushed to the chamber walls by the TPU pellets until they became viscous. As a result more mixing would be required after TPU became viscous to achieve a homogenous compound. To promote proper dispersion of CNFs into TPU's matrix the upper temperature threshold on the material safety data sheet of 220 °C was used. Higher temperatures decrease polymer viscosity, which promotes CNF wetting and dispersion into and throughout the polymer matrix. Proper mixing time and extruder RPM were necessary for adequate CNF dispersion throughout the matrix. Dr. Lozano's scanning electron microscope (SEM) was used to analyze samples after various mixing times to determine when adequate mixing had been achieved.

A SEM microscope analyzed each mixture by scanning a focused beam of electrons across each sample. Detectors sensed sample characteristics as electrons were absorbed or reflected by the sample. SEM photographs of samples compounded at different mixing temperatures are shown in Figures 3.4 and 3.5. Figure 3.4 clearly displays a large clump of CNFs on the surface of the TPU polymer matrix when mixed at 190 ℃. Figure 3.5 displays CNFs mixed into TPU polymer at 220 ℃. The CNFs in Figure 3.5 were wetted by the polymer with fibers sticking out of the matrix instead of lying on top of the polymer matrix in a clump. Another factor indicating CNF dispersion was a change in CNF diameter after mixing. When the TPU matrix properly wets a CNF there isn't any distinction between the beginning of the CNF and the end of the polymer matrix. Wetted fibers had an increased diameter when measured under an SEM because a thin layer of polymer surrounded them. Premixed CNFs from Pyrograf Products Inc. had an average diameter of 150 nm(pyrograf.com). Figure 3.6 displays pure Pyrograf CNFs. Figure 3.7 displays a properly dispersed fiber with a new diameter of 253 nm.

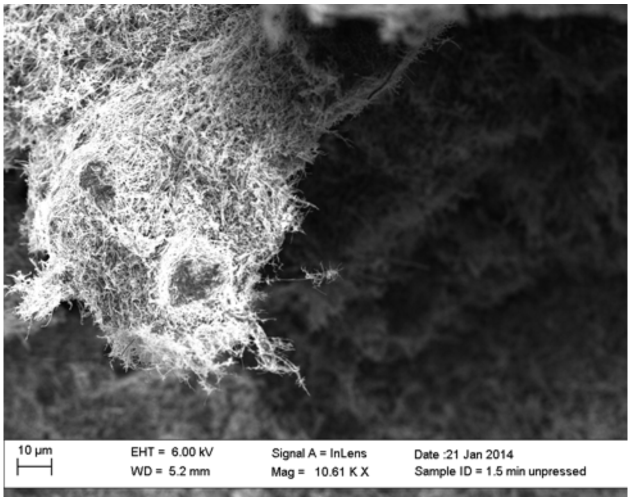

Figure 3.4 190 ℃ mixing Temperature

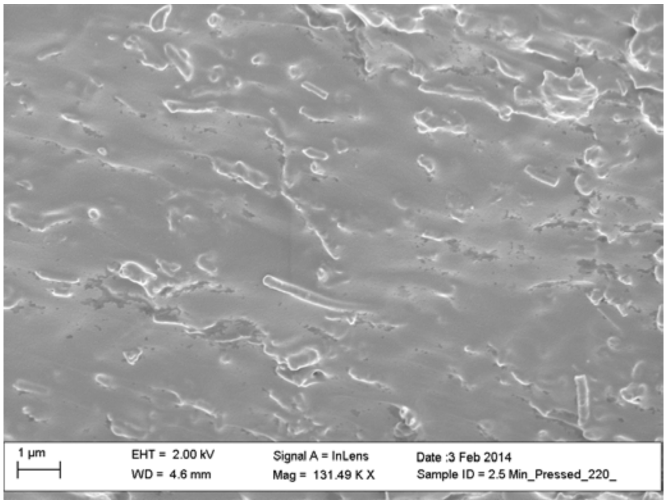

Figure 3.5: 220 ℃ mixing Temperature

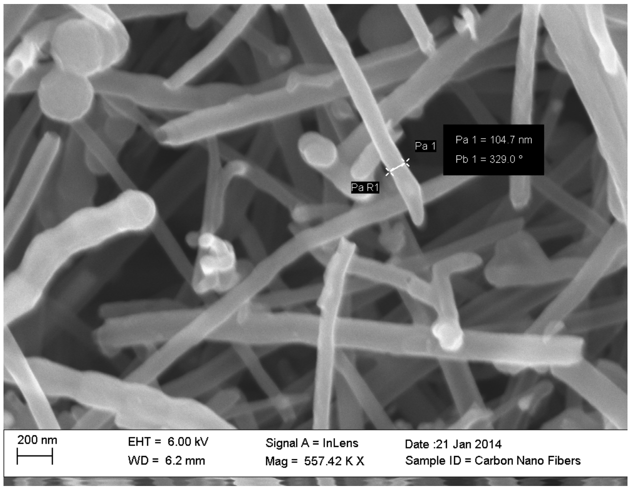

Figure 3.6: Pure Pyrograf CNFs

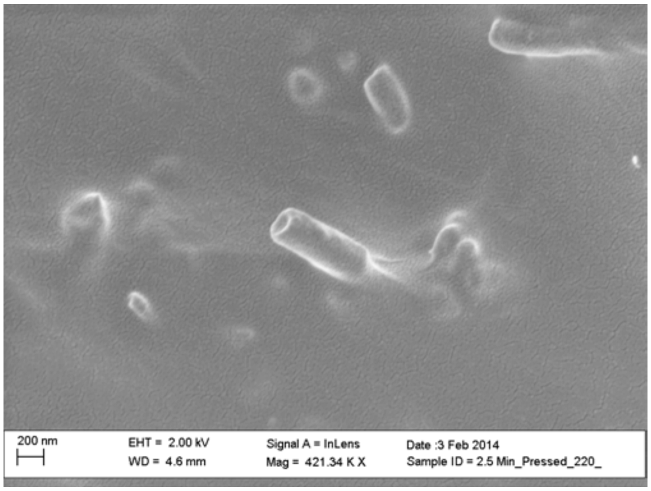

Figure 3.7: CNFs dispersed in matrix

After achieving proper dispersion of CNFs into the polymer matrix by compounding at the proper temperature of 220 ℃ the appropriate mixing time was researched. Samples mixed for 1.5, 2.5, 5, and 10 minutes underwent an SEM analysis to determine when distribution was reached. Figures 3.8 and 3.9 display material taken at 1.5 and 2.5 minute mixing times. These times proved inadequate because agglomerates filled the polymer matrix as shown. Figure 3.8 shows a white film of CNFs covering the TPU matrix after 1.5 minutes of mixing. These fibers are neither dispersed nor distributed. Figure 3.9 displays CNFs embedded into the matrix but a heavy presence of agglomerates still remained. After 5 minutes of mixing the polymer matrix appeared less bright indicating that CNFs were not coating the outside as before, Figure 3.10. The fibers appeared to be more distributed throughout the matrix and dispersed by the polymer. Lastly after 10 minutes of mixing fibers could be seen spread throughout and well dispersed inside the polymer matrix, Figure 3.11.

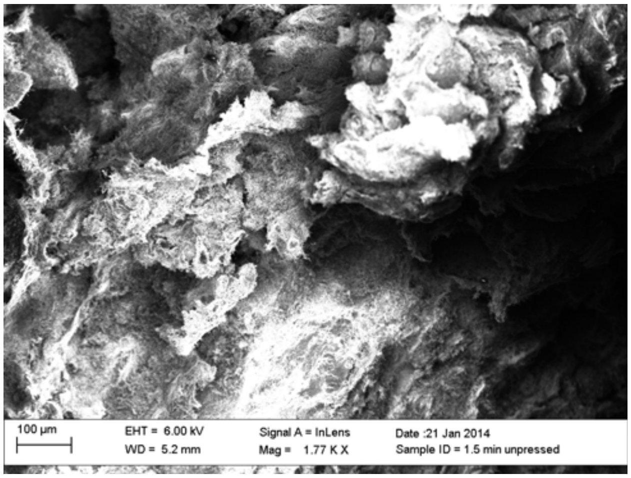

Figure 3.8: 1.5 minute mixing time

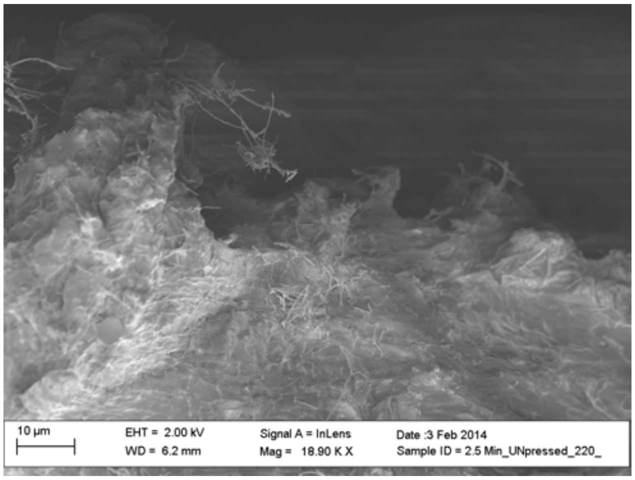

Figure 3.9: 2.5 minute mixing time

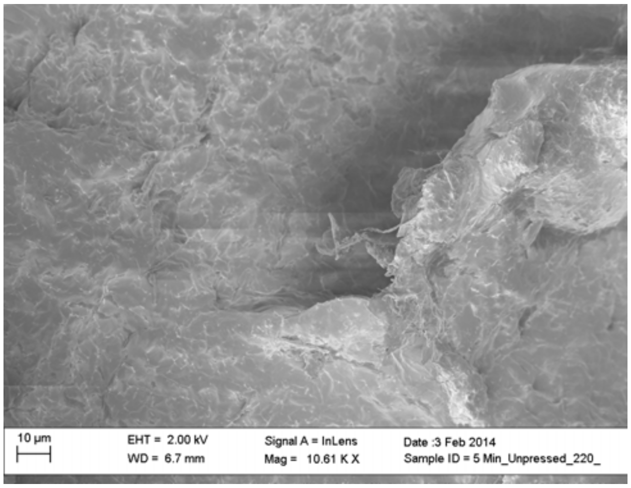

Figure 3.10 5 minute mixing time

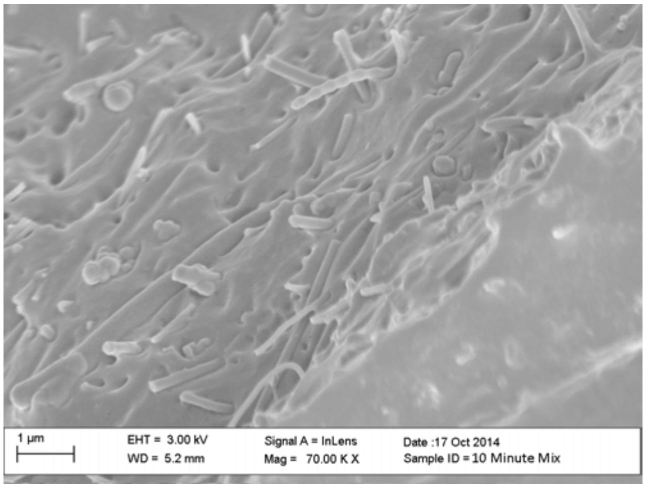

Figure 3.11 10 minute mixing time

Compounded materials were tested at varying percentages of CNFs to determine the effect CNFs had on conductivity. To ensure accurate percentages of CNF in mixing, individual components were pre-made prior to compounding. TPU and CNFs were weighted separately on laboratory scales. To calculate the exact amount of CNFs needed for the desired weight percent, the following equation was used. By manipulation the exact weight of CNF was calculated based on the desired weight percent of the material.

$$\frac{Wt.Carbon\ Nanofiber}{Wt.Polymer+Wt.Carbon\ Nanofiber}\times 100 = Wt.\%\ Carbon\ Nanofiber \qquad (1)$$

$$\frac{Wt.\%\ Carbon\ Nanofiber}{100}\times Wt.Polymer + \mathrm{Wt.}Carbon\ Nanofiber = Wt.Carbon\ Nanofiber \qquad (2)$$

Once the desired measurements of CNFs and TPU were calculated and weighed the Haake Polylab mixer was prepared.

3.2 Haake Polylab Mixer

The Haake Polylab mixing machine was operated through a computer interface, Figure 3.12. The mixing chamber was divided into three different sections M1, M2, and M3. Each section had its own temperature control. For experimentation uniform temperature distribution was desired; therefore, all three chambers were set to the same temperature. The injection molding processing temperature for TPU was listed on the BASF material safety data sheet as 210 – 220 degrees Celsius [25]. Various mixing temperatures were explored for optimum dispersion. 220 ℃ was determined as the optimum temperature after SEM sample analysis. Therefore the Haake Polylab mixing temperature was set to 220 degrees, Figure 3.13.

The rotating screws were each set to 60 revolutions per minute and the mixing time was set beyond what was needed for compounding to ensure adequate mixing. After all the parameters were set the machine was preheated to the desired temperature and then TPU pellets were poured into the hopper. Once the TPU pellets formed a viscous melt inside the chambers the CNFs were added and set to mix for different time lengths. Results from multiple mixing times were examined under a SEM microscope to determine if sufficient mixing had occurred for full dispersion and distribution. The appropriate mixing time was found to be 10 minutes after CNFs were added. After mixing the chambers were opened the compound was removed for molding. The Haake Polylab command screen settings are shown in the Figure 3.13 and a graph of the torque, time, and temperature relationship is shown in Figure 3.14.

Figure 3.12: Haake Polylab Reomixer

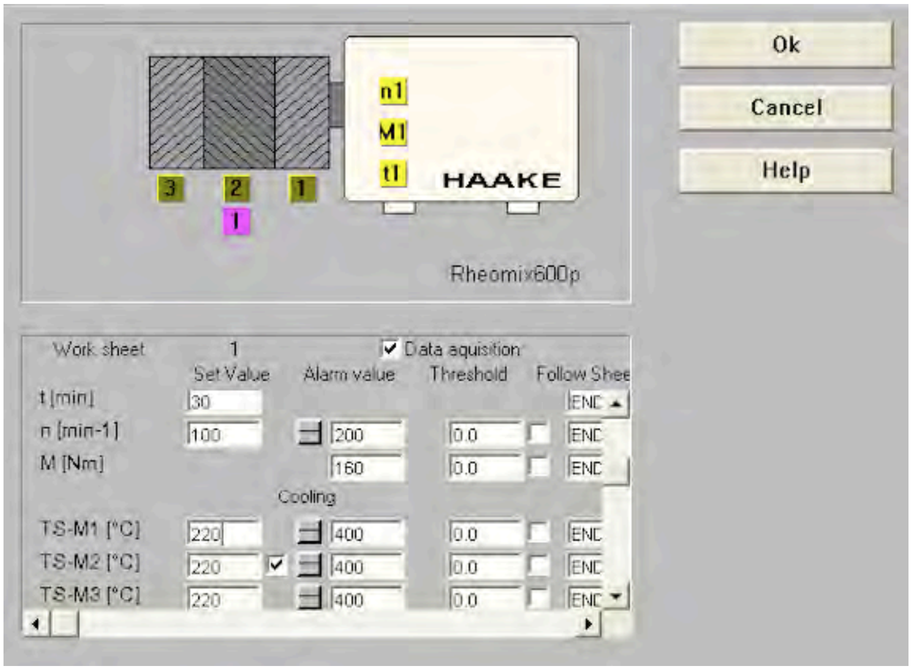

Work sheet 1 ☑ Data aquisition

	Set Value		Alarm value	Threshold		Follow Shee
t [min]	30					ENC
n [min-1]	100		200	0.0	☐	ENC
M [Nm]			160	0.0	☐	ENC
		Cooling				
TS-M1 [°C]	220		400	0.0	☐	ENC
TS-M2 [°C]	220	☑	400	0.0	☐	ENC
TS-M3 [°C]	220		400	0.0	☐	ENC

Figure 3.13: Command Screen Window

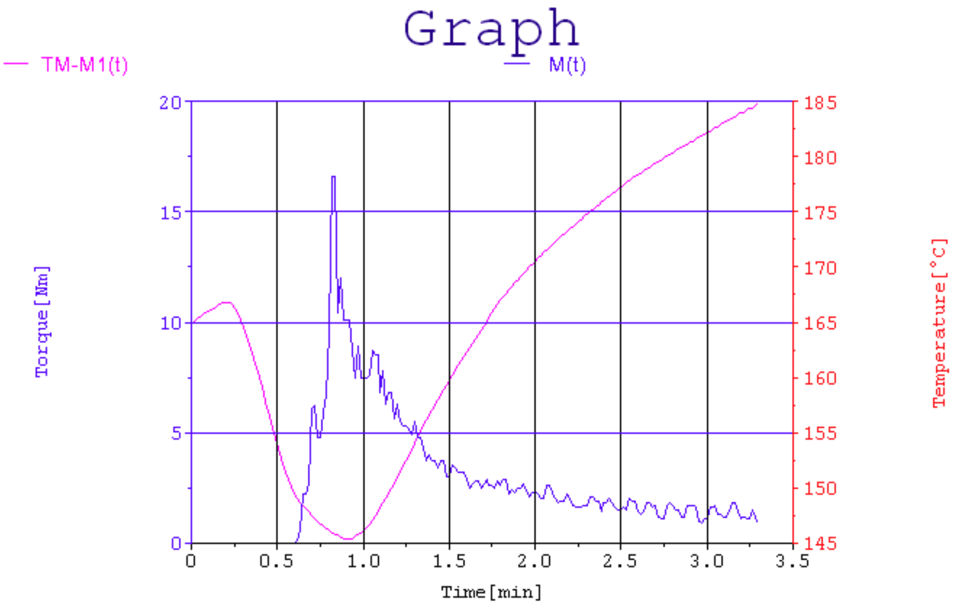

Figure 3.14: Torque and Temperature as a function of time

When the TPU pellets were poured into the hopper the mixing chamber temperature decreased. This was due to the TPU pellets being stored at room temperature prior to mixing. At the onset of mixing the torque spiked upward because a high shear force was required to grind the pellets. However, once the heat distribution equilibrated throughout the TPU its viscosity decreased significantly along with the applied torque. Pellets were carefully added in small increments to not overload the machine past a max torque of 30 newton meters. Once torque levels equilibrated adequate mixing was assumed and CNFs were added. Torque increased slightly upon the addition of CNFs but not significantly compared to the TPU pellets. The torque of the CNF and TPU mixture quickly equilibrated, but this was not an accurate measure of adequate distribution or dispersion.

The Haake PolyLab machine was equipped with a safety mechanism, which triggered an automatic shut down if the torque measured above 30 N·m. Because of this safety measure extreme caution was taken to monitor the torque levels by controlling the amount of TPU poured in. Pouring all the TPU pellets into the hopper at once would trigger a shut down; therefore each batch was broken down into 15 gram increments. After eat portion was completely melted the next portion was added. The graph in Figure 3.14 displays a maximum torque value of 17 N·m after the first portion was added. The torque eventually fell to an equilibrium value of 2 N· m before the next portion was added. CNF did not drastically increase the torque values because of their extremely small volumes. The fibers easily mixed into the TPU negating any possible chance of a shut down. After the CNFs were added they were allowed to mix in the TPU for 10 minutes at 60 rpm and then 2 minutes at 90 rpm.

The Haake PolyLab mixer was not equipped with an extrusion mechanism therefore after all the batches were made each mixing chamber was opened and the mix was manually extracted. Completed mixes were extracted with clean tweezers, copper brushes, and screwdrivers. An aluminum pan was placed underneath the mixing chamber to catch all the entire mix. After each mix was extracted the machine was cleaned by running pure virgin TPU through the mixing chambers. Repeated virgin TPU runs were made until the machine was clean and free of CNFs.

3.3 Pelletization and Drying

The composite material manually extracted from the Haake PolyLab machine was not uniform in shape or size. The CNF-TPU mixes underwent a manual pelletizing process instead of being processed through a chopper to maintain a contaminant free composition. Plastic latex gloves were worn throughout this tedious process to ensure the chemical integrity of the compounded material, Figure 3.15. After the material was pelletized into a uniform size it was dried and prepared for molding.

Figure 3.15: CNF – TPU Pelletization

The purpose of drying materials is to ensure product homogeneity in molding. Trapped moisture can create unwanted air bubbles in final products. Decants are regularly used to absorb moisture when products are in storage but it was also advised to dry them inside an oven before molding. All CNF-TPU batches were allowed to dry in an oven for 3 hours at a temperature of 100 °C, Figure 3.16. This ensured that any moisture trapped in the material was evaporated. Bubble formation in a final product would not only lower aesthetic appearance but also effect properties such as stress and strain tolerances, thermal heat transfer, and electrical conductivity. In regards to thermal and electrical conductivity, air pockets act as capacitors storing energy. This lowers the available channels of electron transfer by adding mechanical resistance.

Figure 3.16: Pellets drying inside oven

3.4 Molding

Two molding techniques were used to press pelletized composite mixes into pucks for testing, compression molding and transfer molding. Compression molding is the traditional process of pressing CNF composites. It was performed by pressing material into a mold on a heated direct press. During this process materials was placed in a bottom mold called a pot and pressed down by a top mold known as the plunger. The process is similar to a piston moving inside a cylinder. The two parts of the molds were fashioned between two heated plates on a direct press.

Transfer molding is a process similar to compression molding except material is extruded through a plate acting as a sprue between a top and bottom part of a mold. Transfer molding contains pot for material and a heated plunger, which presses down into the pot compressing material. However, instead of is staying in the pot, in compression molding the heated polymer is extruded through a hole acting as a sprue on the bottom of the pot and into a bottom mold to form the desired part.

3.5 Compression Molding

Compression Molding offered a low sheer process for pressing material into a mold. The machine used was a Carver Hydraulic Heat Press unit model #3912, Figure 3.17. The press consisted of two heat plates, a hydraulic powered manually unit, two vertical threaded shafts, an electronic power source, cooling water tubes, and temperature gages. The upper plate moved vertically between the two threaded shafts. A through hole on each side of the upper plate allowed it to move freely along the vertical shafts but it was held in place by four nuts. Two nuts on each side sandwiched the plate along the shaft to hold it firmly in place. Once the upper plate was stationed at the appropriate height the press was ready for use.

During operation the lower plate was used to press the appropriate part. It was connected to a hydraulic lift manually operated by a leaver. The plates were heated up through coil resisters and the knobs on the side controlled temperature. Individual temperature gages displayed the corresponding plate temperatures. Keeping the press at a constant processing temperature was challenging, but careful watch over the temperature gages and manipulation of the power knobs held the press near or at the appropriate temperature for molding. Figure 3.17 displays the heat press and its corresponding parts.

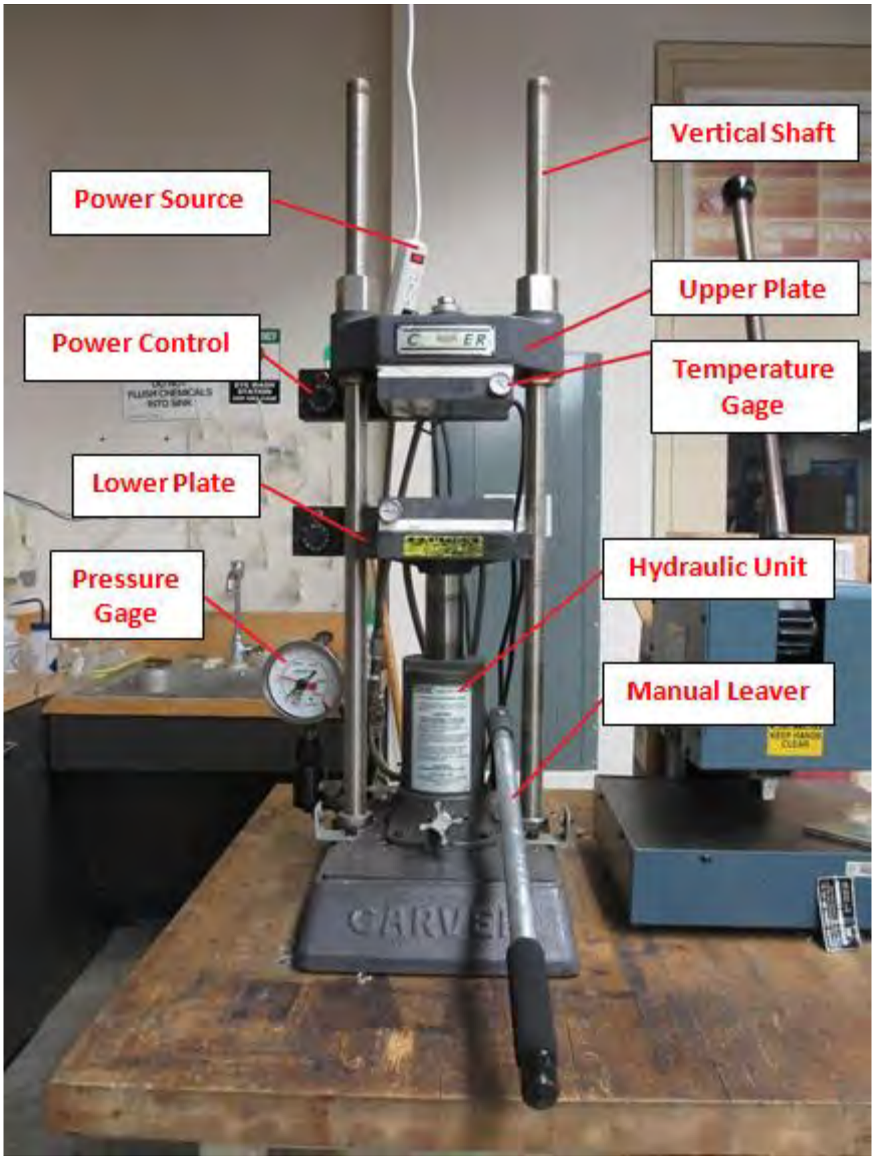

Figure 3.17: Carver Heat Press

The mold used for pressing consisted of three cylindrical aluminum pieces a pot, a plunger, and a disk, Figure 3.18. The thin disk was placed in the pot first and then TPU pellets were added for molding. After the appropriate amount of pellets were added the plunger was fitted above the mold cavity for pressing. The preloaded mold was then placed on the lower plate of the heat press and hydraulically compressed. Dimensions for the pot were: outside diameter of 3.825 inches, inside diameter of 2.535 inches and depth of 1.0 inches. A 0.5 inch hole was drilled through the bottom of the pot to allow for a key to push the sample out after molding. The small disk placed on the bottom of the pot to inhibited flow out of the pot during molding. The disks diameter was 2.500 inches and its thickness was 0.140 inches. The plunger's diameter and depth were both 2.500 inches.

Figure 3.18: Compression Mold

Different pucks were molded for various testing applications. The applications included sample bars for dynamic mechanical analysis (DMA) and MTS testing and inserts for conductivity testing. The DMA tests required bars with specific tolerances where dimensions were no greater than 1.5 inches long, 0.5 inches wide, and 0.125 inches thick. These test bars measured creep and relaxation modulus. Tensile bars, used by the MTS machine, were very similar in dimensions to the DMA testing bars except the middle of the bar tapered down to 0.1 inches providing a wishbone appearance. These bars tested the stress strain relationships of the material under tension. Contrary to the DMA and tensile testing samples, conductivity tests utilized a larger cylindrical puck. Its dimensions were 2.5 inches in diameter and 0.7 inches thick. All the testing samples were made from the same mold, so precise weight calculations were taken into account to determine proper puck volumes. Mass calculations were based off of manipulations of the following formulas.

Puck Volume: $$V = \pi r^2 t \tag{3}$$

$$\rho = \frac{m}{V} \tag{4}$$

Manipulation of the equation yielded the mass required for molding:

$$m = \rho V \qquad (4)$$

Where v, r, t, m, and ρ stand for volume, radius, thickness, mass and density respectively.
10 percent overages in the mass were added to account for material flashing around the plunger during molding. Flashing helped determine the max time limit for compression molding.

Some parameters for molding were given by the product manufacturer but others were discovered through experimentation. For example, all compression molding was conducted between 190 and 210°C, the processing temperature for TPU 1195A55D given by BASF Chemical Company, but the necessary applied mechanical pressure and molding times were determined though experimentation. Molding time and pressure were determined when molding thicker pucks for conductivity testing.

A colleague, Ruben Suarez fabricated a rectangular mold and this mold was borrowed to produce the first puck. The puck, composed of virgin TPU was pressed at 190° C for 5 minutes with 3 tons of pressure applied. This was supposed to provide a baseline for all other pucks, but after molding the puck was cut open to be examined, as shown in Figure 3.19 and Figure 3.20 it contain a granular, heterogeneous nature in the middle.

Figure 3.19: First Puck

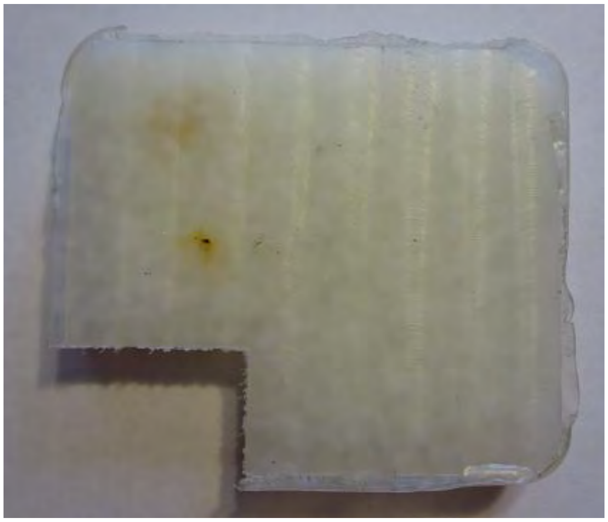

Figure 3.20: First Puck

A heterogeneous composition could not be tolerated because small air pockets act as tiny capacitors inhibiting current flow. To combat this problem a more durable mold was fabricated to allow greater pressure at increased temperatures as shown in Figure 3.21 and Figure 3.22. Two different molding processes were implemented to produce a less granular inside. First virgin pellets were heated to 190° C and allowed to sit inside the mold for 10 minutes to “cook” under heat at little or no pressure. The objective was to bring all the pellets up to a uniform temperature prior to molding, thus improving the homogeneity of the composition. Following the “cook” time 3 tons of pressure were applied until flashing occurred. The second method was to cold press the pellets before heating at 5 tons of pressure and then slowly heat up to 190° C until flashing occurred around the mold. Cold pressing the pellets before heating yielded more homogeneous pucks, but the middle still contained a slight heterogeneous microstructure. These pucks are shown in Figure 3.23 and 3.24.


Figure 3.21: Durable Mold

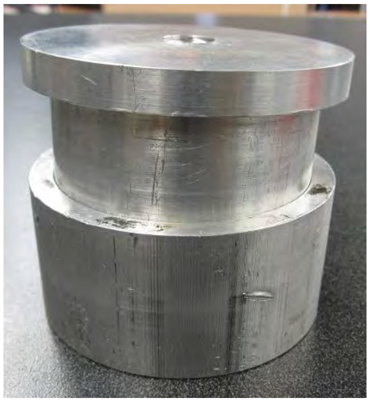
Figure 3.22: Durable Mold

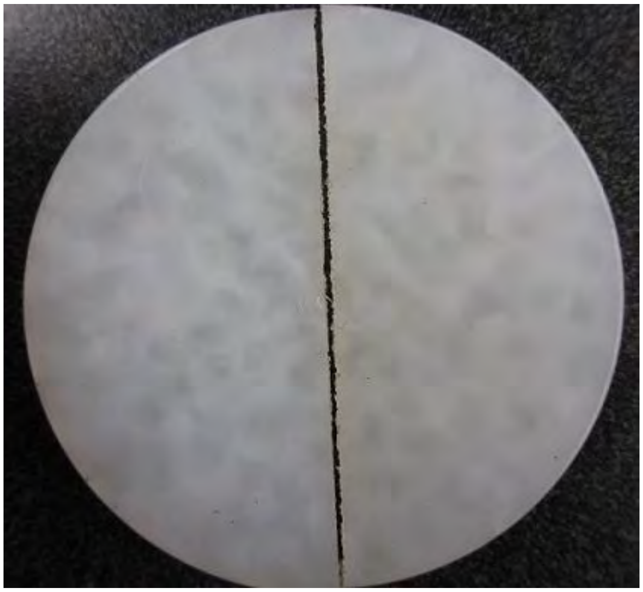
Figure 3.23


Figure 3.24

A completely homogeneous puck was not achieved through compression molding for deeper conductivity testing pucks. Another technique, transfer molding was research to mold these pucks. Because compression molding proved a viable option for thin pucks, a set of DMA and tensile bars were compression molded for testing to compare with other molding techniques.

3.6 Transfer Molding

Transfer molding is a process of molding materials similar to both compression molding and injection molding. Transfer molding is like compression molding because it is slower and a relatively low sheer force is placed on the material, but the mechanics of the system more accurately resemble injection molding. In transfer molding a precise amount of uncured material is preloaded for molding, but instead of placing the mixture directly into the mold as in compression molding material is placed into a pot. The pot is positioned above the mold and heated past the material melting point thus reducing the contents viscosity. The viscous material is then extruded through a sprue at the bottom of the pot into a mold by a plunger, Figure 3.25.

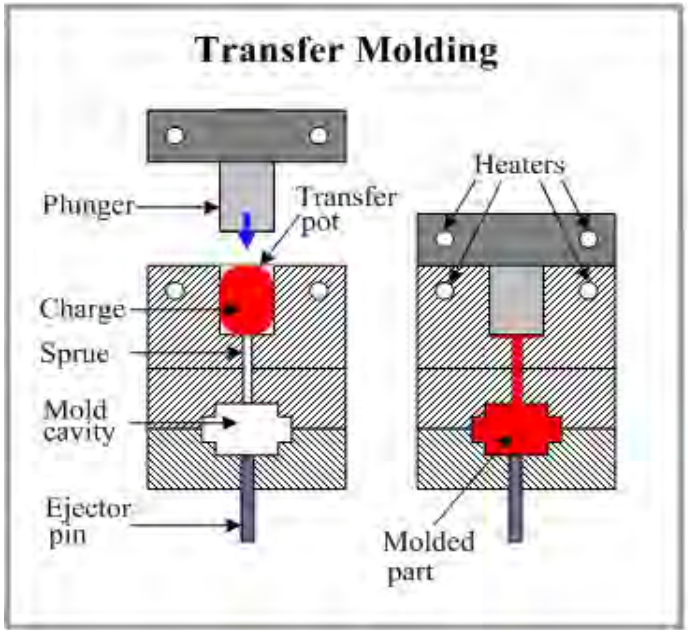

Figure 3.25: Transfer Molding Process [27]

A transfer mold was fabricated on a lathe to fit on the Carver heat press Figures 3.26 – 3.28. The goal was to use to heat and power sources from the press to both heat and operate the mold. An initial prototype made out of aluminum contained a plunger, melting pot, circular disk with a hole acting as a small sprue, lower mold, and a small disk for product ejection. The dimensions of the mold are listed as follows. The plunger had a diameter of 2.5 inches and was 2.5 inches long. The pot consisted of a cylinder that was attached to the disk. The pot’s inner and outer diameters were 2.503 and 3.8 inches respectively while its length was 2.2 inches. The disk, which separated the pot from the mold acted as a gate to only allow passage of viscous material. The addition of a sprue on the transfer mold produced a homogenous puck without air pockets.

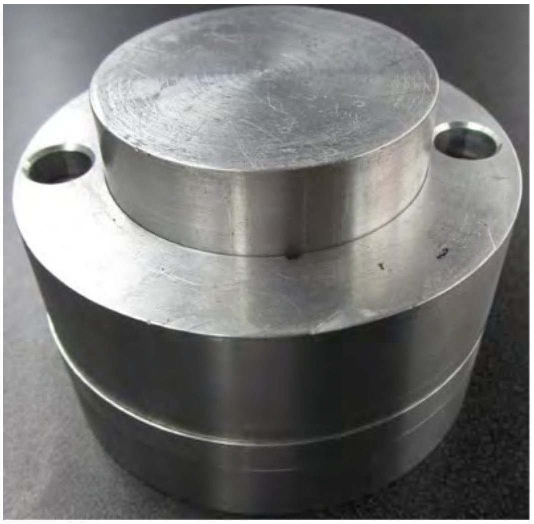

Figure 3.26: Aluminum Transfer mold

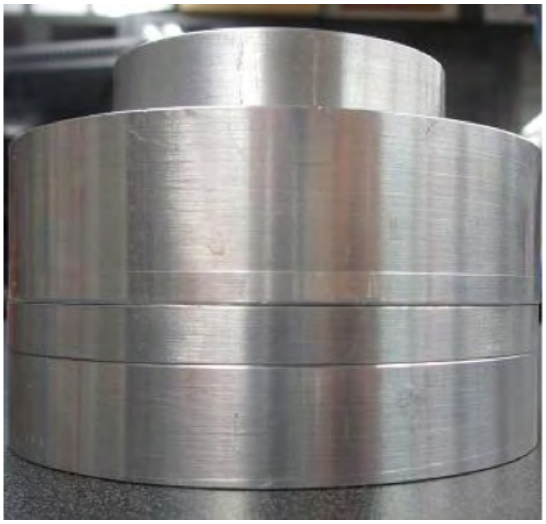

Figure 3.27: Aluminum Transfer mold

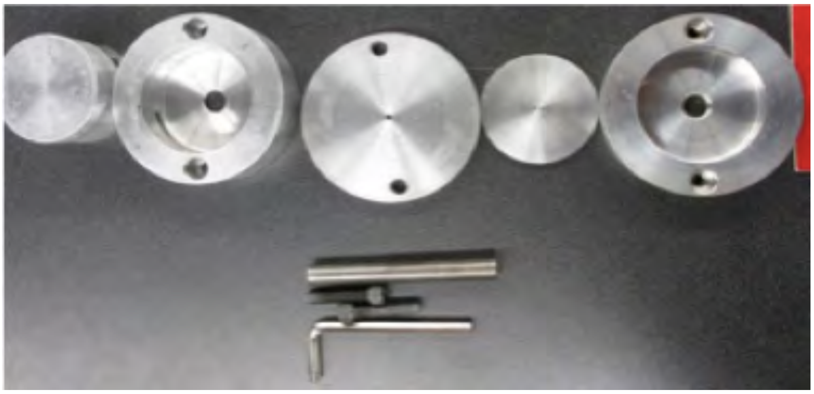

Figure 3.28: Transfer mold disassembled

The aluminum mold heated up very quickly and uniformly on the carver press. This proved to be beneficial in reducing time, yet disadvantageous in controlling the temperature of the bottom mold. With the mold remaining at the same temperature as the pot and plunger a material flow field was evident in processed pucks, Figures 3.29 & 3.30. This produced an unpleasing less aesthetic final appearance and insinuated slight material discontinuities in the form of knit lines. Knit lines are formed when two flow fronts meet each and are unable to weld or knit together seamlessly. These lines decrease the mechanical properties of the molded product, and create weak points where fracture is more probably under stress [28]. These assumptions were verified when pucks were broken under a cryogenic study.

Figure 3.29: 15% CNF-TPU flow field puck

Figure 3.30: Virgin flow field puck

A cryogenic test induces extremely low temperatures on a sample. Failure was induced because cryogenic temperatures lower the material fracture toughness while simultaneously increasing the mode I fracture stress [28]. A cryogenic test can be used to locate weaknesses in a material because fracture will occur at the weakest defect points first, which explains why pucks fracture occurred along knit lines. In cryogenic fracture the internal integrity of the matrix along the fracture remains intact. This is not the case with a saw or knife cut where the polymer matrix around the cut is disrupted. During the cryogenic test transfer molded pucks were placed in a liquid nitrogen bath until fracture. Upon cryogenic fracture discrete groupings appeared separated by knit lines along the flow field Figure 3.31.

Figure 3.31: Cryogenic fractured puck along knit lines

Enhancement of the mechanical properties was not the cardinal point of this study, but knit lines affect electrical properties as well as mechanical. Small visible fissures in the product translate to great chasms on the micro and nano scales. These fissures will have the same effect as the air pockets in the compression molding except unlike compression molding knit lines indicate a molding process that has not been optimized. Manipulating the molding temperature, injection pressure, and/or ventilation gates can eliminate the presence of knit lines. The aluminum mold was an excellent prototype, but noticeable wear marks collected on the pot and plunger during use and material eventually flashed around it instead of flowing through the sprue limiting the maximum amount of applied pressure. Because of the wear on the aluminum mold and the need for process optimization another mold was fabricated out of 4340 steel.

3.7 Steel Transfer Mold

A new mold fabricated out of 4340 steel was designed on solid works, Figure 3.32. 4340 steel is considerably harder than aluminum and has a vastly different heat transfer coefficient. The benefits of a harder material were that discrete, sharp edges maintained their shape and less wear was accrued on the plunger during operation. The plunger was designed to have a radius 3 thousandths smaller than the pot and a copper wear ring fitted on it as a seal. The copper wear ring sat inside a grove on the plunger producing a press fit inside the pot every time it was operated. Because the heat transfer coefficient of AISI 4340 steel is considerable lower than aluminum, 44.5 W/mk and 237 W/mk respectively, temperature distribution in the mold could be carefully controlled [30]. AISI 4340 steel transfer mold showed in Figure 3.33.

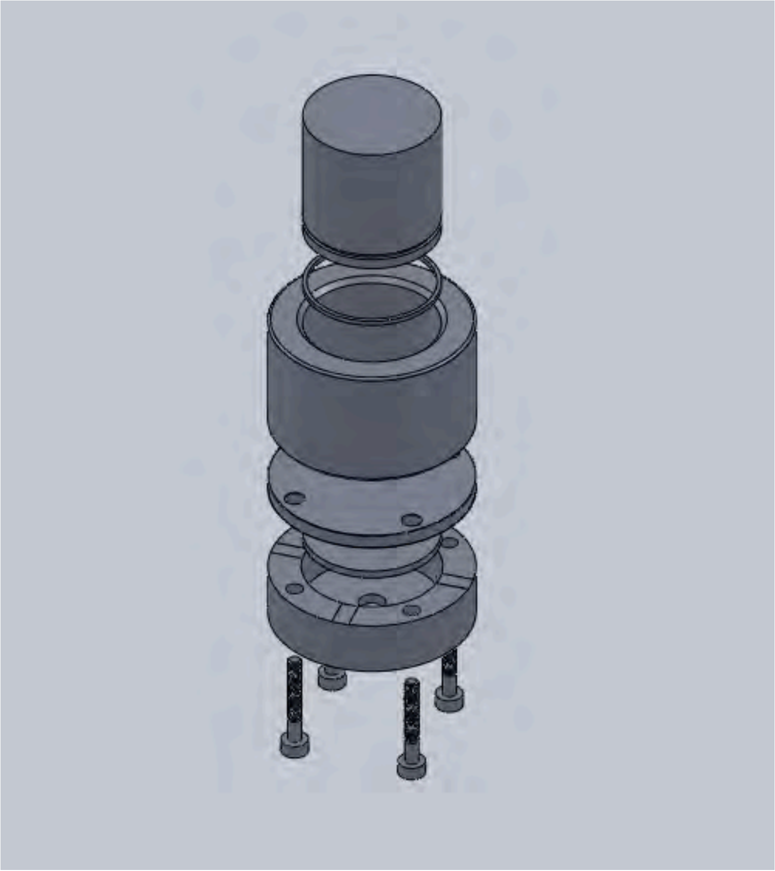

Figure 3.32: Solidworks Representation of Transfer Mold

a.

b.

Figure 3.33: AISI 4340 Transfer mold

Controlling the temperature of the bottom mold proved to be a crucial step in eliminating knit lines in the final product, Figure3.34. Each plate of the Carver heat press had its own independent temperature control knob and thermometers. During injection molding mold are usually kept above the recrystallization temperature [29]. Through experimentation 115 °C was found to be the ideal mold temperature. This temperature yielded clean opaque pucks without knit lines.

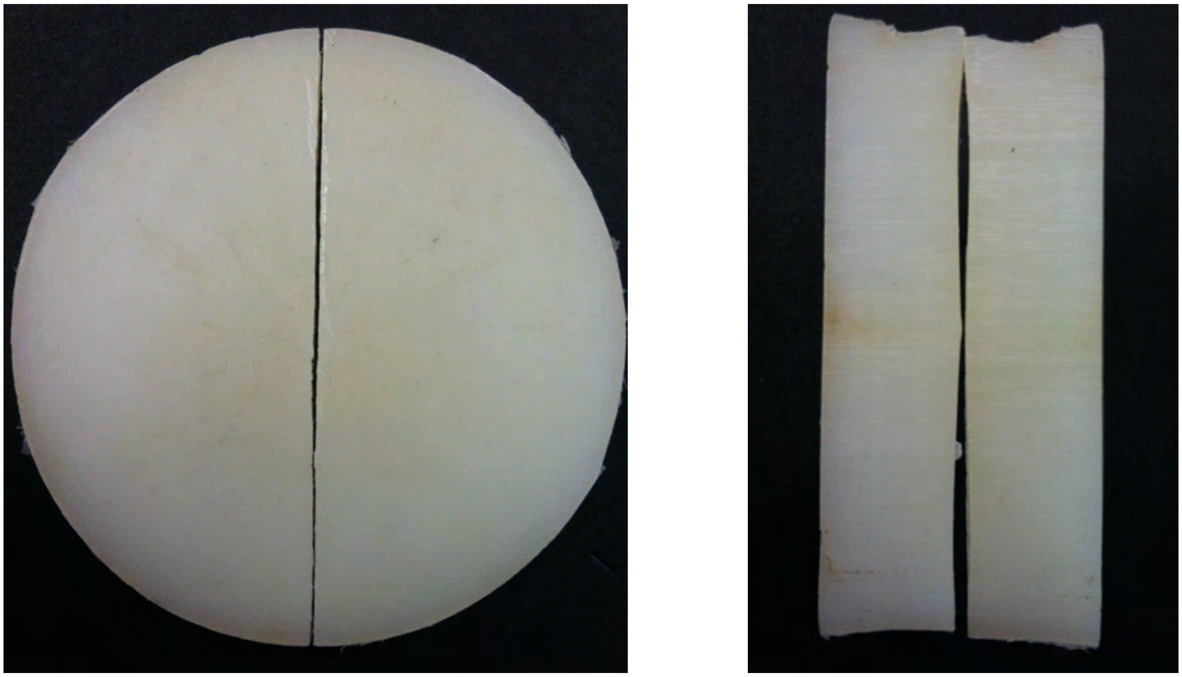
a. b.

Figure 3.34: Virgin TPU puck from AISI 4340 Steel Transfer Mold

The final molding process was to apply and maintain 1.5 metric tons of force on the mold and heat the top mold for 30 minutes. The top plate was heated to 230 °C while the bottom plate was set at 115 °C. 230 °C was well above the listed viscous softening point but a greater heat differential between the plate and the mold reduced the heating time. A pressure drop on the gage indicated material flow into the bottom mold. Pressure was manually maintained at 2 metric tons during the operations. Once flashing occurred through the release gates in the bottom mold a water-cooling system was activated. The cooling system was comprised of a tubing apparatus, which ran through the heating plates. As the heating plates cooled the mold followed. Because the mold retained heat so well, when the mold temperature reached 70 °C it was quenched in water to rapidly cool. The entire process lasted for approximately 1 hour.

3.8 Conductivity Testing

Multiple testing methods were implemented on pucks to resemble practical industry settings. All testing setups had similar parameters. Pucks were tested on an MTS machine while a voltage difference passed when loads were applied. All the testing setups contained the same power supply, multimeter, aluminum sheets, wires, and air valve, Figure 3.35 a – d.

Figure 3.35: a. Two Aluminum Plates

Figure 3.35: b. Multimeter

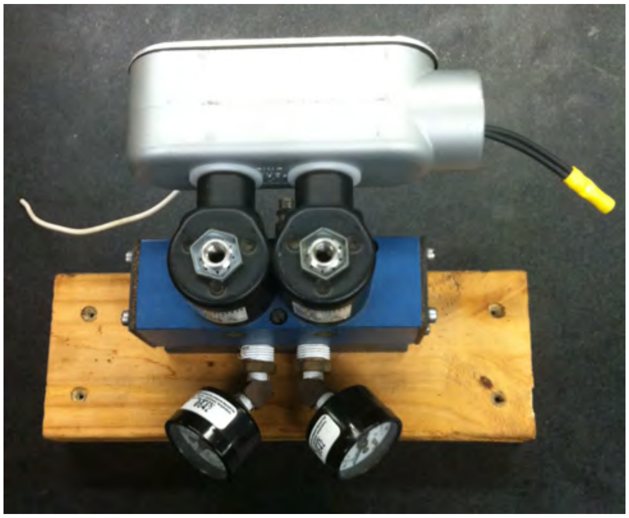

Figures 3.35: c. Air Valve

Figure 3.35: d. Multimeter

To satisfy the requirements for the rail application and air valve had to be triggered for the test to be considered successful. A current of 260 milliamps had to pass through the composite to trigger a solenoid driven air valve. For the industry application the solenoid had to maintain functionality for actuation on an empty and fully loaded rail car. Therefore the composite must pull at least 260 milliamps of current when a max of 27,500 pounds of load are applied corresponding to a loaded car and 2,750 pounds corresponding to an empty car. Other classes of rail cars transport greater cargo loads but testing these loads was not imperative because conductivity through the pad increases as load is applied until a maximum threshold is reached. This is due to CNFs moving closer together opening up newer pathways for current flow as the composite material undergoes compression. The industry application pad's surface area was 27 in^2, while prototype pucks had an area of 4.9063 in^2. Thus an empty railcar imposed a stress of 101 psi on the pad. The tested pucks experienced the same stress at a load of 499 pounds. At this minimum load 260 milliamps of current had to pass through the puck to trigger the valve. During testing 22 volts of electricity were applied to the setup. 24 volts of electricity are applied in current rail applications but testing at 22 volts allows for a factor of safety to ensure manufactured pads will exhibit conductivity at 24 volts.

3.9 MTS Machine Setup

The prototype pucks were tested on an MTS machine to simulate loading the material may undergo. Current fluctuations were studied as loads changed on the machine. The MTS machine consisted of two metal compression plates, which applied pressure. Plastic plates were fashioned above and below the aluminum plates sandwiching the puck. This set up forced current through the puck, which was in series with the power supply, valve, and multimeter.

This test allowed for quick, effective testing of small portions of composite material to be performed. An example of the setup is displayed below in Figure 3.36.

Figure 3.36: MTS Testing

CHAPTER IV

RESULTS AND DISCUSSION

Following the development of material compounding and molding, tests were preformed to determine the effect of CNFs on TPU material properties thermogravimetric analysis, differential scanning calorimetry, thermal conductivity, electrical conductivity, durometer, tensile, abrasion, dynamic modulus, creep, and hysteresis tests were all performed on the composite. The results were analyzed to develop and discover material trends as CNF percentage increased. These trends were used to make essential predictions pertaining to the effect CNFs had on elastomers. Electrical conductivity testing was the principal test performed dictating the composite material's viability in extreme service.

4.1 Thermogravimetric Analysis

Thermogravimetric analysis (TGA) is commonly used to measure physical and chemical property changes of a sample as it undergoes a constant heating rate or exposure to a constant temperature for a set amount of time. The percent weight loss of the sample relative to the initial weight is measured as the sample is decomposed. The rate of material decomposition varies with respect to temperature because specific polymer components decompose at select temperatures. TGA curves are routinely used for determining the presence of volatiles, decomposition patterns, the presence of organic or inorganic content, among other things. In this study TGA tests were performed to determine actual fiber loading achieved in samples and to investigate the effect of CNFs on TPU decomposition behavior in a nitrogen environment.

Prepared samples of 5 to 10 mg were placed in aluminum pans inside the machine. The heating rate was set to ramp from room temperature to 525 ℃ at a rate of 5 ℃ per minute. 0, 11, and 22 wt.% CNF-TPU were tested. 0 wt.% CNF-TPU was analyzed first under the TGA to develop a baseline model for how TPU 1195A decomposed, Figure 4.2. The curve displayed two strong decomposition steps. This was expected because TPU consists of two linear block segments of copolymers, a hard segment and a soft segment. From Figure 4.2 it is concluded that 45.27% (3.92 mg) of TPU decomposed between 304.00 and 327.58 ℃ representing the soft segment and 51.15% decomposed between 347.00 and 525.00 ℃ representing the hard segment. The degradation temperature associated with the first and second decompositions will be referred to as T_{d1} and T_{d2} respectively.

Figure 4.1 displays all the TGA curves overlaid for comparison. A clear distinction can be made between the 0, 11, and 22 wt.% CNF-TPU. Increasing CNF loadings tends to shift the decomposition curves to higher temperatures. The onset T_{d1} decomposition temperatures for 0, 11, and 22 wt.% CNF-TPU were 304.00, 300.94, and 310.49 ℃ respectively revealing a slight temperature shift at higher loadings (Figures 4.2 – 4.4). Shifting however was more noticeable at the 50% weight loss degradation temperature ($T_{50wt\%}$). The $T_{50wt\%}$ for virgin and 22 wt.% CNF loading were 347.00 ℃ and 385.98℃ respectively, translating to a 38.98 ℃ shift higher. This can be attributed to multiple factors.

First, optimally distributed and dispersed CNFs form weak intermolecular bonds with adjacent molecules. Although these interactions are weak singularly the compilation of millions of weak Van der Waals cannot be over looked [25]. Van der Waals forces increase the necessary amount activation energy needed for decomposition because they add dipole-dipole forces. These dipole-dipole forces must first be broken before chemical bonds can be degraded. Secondly, higher percent loadings of CNFs account for the available intermolecular space in the TPU matrix [31]. Restricted molecular mobility was the primary cause of the heat retardation effect. Heat travels through vibrational waves called phonons. When molecular freedom is restricted because of less intermolecular space molecular vibrations are damped. The dampening of molecular vibrations decreased TPU’s sensitivity to temperature change. Higher fiber loadings accounted for more intermolecular spaces increasing the amount of heat retard.

Finally, after Van der Waals forces have been overcome and molecular bonds are broken the free radicals which are produced by initial decomposition do not propagate additional decomposition reactions as usual in unmodified polymers. Free radical production leads to decomposition reactions that play a prominent part in polymer degradation. Normally free radicals react and break down organic compounds producing more free radicals and propagating their reactions. The presence of CNFs however, retards the effect of free radicals on organic compounds. CNFs act to adsorb available free radicals as they are produced inhibiting and neutralizing future decomposition reactions [32]. All of the reasons stated above explain the apparent shifting of decomposition curves in the TGA to higher temperatures.

Thermogravimentric Analysis

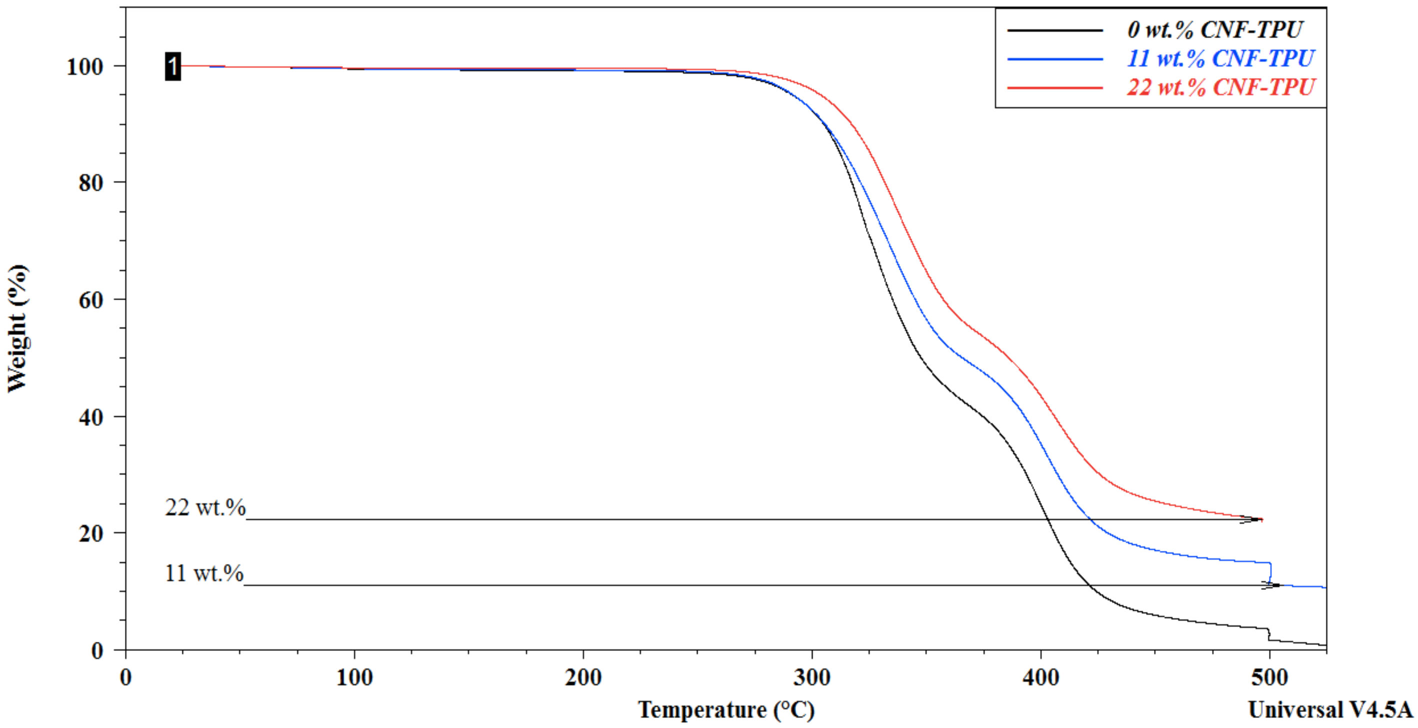

Figure 4.1: Overlay of TGA Curves

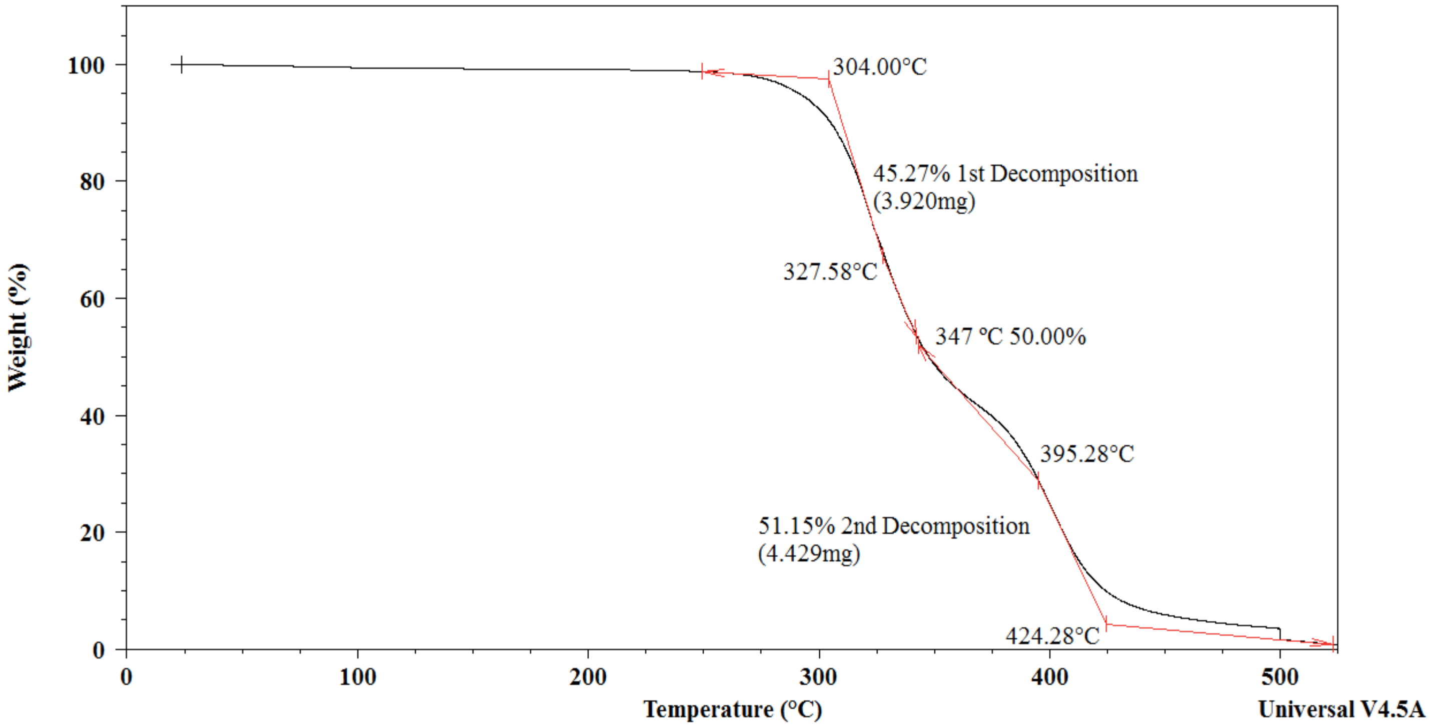

Figure 4.2: Virgin 1195a TPU TGA curve

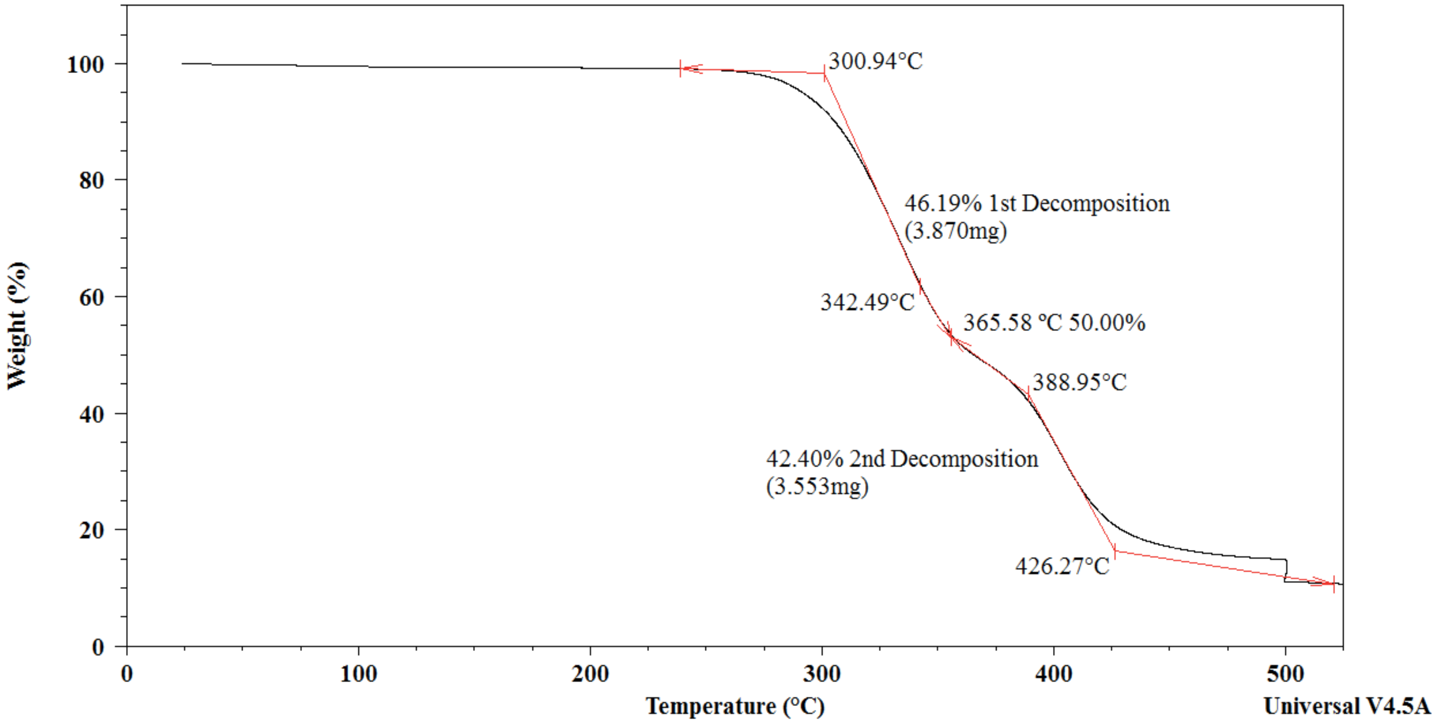

Figure 4.3: 11% CNF-TPU TGA curve

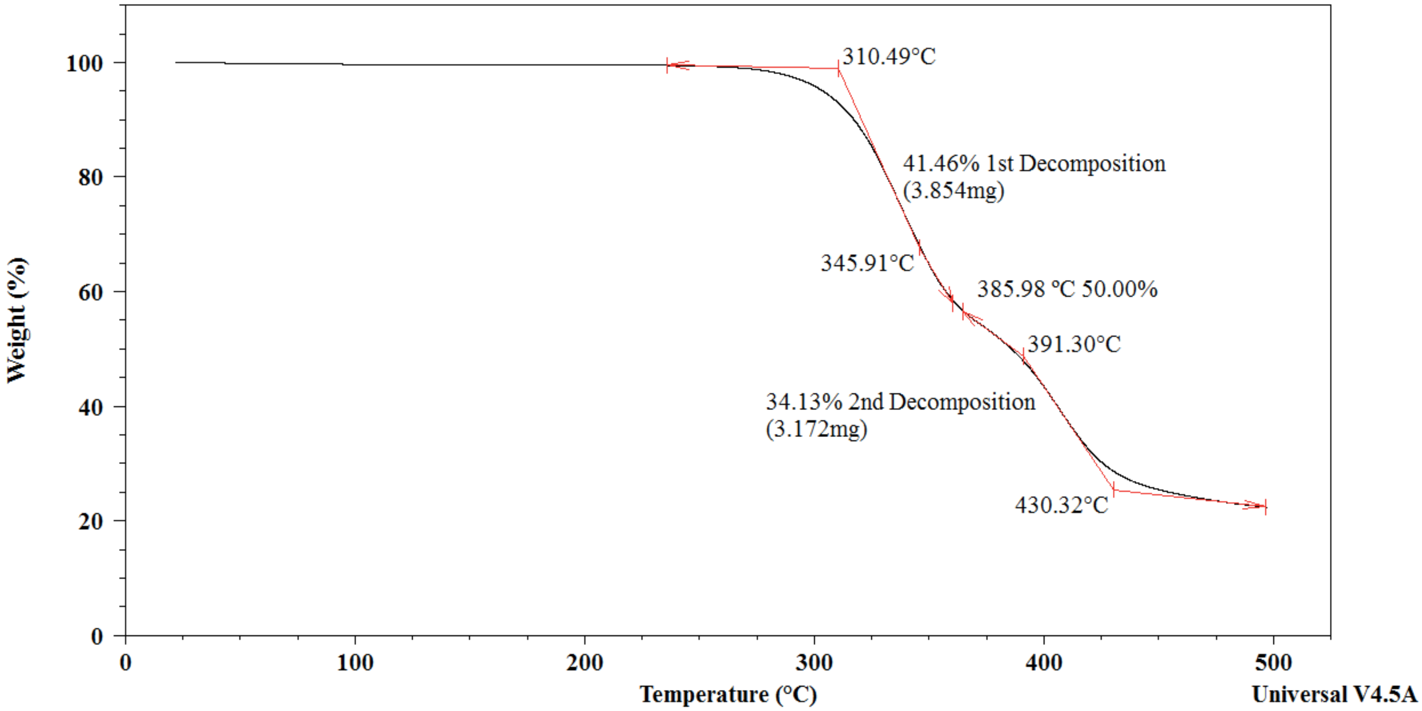

Figure 4.4: 22% CNF-TPU TGA Curve

4.2 Differential Scanning Calorimetry

Differential scanning calorimetry (DSC) is a research technique used to monitor physical changes in matter by measuring the amount of heat energy required to increase the temperature of a sample. As polymers undergo phase changes like glass transition, crystallization, melting, and decomposition the amount of heat required to increase the temperature varies. Measuring the temperature range of these changes and the amount of heat energy required to produce them, provided a blueprint for how the polymer reacted under thermal stress.

Thermoplastic polyurethane is a block copolymer containing a mixture of hard and soft segments. The hard segments (HS) of Elastollan composed of diisocyanate residue crystals are spread sporadically throughout soft amorphous segments (SS) formed from a long flexible polyether/ester [25]. In the solid state, the segments tend to segregate. Upon heating, the hard segments become increasing miscible with the soft segments as the crystals formations break down. When the crystal melting temperature of the HS are exceeded the polymer transforms into a completely homogeneous viscous melt. The nature, concentration, and interactions of the HS determine TPU's viscous melting point. Subsequently upon cooling the HS and SS separate again into blocked segments [33]. TPU receives its unique characteristics of strength and flexibility from a combination of HS and SS interactions. Hydrogen bonds form cross-links between adjacent HS to reinforce the polymer and provide rigidity. SS disrupt these interactions to provide TPU with an elastic component [34]. The amount of HS and degree of miscibility within SS dictates a polymer's characteristics, producing a unique DSC curve with multiple peaks and valleys. DSC tests were run on virgin and composite material to fingerprint the polymer and to characterize the effects CNFs had on TPU.

Figure 4.5 displays multiple DSC runs performed on 0%, 11%, and 15% by weight wt.% CNF loadings. As predicted CNFs produced DSC curve shifts indicating distinct affects on TPU. The degree and type of effect CNFs had on the composite will be analyzed in the following paragraphs after a thorough discussion of the virgin TPU curve. Several key features like melting points, and an endothermic decomposition are displayed in the complete virgin DSC curves, Figures 4.16 and 4.17. The virgin TPU's viscous melting point was signified by two endothermic valleys at between 200 – 215 °C, Figure 4.7. These values correspond with BASF's listed processing temperature for TPU, 195-220 °C [25]. A polymer's processing temperature is an accurate indicator of melting point because polymers cannot be injection molded unless they first are converted to homogeneous viscous melts. A recrystallization peak can be seen on the controlled cool down at 113 °C, Figure 4.7.

The two valleys in the DSC curve denote two distinct HS ordering types, Type I and Type II, which lead to a material with multiple melting points. A study performed by Frick and Rochman concluded that the two points are due to disordering of multiple hard segment types through phase separation and phase mixing. The initial point representing HS Type I was influenced by a higher degree of phase mixing where as the later point representing HS Type II was influenced by a higher degree of phase separation [33]. The CNF loaded composites displayed similar melting point peaks, however the peaks were within a smaller temperature range forming a broader, less distinct peak as seen in Figure 4.8. A reasonable explanation for this effect is that CNFs influenced the degree of phase mixing between the HS and are responsible for diminishing the initial peak representing Type I HS. An additive can initiate such an effect as cited by Frick. In his study excess isocyanate increased the miscibility of HS in SS domains, increasing phase mixing. As a result the latter peak which arises from phase separation, Type II diminished. In the present study, the peaks broadened and diminished indicating that CNFs diminish the degree of phase mixing and increased the amorphous content by inhibiting crystallization. Figure 4.8 displays a close up of TPU's melting point region and shows melting peaks diminishing.

Beyond the melting points the polymer underwent endothermic and exothermic decompositions as shown in Figure 4.6. The endothermic decomposition occurred between 278 and 350 °C and corresponded with the first decomposition with the first decomposition segment of the TGA curve. This decomposition refers to the degradation of TPU's amorphous segment. In Figure 4.5 there is a temperature shift consistent with CNF loading. Increased CNF loadings led to endothermic peaks shifting to higher temperatures. This is attributed to CNFs accounting for the available intermolecular spacing and pinning down the polymer chains, which inhibits lattice vibration. Inhibited lattice vibration retarded the polymer to decompositions to higher temperatures, which was consistent with the TGA analysis.

The 11 and 15 wt.% CNF-TPU samples displayed smaller endothermic peaks indicating lower energy use, which was attributed to two factors. First, the 11 and 15 wt.% CNF-TPU samples have less polymer per sample to degrade, but second, CNFs are good conductors of thermal energy. Adding a good conductor of thermal energy to a normally low thermally conductive material increases the thermal conductivity coefficient, and there by decreases the amount of energy required to heat a sample. The sample's increased thermal conductivity coefficient allowed less energy to be used in heating the sample, see the Heat Transfer section for a more detail explanation. By integrating the area above the endothermic valley it was determined that virgin TPU consumed 253.8 J/g during decomposition while 11 and 15 wt.% CNF used 191.6 and 174.8 J/g respectively, Figures 4.19 and 4.20. However, further examination determined the amount of joules per gram of polymer consumed during decomposition by dividing the received decomposition values by the percentage of polymer in the composite. The quotient revealed that 11 and 15 wt.% CNF composites actually accounted for 215.28 and 205.65 J/g respectively. These values were lower than the 253.8 J/g used in decomposing the virgin TPU. Therefore CNFs positively impacted the uptake of heat energy in TPU composites.

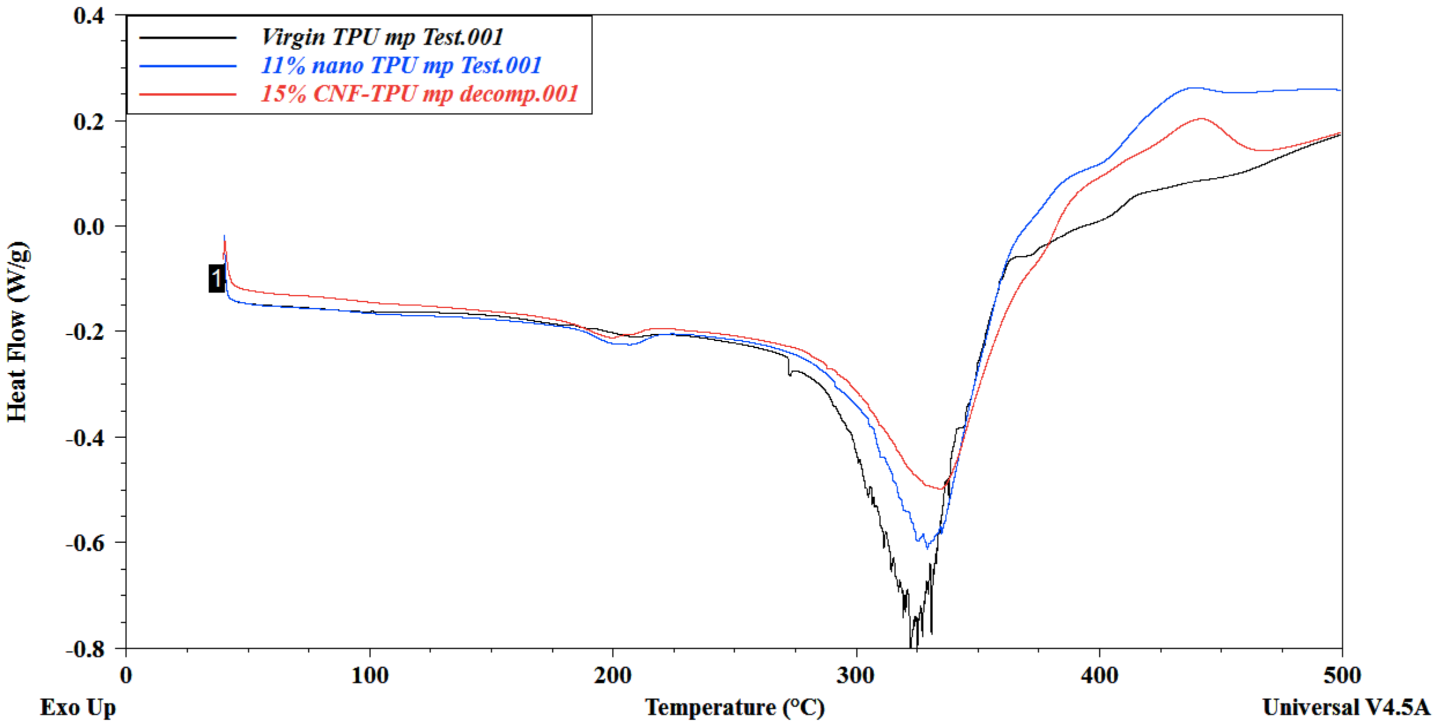

Figure 4.5: 0, 11, and 15 wt.% CNF composite DSC curves

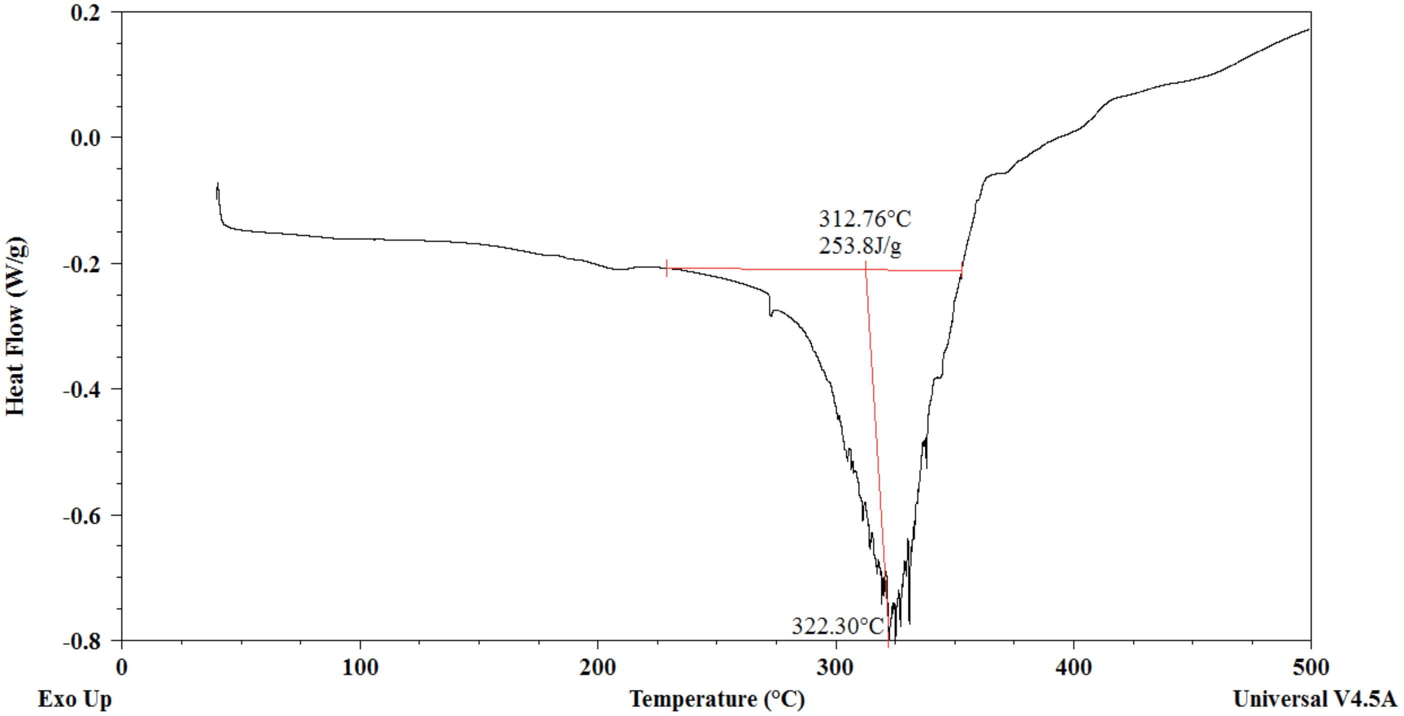

Figure 4.6: Virgin DSC curve

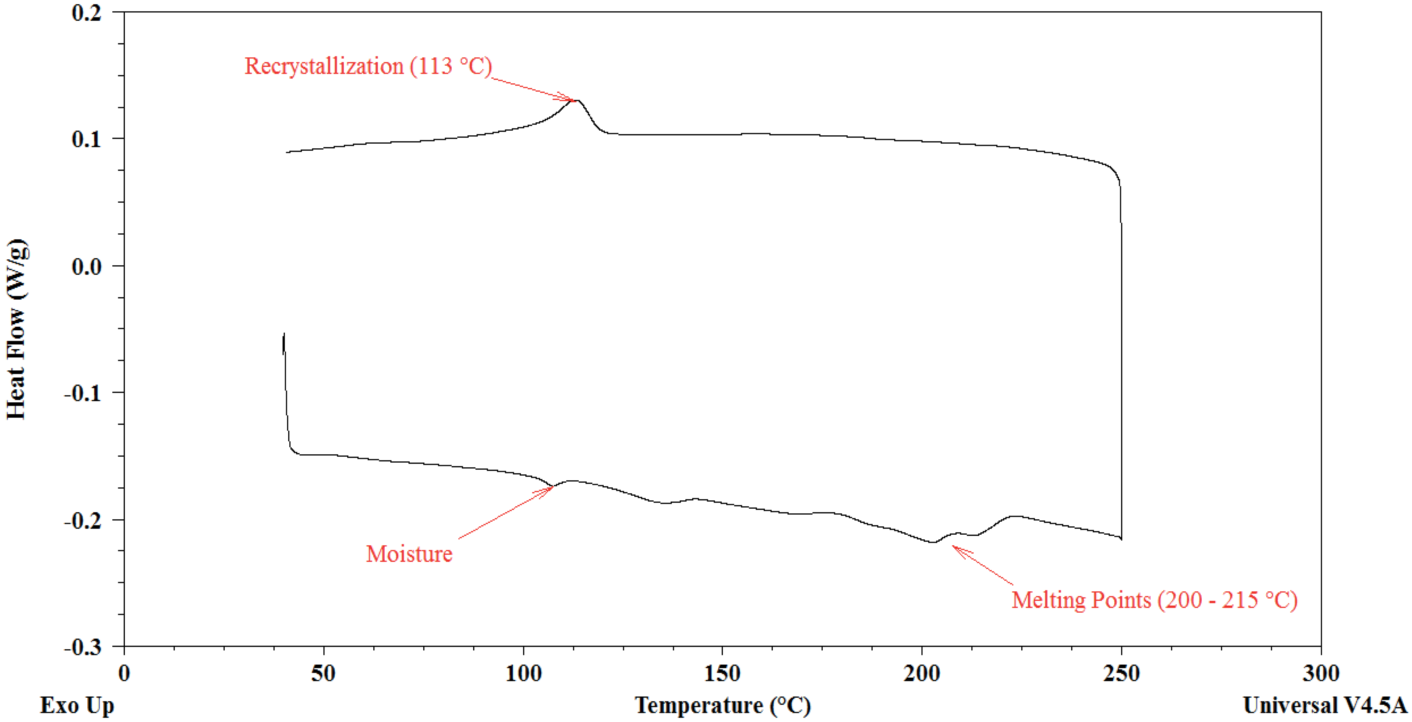

Figure 4.7: Virgin TPU DSC curve with melting points, and recrystallization

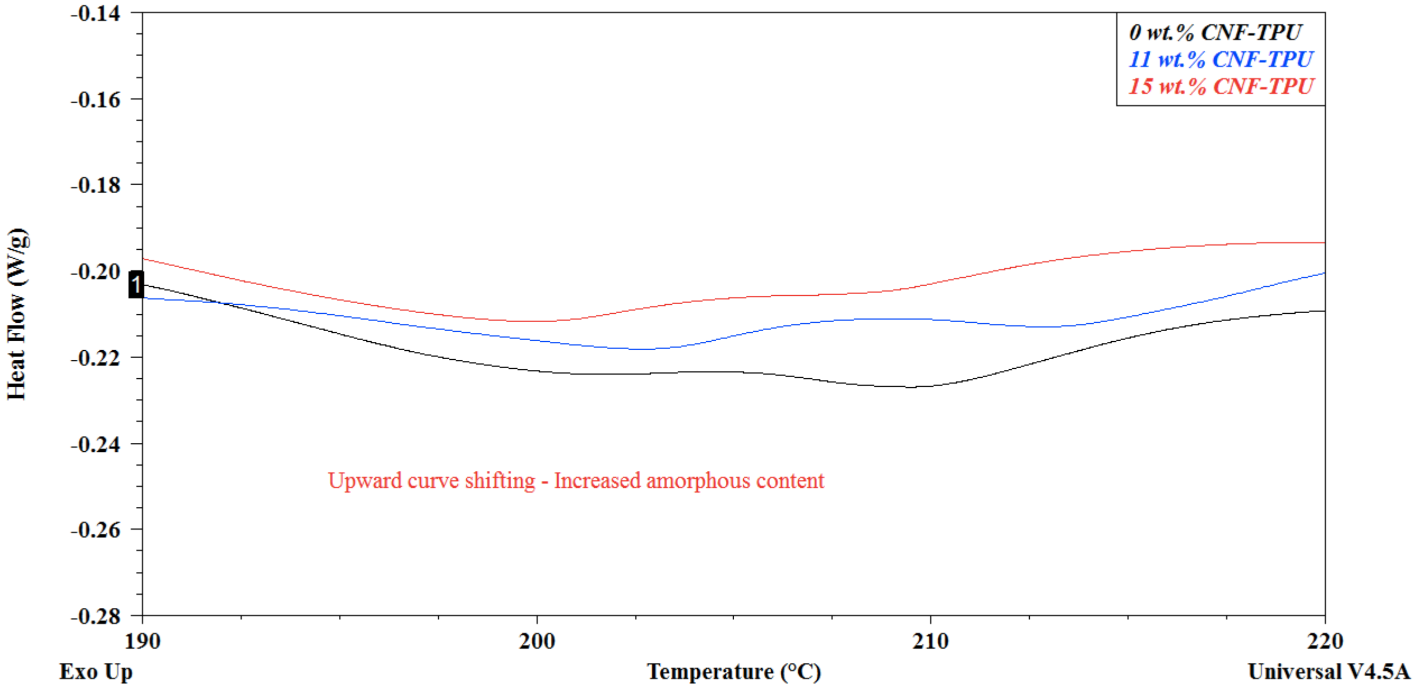

Figure 4.8: Amorphous region increase around at melting temperatures

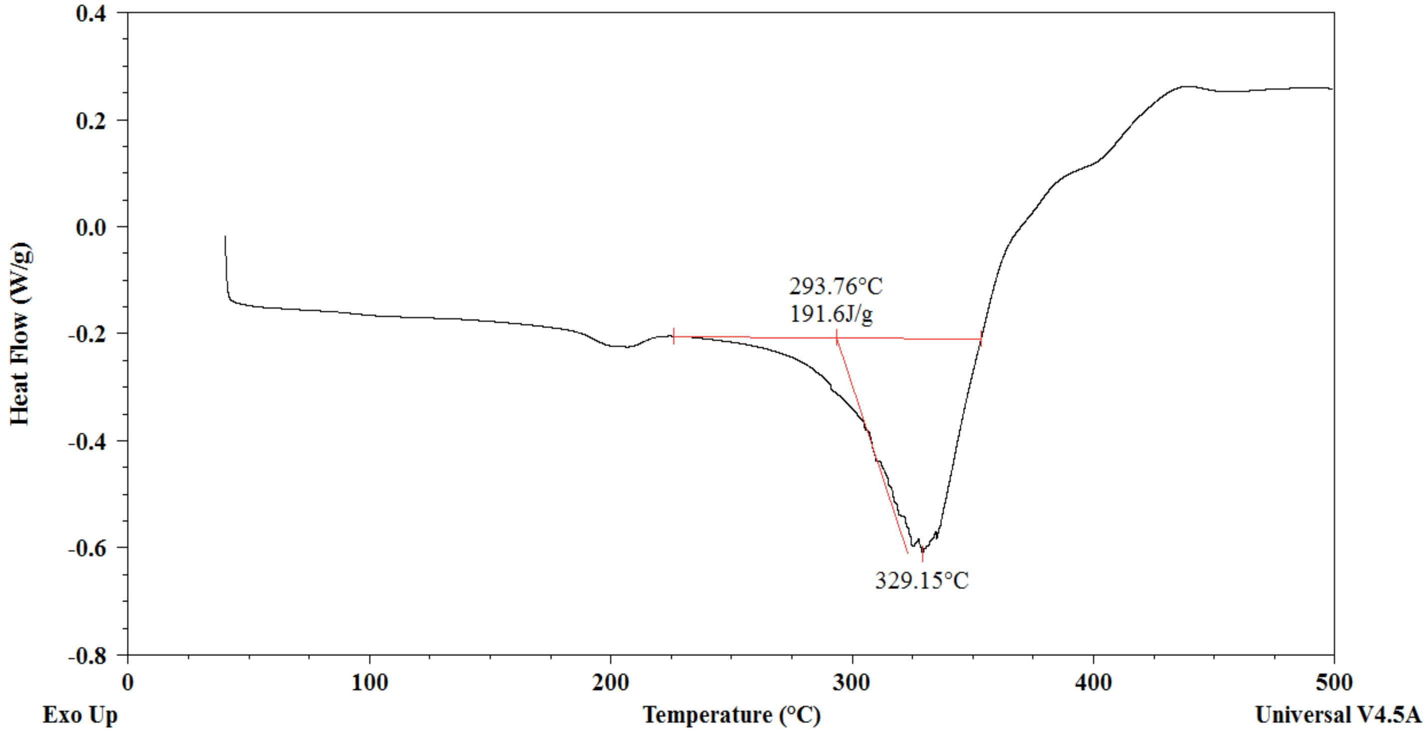

Figure 4.9: 11 wt.% CNF-TPU endothermic peak

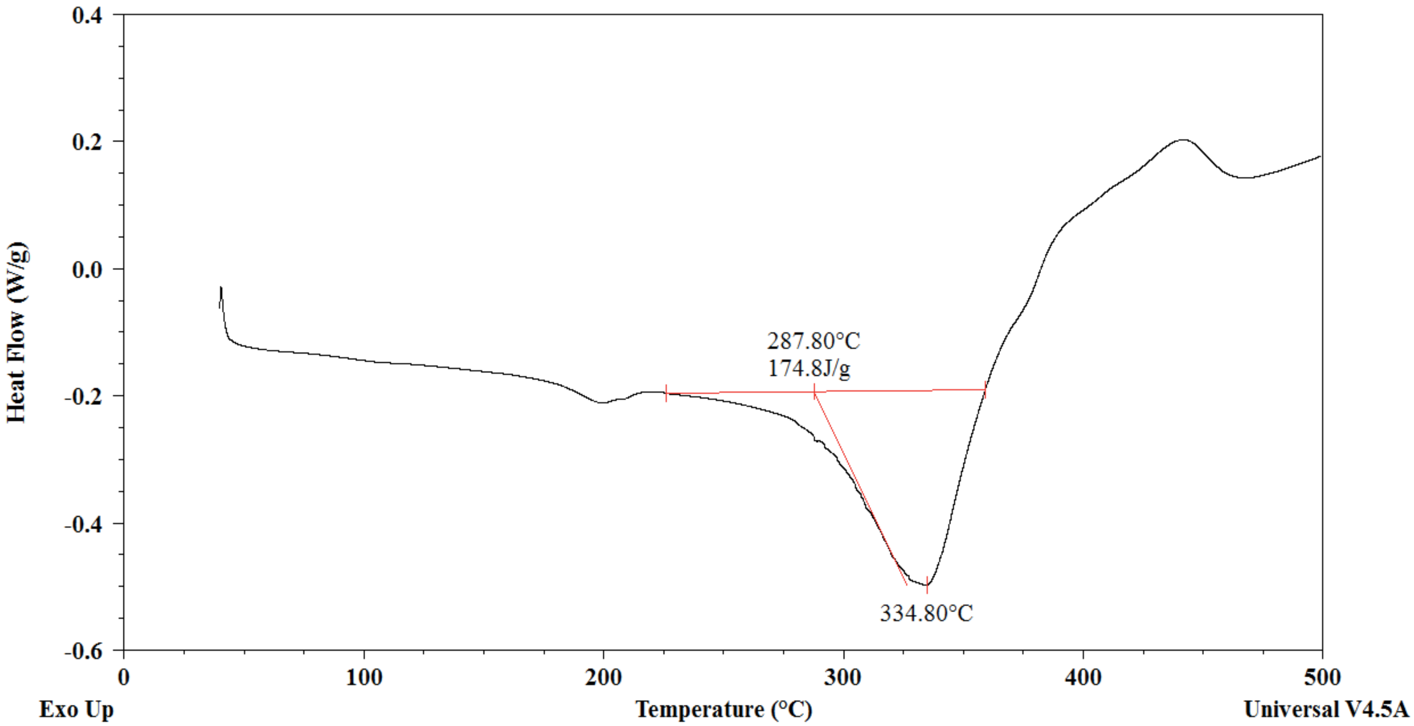

Figure 4.10: 15 wt.% CNF-TPU endothermic peak

4.3 Thermal Conductivity Testing

CNFs display promising characteristics to enhance heat transfer coefficients and facilitate heat dissipation in composite materials used in high heat applications. Individually CNFs, and CNT display superb thermal conductivity and this characteristic prompted an examination to determine their effect on the heat transfer coefficient of TPU. Studies have shown CNFs to uniquely contain negative coefficients of thermal expansion, high aspect ratios, and exceptional thermal conductivity, up to 1950 W/m·K in some cases [35]. Polymers undergo high expansion under thermal loading, therefore when designing a composite material it is important to take into account the thermal expansion coefficient of the additive. The extremely high surface area to volume aspect ratio that CNFs embody allows for a high degree of interfacial contact between

CNFs and a polymer. Good interfacial contact is one element in permitting heat transfer from the polymer to the composite additive. This dissipation of heat increases thermal stability and decreases the thermal expansion a polymer part may experience. Many factors determine the thermal conductivity of a composite. Of primary importance are the conductivity, orientation, dispersion, filler aspect ratio, and interfacial thermal resistance of the additive. Orientation of CNFs in the desired direction of heat transfer enhances heat dissipation in a composite significantly [36]. It is interesting to note that there is no percolation threshold for thermal conductivity. Thermal conductivity continues to increase with the addition of CNFs [6].

For the mixing performed in the Haake PolyLab system orientation of fibers was not controlled, however composite mixes exemplified enhanced thermal conductivity when compared to unmodified specimens. In the thermal conductivity test, transfer molded pucks were measured to determine the depth and area as shown in columns 6 and 7 of Table 2 respectively. A small OMEGALUX flexible round heater was attached to a power supply and a thermocouple placed on one side, Figure 4.11. A puck was placed adjacent to the thermal couple and another thermal couple was place on the other side of the puck, Figure 4.12. The thermal couples were both attached to an Omega Supermeter^{TM} multi meter and temperature differences across the pucks were measured. The heater, puck, and thermal couples were wrapped in fiberglass insulation and clamped down to eliminate any heat loss through the sides. The final experimental set up is shown in Figure 4.13. Temperature readings were taken after steady state heat flow was achieved in the system. Steady state was determined when the temperature difference between both sides of the puck remained constant for at least 10 minutes. When this occurred the test was ended and thermal conductivity values were calculated.

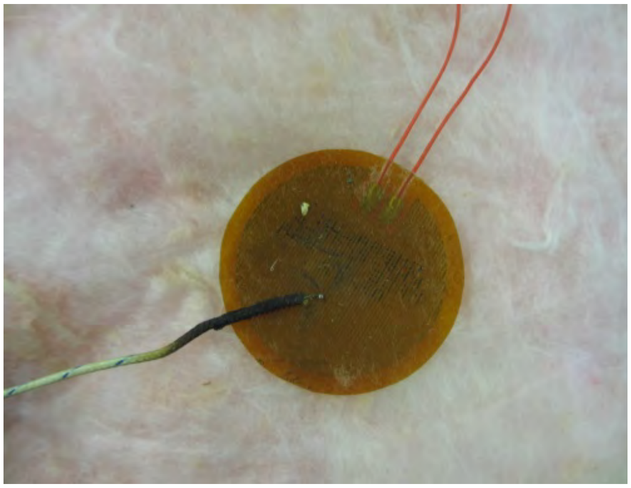
Figure 4.11: Heater with Thermocouple

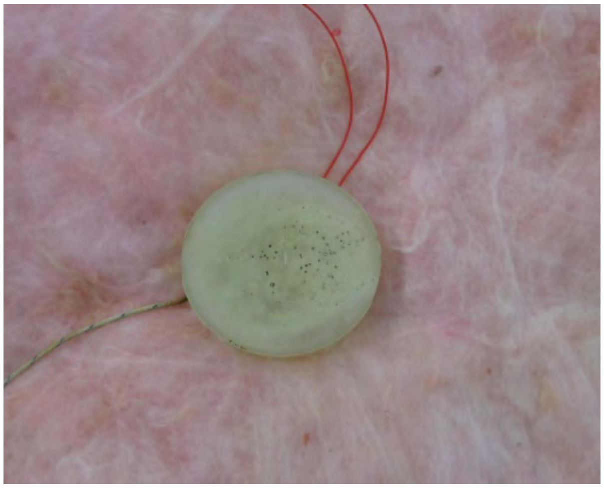
Figure 4.12: Virgin puck

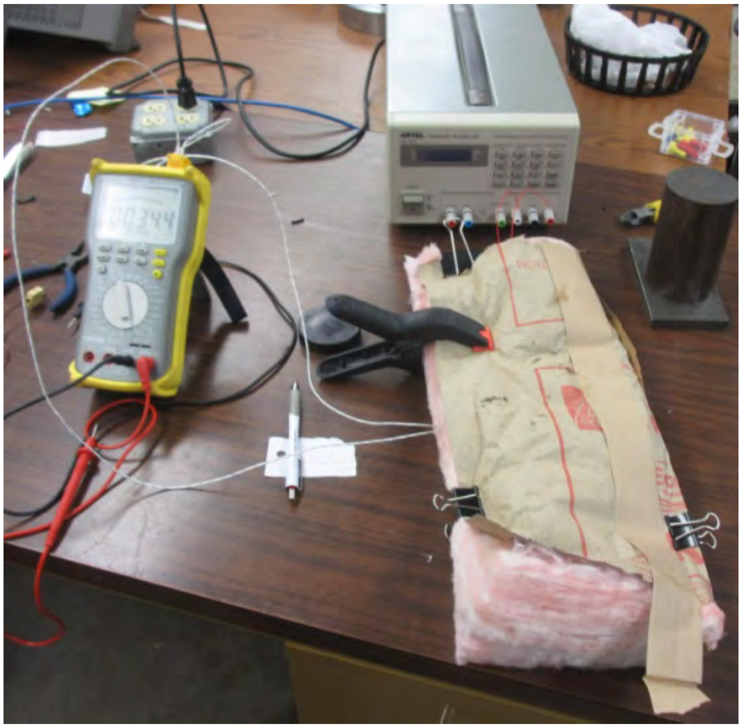
Figure 4.13: Complete set up

The following equations were used to determine the thermal conductivity coefficient of the pucks:

$$Q = Voltage \times Current = VI \tag{6}$$

$$Q = kA\frac{dT}{dX} \tag{7}$$

Equation (7) manipulated to solve for the thermal conductivity coefficient, k:

$$k = \frac{Q\ dx}{A\ dT} \tag{8}$$

The power input, Q, respective temperatures, T1 and T2, temperature difference, dT, puck depth, dx, surface area, A, and thermal conductivity coefficient, k are all listed in Table 2. The test results for virgin TPU were consistent with the listed values of 0.19 – 0.25 W/m·k [25] for Elastollan 1195a. The measured value of 0.205 W/m·K indicates that the test set-up was adequately limiting lateral heat losses. From Table 2, it is clear that CNFs greatly enhanced the thermal heat transfer coefficient of the composite material. The 9 wt.% CNF loading increased the coefficient by 48.21%, 11 wt.% by 62.09%, and 15 wt.% by 146.94 wt.%. The trend of increasing heat transfer coefficients as function of CNF loading was expected since a percolation threshold cannot be reached as previously stated. Figure 4.14 is a graphical representation of the heat transfer coefficient, k, values. The linear increase in value follows the law of mixing.

Table 4.1 – Thermal Conductivity Values

% CNF	Q [W]	T1 [°C]	T2 [°C]	dT [K]	dx [m]	A [m^2]	K [W/m·K]
Virgin	2.4	111.3	60.4	50.9	0.01387	0.00318	0.20566
9	2.4	77.7	44.7	33	0.01316	0.00314	0.30481
11	2.4	77.1	31.6	31.6	0.01387	0.00316	0.33336
13	2.4	93	70	23	0.01369	0.00323	0.44502
15	2.4	77.6	56.2	21.4	0.01431	0.00316	0.50787

Although the values received from thermal testing showed that CNFs made a sizeable impact on thermal conductivity, it was significantly less than what was predicted based on how CNFs affected electrical conductivity. CNFs did not increase the thermal conductivity as much as electrical conductivity because heat is transferred primarily through phonons, lattice vibration waves causing atomic vibrations. Phonons are more likely to travel through the matrix of a CNF/polymer composite because polymer molecules can vibrate under excitation. This is why when comparing the thermal conductivity ($k_{\text{nanotube}}/k_{\text{polymer}}$) and electrical conductivity ($\sigma_{\text{nanotube}}/\sigma_{\text{polymer}}$) there is stark difference between them ~10^4 and 10^{15}-10^{19} respectively [37]. The difference is primary attributed to the nature of phonons, which preferring to transfer through a vibrating medium and the interfacial resistance between CNFs and polymers.

Huxtable et al. stated that constraints on transmission of thermal energy across the interfaces of CNFs and CNFs and the polymer matrix are caused after a high-frequency phonon becomes coupled with another phonon and transform to a lower frequency. This reaction has to take place in order for any exchange with the surrounding media [37]. This explains why the CNF-TPU composite exhibited low thermal conductivity even though individual fibers exhibit high thermal conductivity. However, studies have shown that when functionalized CNFs covalently bond to a polymer matrix the thermal interfacial resistance is drastically decreased 38. Reducing the interfacial resistance greatly increases the thermal conductivity. Nonetheless the results from the thermal review revealed that the addition of CNFs to TPU does increase thermal conductivity even if it pales in comparison to the effect CNFs have on electrical conductivity.

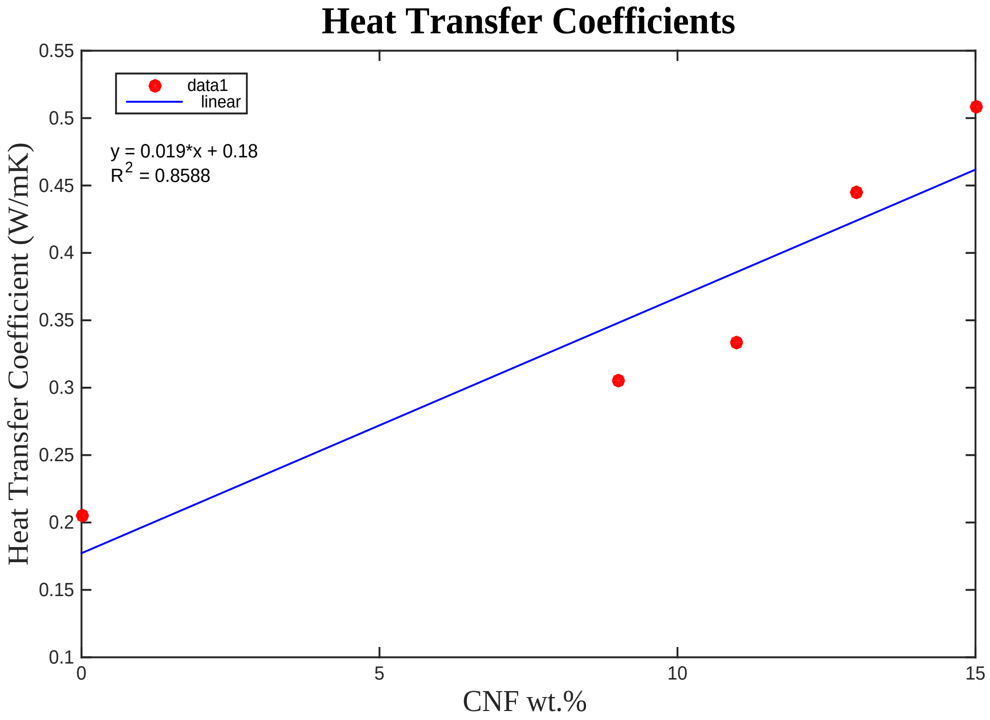

Figure 4.14: Heat Transfer Coefficient vs. CNF wt.%

4.4 Electrical Conductivity Testing

Pyrograf III CNFs are functionalized to be electrically conductive, making them attractive additives for composites. Because polymers generally lack electrical conductivity this limits their uses in some areas. An electrically conductive polymer would open a new realm of possible applications. The conductivities of polymers are nearly zero while a CNF will range from 10^{15} to 10^{19} making them the ideal additive [37]. CNF-TPU composite materials were tested under a constant voltage at different loads to determine the necessary percentage of CNF to reduce resistivity and to study how load influenced conductivity. Following the parameters outlined in chapter 3, a test was set up to measure resistivity on an MTS machine to compress a molded puck while an electrical potential of 22 volts was applied through the compressed puck.

The results clearly show that TPU, which is naturally nonconductive, can be enhanced with CNFs to become a conductor. CNFs allow electrical current to flow via two mechanisms, direct contact and tunneling [6]. Direct contact takes place when adjacent CNFs touch each other forming a corridor for electron travel. The current flows through the material solely by these pathways. Direct contact is usually the predominant electron transport mechanism in composites when CNFs are not properly distributed throughout the polymer matrix due to inadequate mixing. Although direct contact can provide conductivity in a composite at low CNF percentages it is not always the preferred method to enhancing polymers. Scaling up a direct contact composite is difficult because maintaining product uniformity becomes nearly impossible. For this reason tunneling electrical current is preferred over direct contact even though it requires higher CNF percent loadings driving costs up. In tunneling the CNFs are within 10 nm of each other. At this distance electrons have the ability to jump from adjacent nanofiber to nanofiber even though the polymer may completely surrounds each individual fiber

[6]. When CNFs are independently spread out from each other mechanical properties are optimized because there are fewer brittle concentrations of agglomerates.

The present study demanded producing a composite with optimum mechanical and electrical properties therefore it was necessary to determine if conductivity was a result of tunneling or direct contact. To accomplish this 11 wt.% CNF-TPU batches were produced at 2.5, 5, and 10 minute mixing times. Their resistivity was measured and the results revealed that lower mixing times translated to lower resistivity, Figure 4.15. Resistivity was calculated using the following equations

$$R = \frac{V}{I} \tag{9}$$

$$\rho_v = \frac{RA}{t} \tag{10}$$

where R, V, I, A, t, and ρ_v represent resistance, voltage, current, area, thickness, and resistivity respectively. Since increased mixing time produced higher resistivity it was concluded that much of the conductivity at lower mixing times was due to direct contact instead of tunneling. Samples were examined under an SEM microscope and lower mixing time composites contained a higher degree of CNF agglomerates, substantiating the initial interpretation of results. Another method of determining the dominant current pathway is through examining the current-voltage relationship. A linear current-voltage relationship indicates direct contact between fibers whereas a power law current-voltage relationship will be present when tunneling is the dominant mechanism of current flow [39].

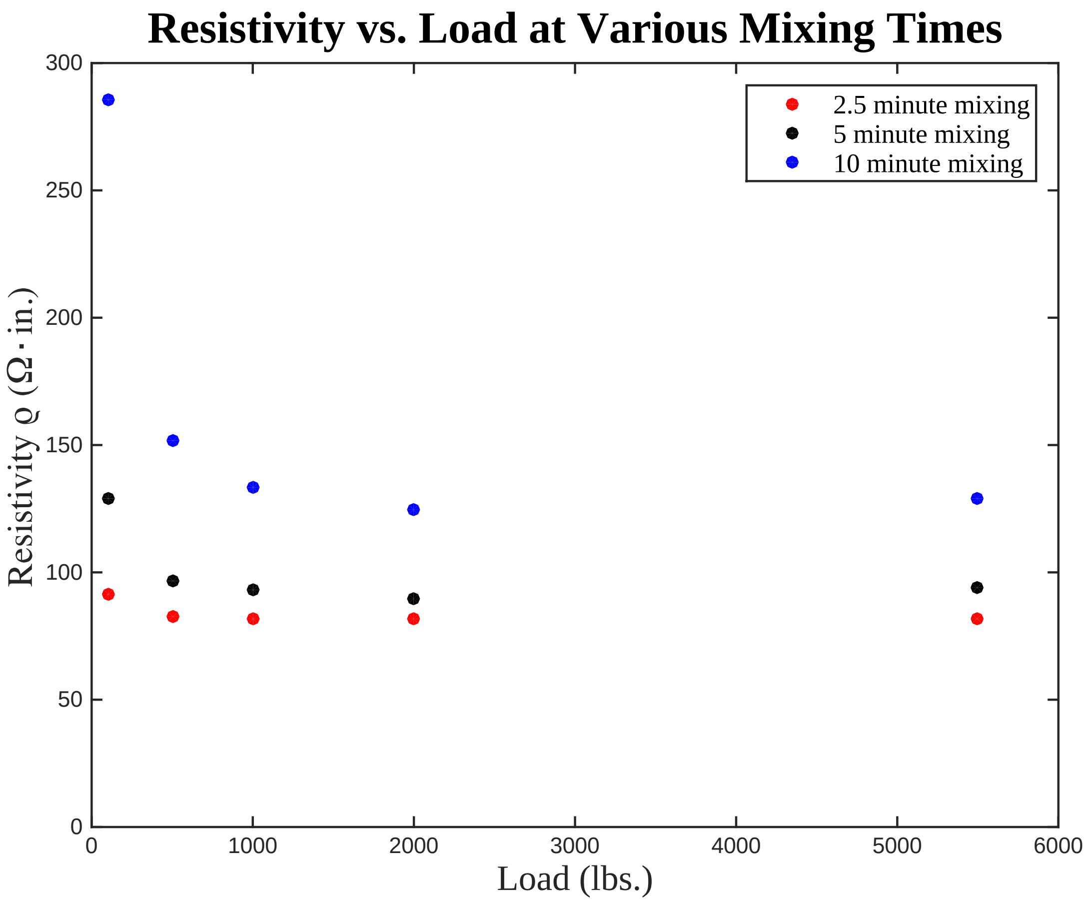

Figure 4.15: Resistivity vs. mixing time for 11 wt.% CNF-TPU samples

Finding the correct mixing time to have sufficient distribution and dispersion took priority over other factors like percolation threshold and current potentials. Figure 4.16 presents different dispersion and distribution scenarios. Pictures (a) and (b) both show clumping and bad dispersion of CNFs into the polymer matrix. Although there is good distribution in picture (b) both structures yield no conductivity. Pictures (c) and (d) show situations of electrical conduction. Picture (c) is an example of electrical conduction by means of direct contact where as picture (d) presents a tunneling situation. As displayed picture (d) has good distribution and dispersion compared to picture (c) which only has good dispersion. Note that the cartoon images are illustrations of 2-dimentional systems. Actual polymer composite matrixes are 3-dimentional networks composed of CNFs evenly distributed and dispersed pointed in all directions from each other. The preferred direction for CNFs to be fashioned is along the flow of current. When CNFs are directed in this manner the potential current flow is at a maximum. Before conductivity can be optimized by CNF manipulation the percolation threshold must be met.

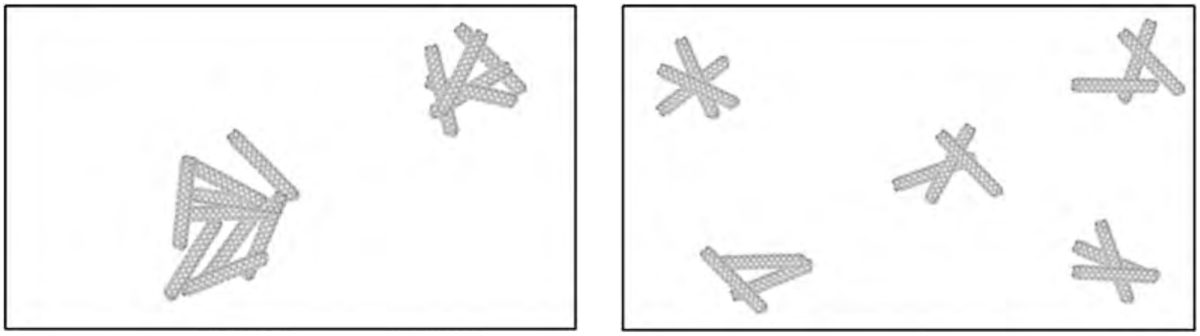

a. No Conductivity: Bad dispersion & distribution

b. No Conductivity: Bad dispersion, good distribution

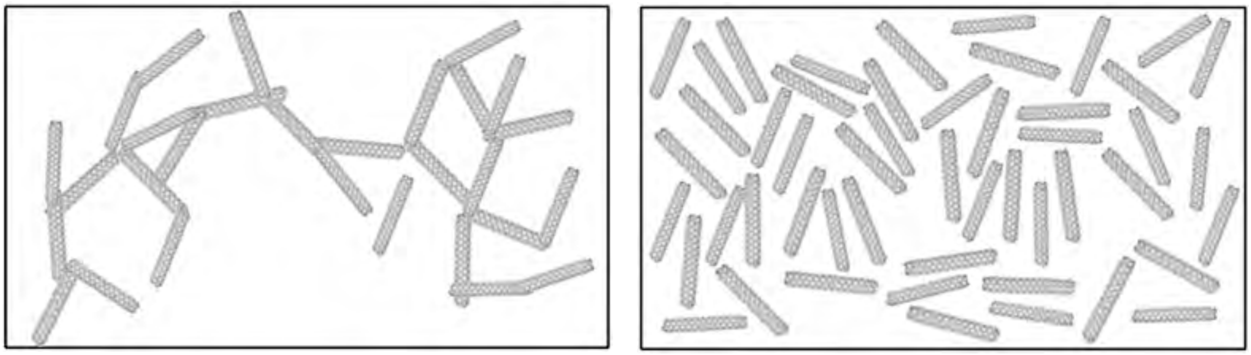

c. Direct Contact Conductivity: Good dispersion, bad distribution

d. Tunneling Conductivity: Good dispersion & distribution

Figure 4.16: Distribution and dispersion

The percolation threshold is the critical concentration point at which a composite compound transforms from performing as an insulator or semiconductor into a conductor. At the percolation point there is a drastic decrease in resistivity because a CNF network has been formed inside the polymer composite. Doping the composite with more additive after the percolation threshold will not result in significant further increase in conductivity. If a noticeable increase does occur however, it can be attributed to a direct contact CNF network instead of a tunneling network [6]. Since tunneling was the preferred method of conductivity proper compounding methods were developed before any conductivity tests were preformed. A study of the effects of resistivity vs. load was performed for 7, 9, 11, 13, and 15 wt.% CNF-TPU composites. The composite resistivities are displayed in Figure 4.17.

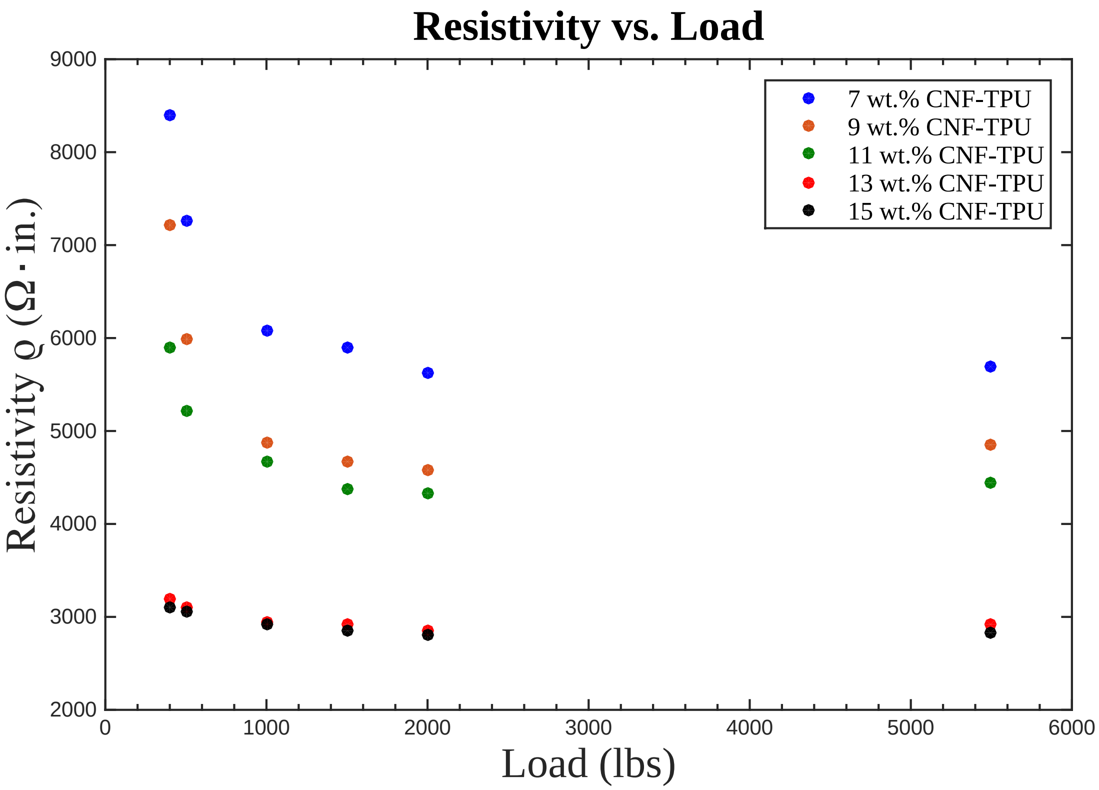

Figure 4.17: Conductivity vs. load plot

From the plot in Figure 4.17 a noticeable decrease in resistivity can be seen between 11 and 13 wt.% CNF loadings. This gap represents the percolation threshold in the present study. The fact that 15 wt.% CNF-TPU did not significantly increase conductivity increases confidence in the existence of a percolation threshold between 11 and 13 wt.%.

Properly dispersed CNFs in composites alter mechanical properties, thus opening new possibilities for applications in high load environments. Therefore tests were preformed at high loads to determine how load affected conductivity. Figure 4.17 shows that load decreased resistivity. Every sample experienced a decrease in resistivity between 0 and 1,000 PSI of applied stress. This was attributed to the tested polymer pucks becoming denser under compression, fibers being pushed closer together opening new tunneling pathways, and surface resistance reduced. Above 1,000 PSI there was only a slight decrease in resistivity and at extremely high loads like 5,500 PSI there was even a small increase. The resistivity increase was attributed to the polymer relaxing under pressure and CNFs reorienting to lower energy configurations that were more perpendicular to the applied force. Over all the test results indicate that CNF doped TPU composites can be used in electrical applications to carry current and will decrease in resistivity when an external load is applied.

4.5 Hardness Durometer Testing

Durometer testing was performed on an array of sample composites containing various, incrementally increasing CNF weight percent. The study was performed on molded pucks to characterize the effect of CNFs on overall material hardness. Each test was performed on a Shore Durometer Type D from Instrument & MFG following the ASTM D2240 standard. To achieve reliable reading five different test points were selected on each puck, which are displayed as white spots in Figure 4.18. The results were compiled with averages and standard deviations calculated as displayed in Table 1. The BASF product sheet listed the virgin material hardness as 95A [25]. This value translates to 45D on hard shore D scale. Testing gave an average Shore D hardness of 46.2. This reading was less than 5% from the material specifications at a difference of 2.63%, which indicated accuracy and fidelity for future tests. As predicted, sample hardness increased with increased CNF content along the Shore D hardness scale. The proportional and steady increase of the hardness with increasing CNF content indicated there was an even distribution of CNFs in the polymer. Low scatter in the result indicated by the small calculated standard deviations also indicated that fibers were well dispersed. Figure 4.19 displays a graphical representation of the average durometer recordings.

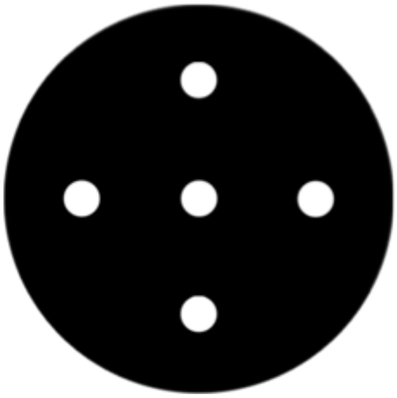

Figure 4.18: Test point on molded pucks

Table 4.2: Durometer Hardness Data [Shore-D]

CNF wt. %	**0**	**7**	**9**	**11**	**13**	**15**
Average	46.2	49.2	51.6	53.0	54.0	54.2
Standard Deviation	0.83	1.48	1.52	1.23	1.41	2.17

*Average of 15 trials

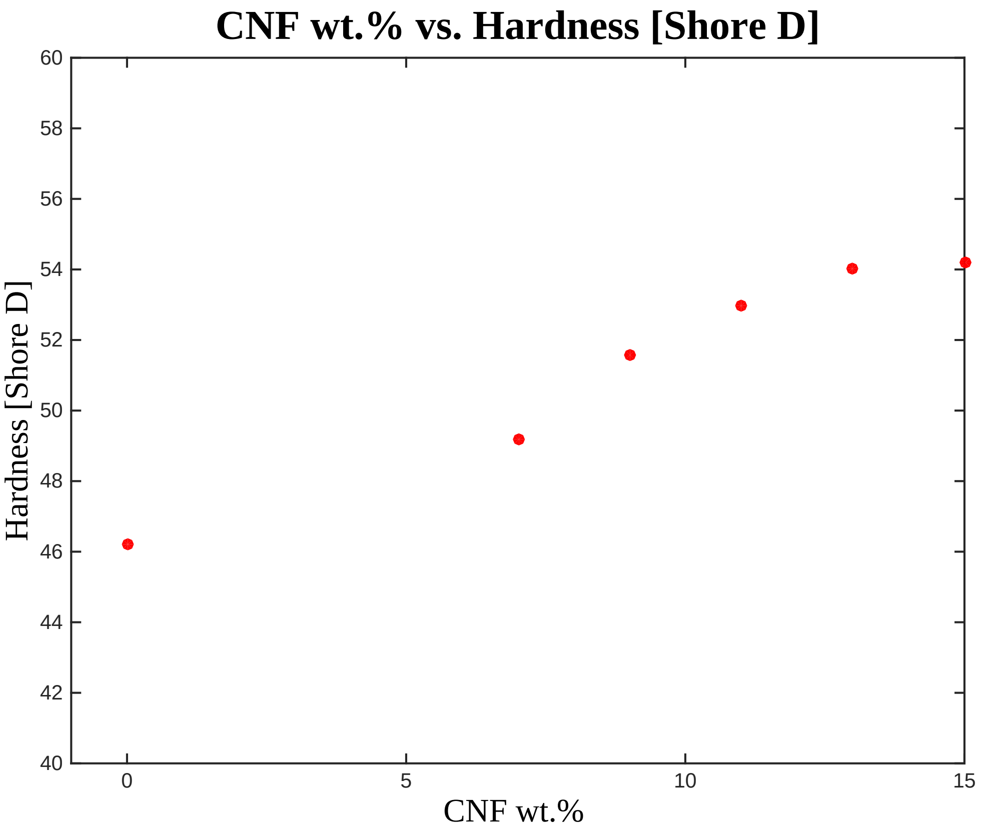

Figure 4.19: Plot of average Hardness vs. CNF wt. %

4.6 Tensile Stress/Strain Testing

Tensile tests bars were molded to test the stress/strain properties of the composite and virgin material on an MTS machine. Comparisons were made between virgin and various CNF composites to determine how CNFs affected material properties like Young’s modulus, strain to failure, yield strength, and ultimate tensile strength. In general additives tend to increase one property while diminishing another. This proved to be true in the present study. As displayed in Figure 4.20 the Young’s modulus increased in proportion with CNF concentration while strain to failure decreased in composite materials. These results corresponded with the durometer testing, which showed a steady increase in hardness as CNF concentration increased. The degree to which CNFs performed the described tasks depended on the weight percent, CNF aspect ratio, dispersion, distribution, and polymer-CNF interfacial adhesion [40]. Increasing the CNF aspect ratio, dispersion, distribution, and polymer-CNF interfacial adhesion tends to enhance tensile properties. In an ideal system CNFs carry the stress in a composite polymer while not reducing matrix elongation. At lower fiber concentrations it appears that CNFs accomplish this and but, as CNF loading increases, strain to failure was affected also.

The strain to failure decreased linearly as CNF content increased. The virgin TPU sample strained just over 6% while the 15 wt.% CNF-TPU sample elongated slightly more than 2%. The cause for such a drastic decrease in percent strain was attributed to the presence of CNF agglomerates. Although a considerable amount of work was done to optimize dispersion and distribution, inevitably as CNF concentrations increased the probability of agglomerates forming also rose. Completely eliminating CNF agglomerates at concentrations higher than 5% was nearly impossible. A study by Barick and Triphathy found a similar effect. They concluded that composites samples with CNF content above 7 wt.% exhibited a pronounced decrease in strain to failure regardless of the level of mixing [41]. Agglomerates acted to produce stress concentrations in the matrix as well as reduced resin ductility due to resin starvation and constrained deformation. These concentration produced cracks that were the initial points of fracture. Outside of agglomerates, CNF composites fracture due to deterioration of interfacial bonding between the polymer and the CNF. This deterioration leads to tearing and crack development [41].

CNFs restrict polymer mobility limiting ductility and plastic deformation. According to Figure 4.20 the virgin sample entered plastic deformation at a lower stress than all the CNF composites. The virgin sample also sustained plastic deformation to a higher strain level before failing. The CNF composites were able to maintain elastic deformation longer but could not plastically deform to the same degree as the virgin sample. These observations support the previous claims that CNFs initially carry the applied stress and limit polymer ductility. If composite samples had plastically deformed as much as pure TPU samples then crack development due to polymer-CNF interfacial separation would not have been a major failure mechanism. Since more elastic deformation was displayed in the CNF composite stress strain curves it was concluded that CNFs acted to carry the stress applied to the tensile bar by reinforcing it. A composite material enters plastic deformation when the applied stress has overcome the intermolecular bonds and begins to break down the polymer network. Table 4.4 displays the modulus, yield strength, limit of elastic strain, strain to failure, and work to failure for 0, 5 11, and 15 wt.% CNF-TPU specimens. Figures 4.21 and 4.22 display the strain to failure and elastic strain vs. CNF content respectively.

Table 4.3: Material Tensile Properties

CNF wt.%	**0**	**5**	**11**	**15**
Modulus (MPa)	28.12	85.36	115.58	116.26
Yield Strength (MPa)	6	10	13	15
Limit of Elastic Strain (mm/mm)	0.2	0.18	0.15	0.13
Strain to Failure (mm/mm)	6.13	5.15	4.04	2.01
Work to Failure (N·mm)	35,764.52	17,219.47	22,867.29	9,175.11

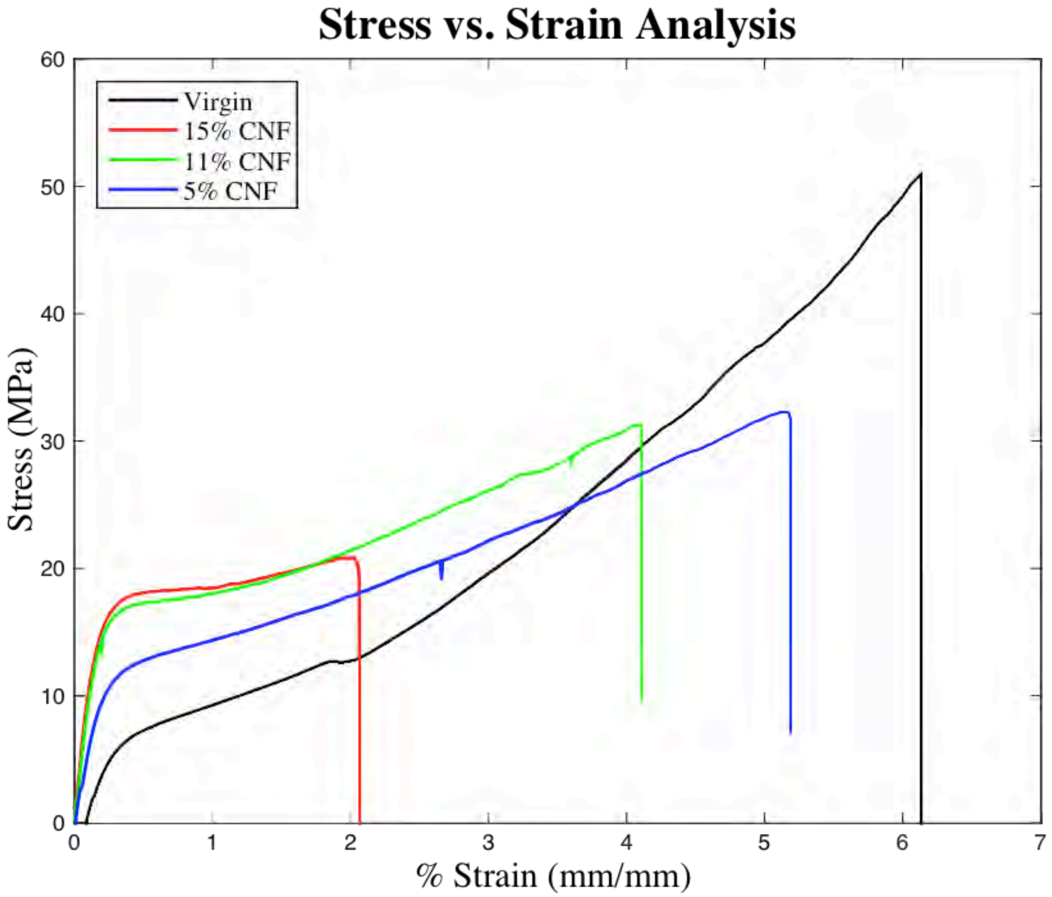

Figure 4.20: Stress/strain curve of virgin and composite material

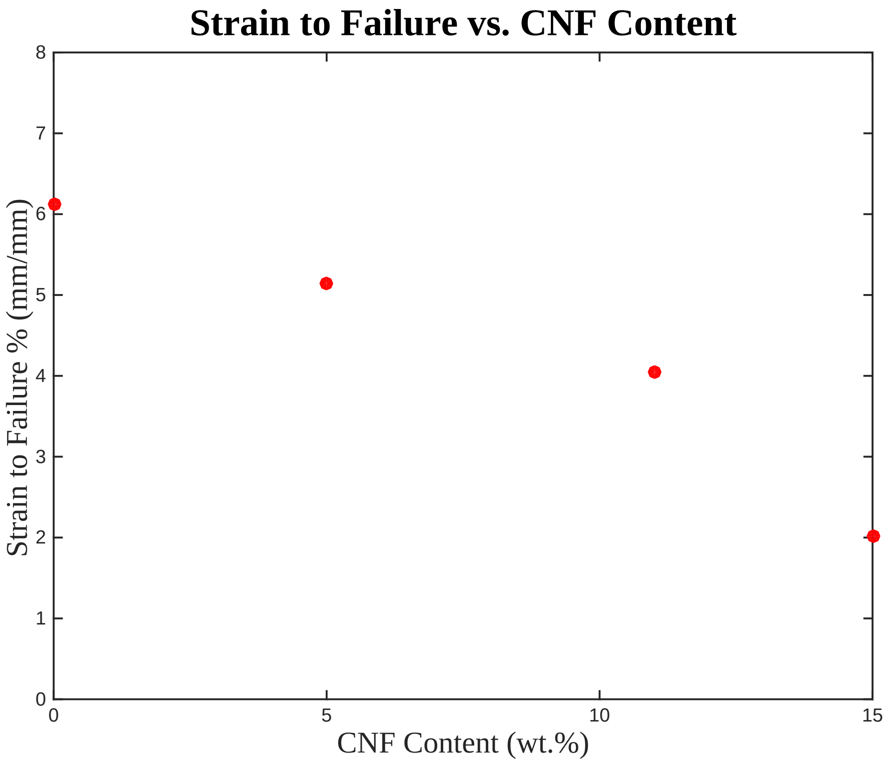

Figure 4.21: Strain to failure vs. CNF content in composite samples

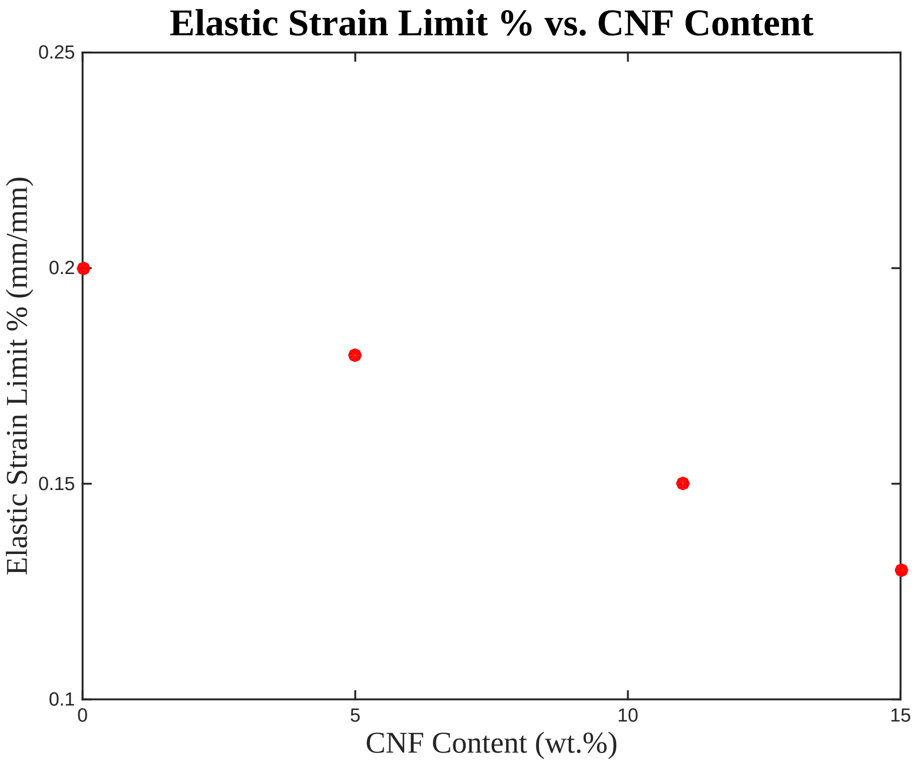

Figure 4.22: Elastic strain limit % vs. CNF content in composite samples

4.7 Abrasion Testing

Abrasion is the wear experienced by displacement or rearrangement of a softer material due to rubbing or scuffing against hard sharp particles. Elastomers are known to be extremely wear resistant and polyurethanes are the most wear resistant of this family. They are commonly utilized in high wear situations including conveyor belts, footwear, wheels on trucks, etc. Abrasive wear is common in industry because complex mechanisms are often composed of multiple components made out of different materials. Composite materials are becoming more prevalent in industry increasing the need to understand their abrasive characteristics. Abrasion is especially important because the nature of a material under abrasion; is a reflection of multiple properties such as low strain dynamic, high strain tensile, compression, and thermal response [42]. CNF-TPU composites will be extensively used in the future because of their compatibility with each other; therefore an abrasion test, in particular was deemed a critical part of this study.

The tests were performed on a Taber 5150 surface abrader. ASTM 1044 protocol was followed to perform the test on three separate specimens compression molded from a custom fabricated mold. The specimens were composed of an unmodified Ellastolan 1195a TPU, a 15 wt.% CNF-TPU composite, and a higher molecular weight TPU made from grinding down a railway steering pad and then compression molding it. Standard H-18 abrasion wheels were used on all specimens. Instead of studying how much wear accumulated on a test specimen during a set number of cycles; trends were studied by measuring each sample’s weight after every 10,000 cycles up to 50,000 cycles. This allowed the wear response to be plotted and the response subjected to a linear regression analysis in MatLab. The linear fittings provided line slopes allowing future specimen weights to be predicted based on previous trends.

In Figure 4.23 trends are displayed with linear fittings applied. The graph indicates the weight loss per 10,000 cycles. Because trends were desired the slope was the most important feature extrapolated from the graph. Achieving a consistent starting weight was difficult because each compression-molded specimen exhibited a unique amount of flash during molding, but after the samples were manipulated to have the same initial starting weight tests were preformed. The linear best-fit lines were added to provide slopes and R^2 values.

The virgin TPU specimen displayed results that were slightly better than those found on BASF's product sheet. BASF's material data sheet for 1195a TPU had 30 mg of wear loss per 1000 cycles [25]. This translates to 1.5 grams lost for 50,000 cycles in a perfect environment. Our tests however, displayed a total loss of 0.431 grams after 50,000 cycles. In Figure 4.23 the 15% CNF-TPU specimen clearly experienced more abrasion compared to the other two pure TPU specimens. In total the 15% CNF-TPU composite experienced a loss of 1.607 grams due to abrasion compared to 0.431 and 0.202 grams lost from the virgin TPU and rail steering pad material respectively. In total the weight loss for the 15% CNF-TPU composite was only 1.176 grams more than the virgin TPU. This loss can be explained by a disruption of the hydrogen bond interaction between the rigid segments of TPU. The hydrogen bonding between the rigid segments of TPU react with each other to form strong bonds with high cohesive energy [42]. These bonds in particular are responsible for the good abrasion resistance. Extensive inter-strand hydrogen bonding is evident under infrared spectroscopy between the –NH– (proton donor) and C=O (acceptor) functional groups of hard segments [44]. This leads to enhanced abrasion resistance in TPU polymers with increased hard segmentation [42]. A conclusion can be made that CNFs disrupt this intermolecular bonding when they are inserted in the matrix. The hydrogen bonding, which provided strong interactions between polymer chains was replaced with weaker Van der Waals dipole – dipole forces. The Van der Waals interactions between the CNFs and the polymer chains lessen the number of direct interactions between polymer chains. As Van der Waals dipole-dipole reactions increased, hydrogen bonding between polymer chains decreased with a corresponding reduction in the abrasion resistance of the material.

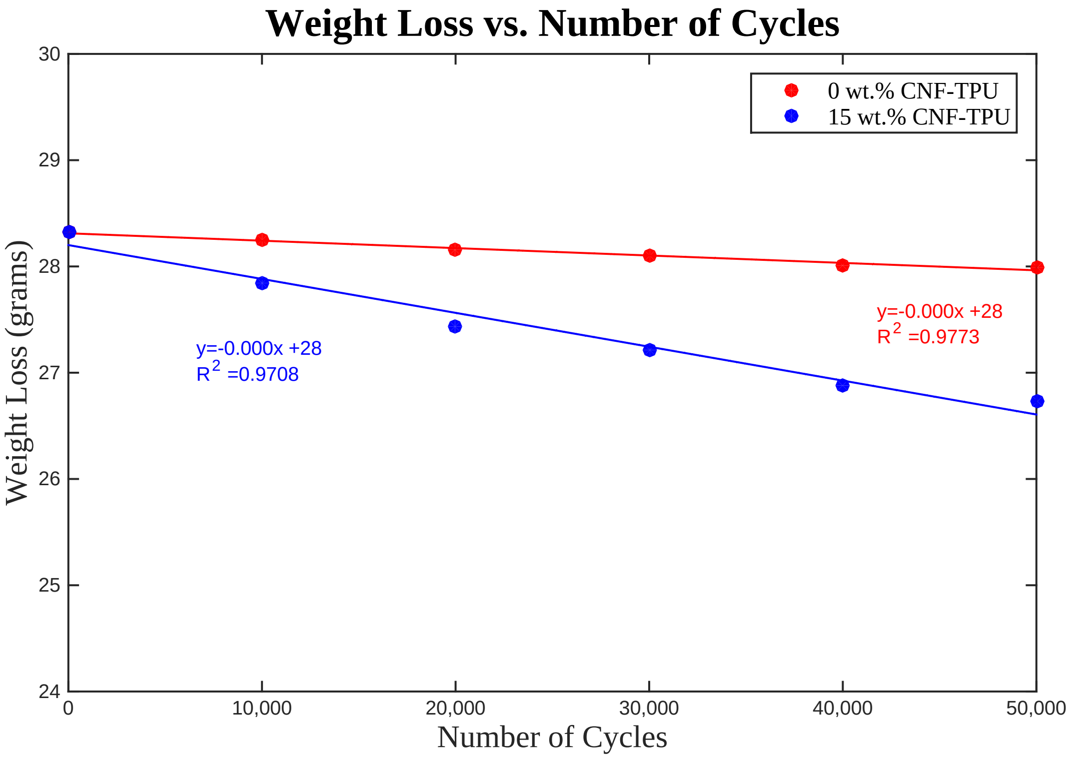

Figure 4.23: Weight loss vs. number of cycles

In addition, the presence of CNFs in the TPU matrix limited the number of degrees of freedom for each molecule. By limiting molecular movement, rigidity is increased and less energy is absorbed by the polymer making it more susceptible to abrasion. These two factors combined are responsible for the increased wear on the 15% CNF-TPU composite on a chemical level. Macro interactions such as tearing were suspected and investigated as well to understand their implications for the changed wear behavior.

Macro interactions of wear and abrasion resounded from a combination of micro chemical and physical changes. To better analyze these macro changes, the dust from abraded samples was viewed under an SEM as shown in Figures 4.24 & 4.25. In Figure 4.24 virgin TPU dust is displayed in chunks with H-18 abrasion wheel particles spread throughout. The polymer particles broke off in discrete pieces. This can be explained by the fatigue and wear mechanism. Studies have shown that wear in polymers is dependent on surface roughness but in general a poor correlation exists between polymer hardness and wear [45]. The reason for this poor relationship is because polymer wear is more closely associated with fatigue crack growth rather than plastic deformation [46]. Polyurethane elastomers under fatigue develop cracks through micro tearing of the surface by frictional forces. The cracks initially grow downwards but as the tongue or ridge grows the crack turns upwards freeing a particle fragment of polymer [47]. Polymer debris continues to be removed as this micro tearing reaction propagates. The introduction of fatigue cracks has been found to be dependent on the abrader angle of incidence and amount of energy a polymer can absorb.

Hutching's studies of TPU erosion found the angle of incidence between the polymer and the abrader to be a dominant factor in determining wear correlations [46]. He also found that solid particle erosion was not dependent on glass transition temperature or mechanical properties like durometer, tensile strength or elongation. The main contributing factor however, was related to the amount of kinetic energy from the erosive particle the polymer could absorb. This principle means that polymers, which can absorb high amounts of kinetic energy without breaking, rebound to their original form after abrasion and exhibit excellent abrasive qualities.

Hutching's assumptions correspond with the chemical bonding of TPU described previously. The powerful crosslinking provided by hydrogen bonds between the hard segments of TPU allow greater amounts of abrasion energy to be absorbed before the failure of the hydrogen bonds. The magic in hydrogen bonding is that they are not part of the actual polymer backbone therefore they can absorb abraded energy and break without any destruction of the actual polymer itself. Because they are composed of attractive forces hydrogen bonds may actually break and then reform repeatedly during abrasion adding resistance. This was evident under higher magnification examinations of the abrasion dust between 15 wt.% CNF-TPU and virgin TPU. The CNF composite fragments broke off in larger chunks of CNFs and TPU while the virgin TPU appeared to have been pulled off like chewing gum, Figures 4.26, 4.27. Virgin TPU abrasion dust contained a higher degree of abrasion wheel particles as well. Therefore by removing some of the hydrogen bond crosslinking between polymer chains, the CNFs also lessened the amount of kinetic energy the TPU could absorb before cracks developed. Fatigue cracks developed at a higher rate in the CNF-TPU composite and Figure 4.26 clearly displays larger broken off chucks of TPU and CNFs meaning cracks can grow deeper in the composite polymer matrix before turning back up.

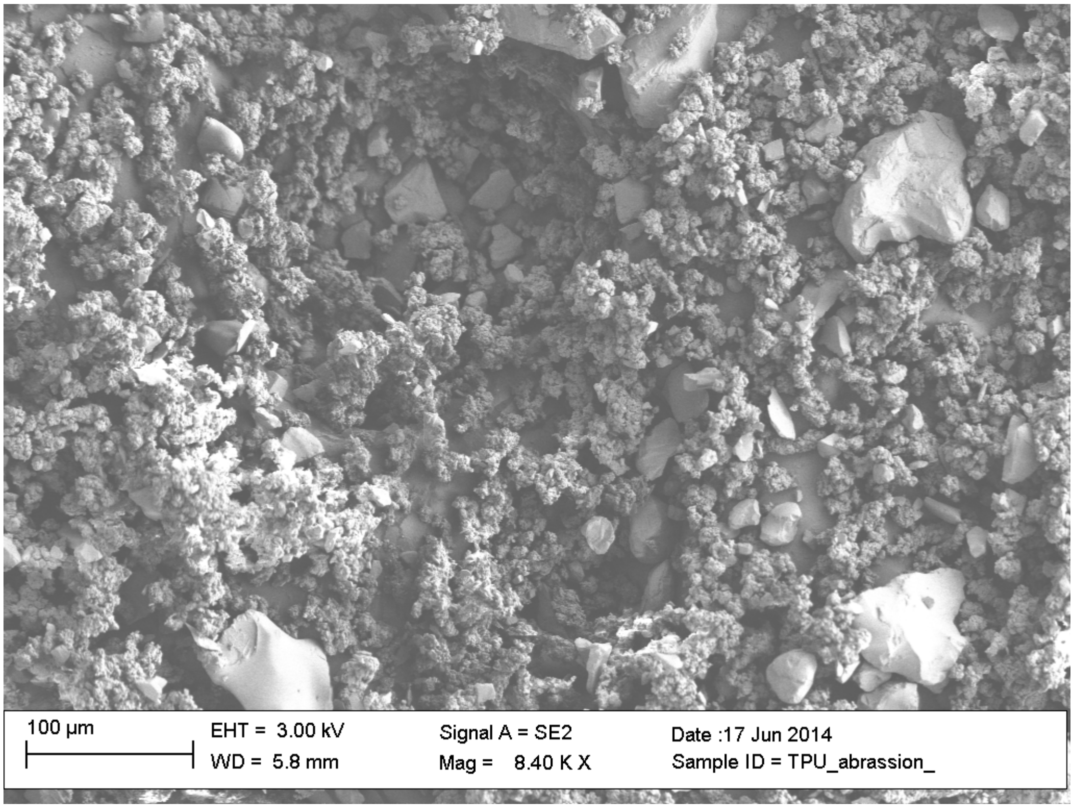

Figure 4.24: Virgin TPU with abrasion particles spread throughout

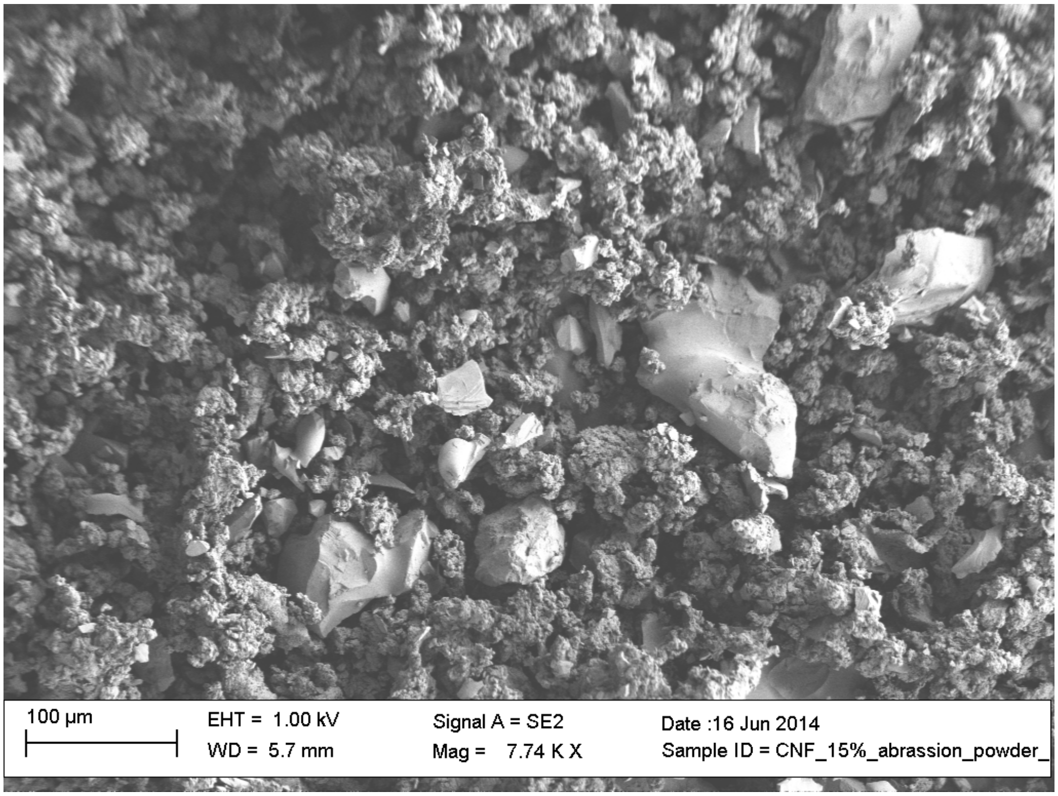

Figure 4.25: 15% CNF-TPU composite with abrasion particles spread throughout

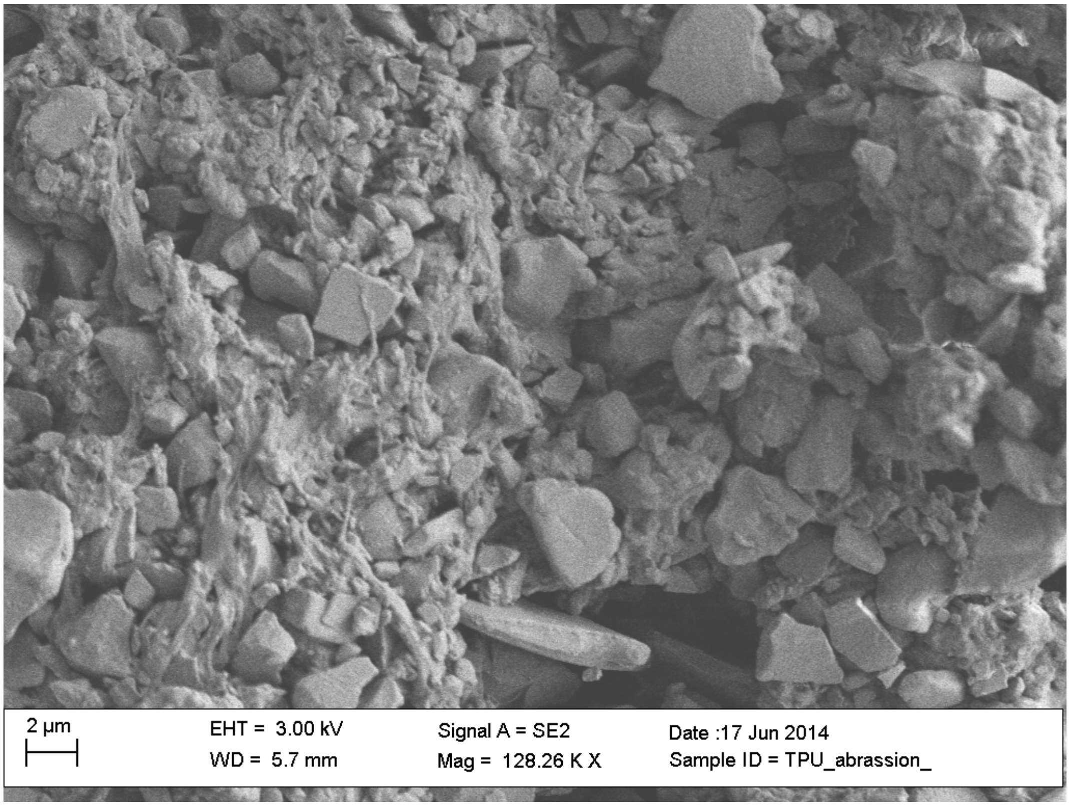

Figure 4.26: Virgin TPU abraded dust

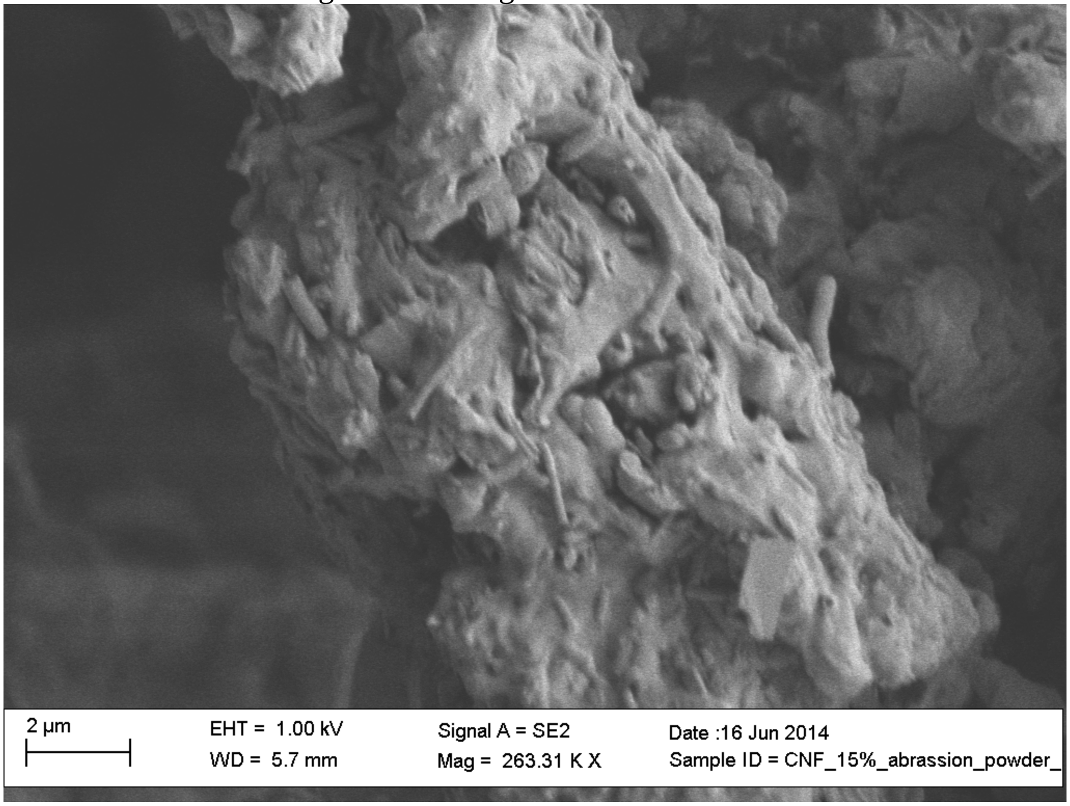

Figure 4.27: 15 wt.% CNF-TPU abraded dust clump

4.8 Creep Testing

Rectangular test bars were tested in a dynamic mechanical analyzer (DMA) Q800 manufactured by TA Instruments. The machine has a creep testing mode which was used to evaluated the long term static behavior of CNF-TPU composites. The tests were run at various temperatures to permit creation of a master curve at any temperature of interest and at extended times. The applied static stress was 5 MPa which is safely in the linear elastic region of the material's tensile stress/strain curve. Material creep compliance and strain were measured as the stress was applied for 10-minute durations at a five degree increments in temperature between 35 ºC and 150 ºC. Rectangular specimens of 35 mm x 12.5 mm x 1.60 mm dimensions containing 0, 5, and 15 wt.% CNF concentrations were evaluated. Time-temperature superposition (TTS) was used to create a master curve displaying long-term creep behavior.

Figure 4.28 displays a curve of the creep compliance with respect to time. The 0 wt.% CNT-TPU curve shown clearly displays the instantaneous, primary, and secondary creep regions. The tertiary creep region is not shown because tests were not run to failure. The 5 and 15 wt.% CNF-TPU composites yielded similar curves to the virgin material containing instantaneous, primary, and secondary regions but at different creep compliance values.

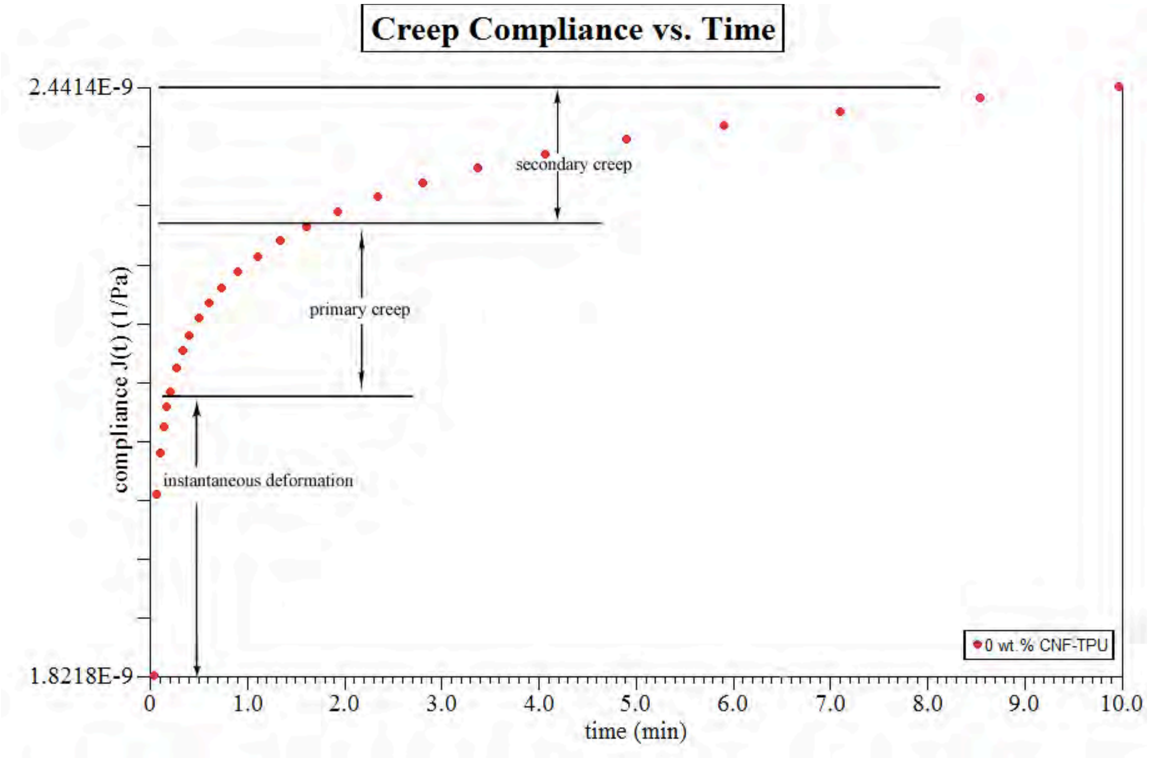

Figure 4.28: Creep vs. Time with creep regions

Figure 4.29 displays 0, 5, and 15 wt.% CNT-TPU creep curves at 35 ºC. The 5 and 15 wt.% CNF-TPU composites are clearly less compliant than the 0 wt.% CNF-TPU. This is because CNFs inhibit creep by filling in intermolecular space and pinning molecules as they reinforce the polymer matrix [31]. Under stress, pinned molecules cannot relax, stretch, and re-orient themselves and therefore the material cannot creep as easily [48]. Similar results have been reported when CNFs reinforced other polymers [49].

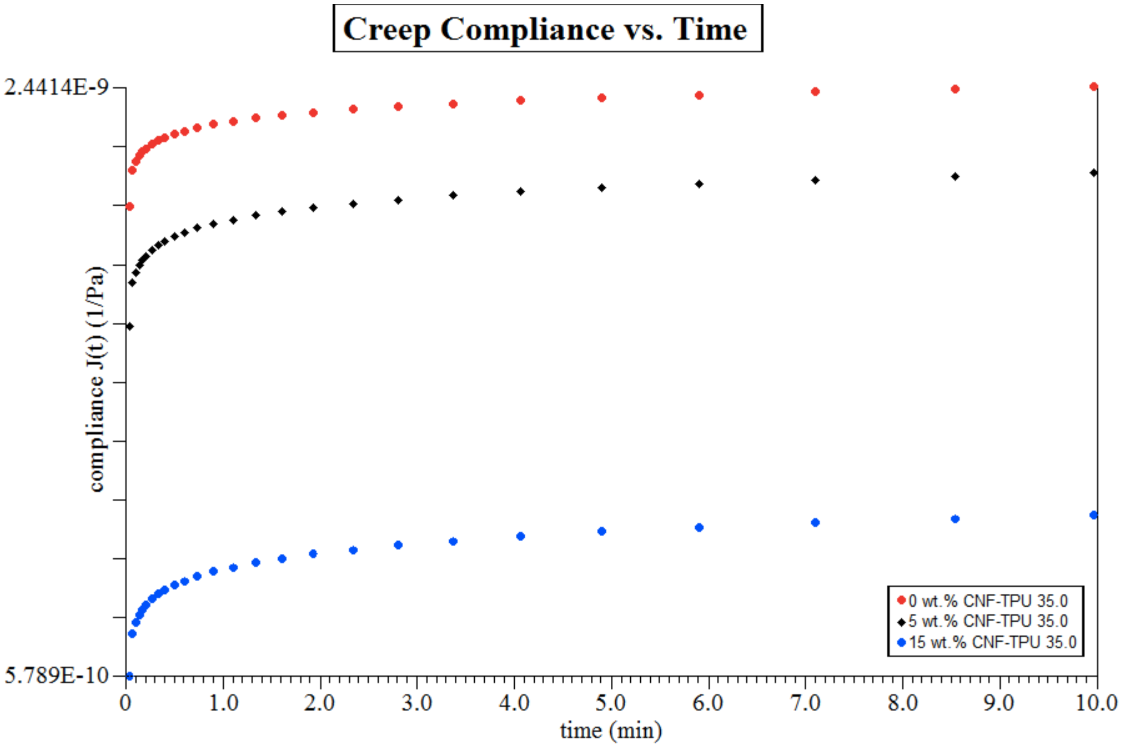

Figure 4.29: 0, 5, and 15 wt.% CNF-TPU Creep Compliance vs. Time

Figure 4.30 displays the TTS of 0, 5, and 15 wt.% CNT-TPU concentrations. TTS is a convenient way to shift data to predict long-term material behavior by accelerating material response by raising the test temperature. The shift factor can be determined using the Arrhenius equation:

$$log\alpha_T = \frac{Q}{2.303R}\left(\frac{1}{T} - \frac{1}{T}\right) \qquad (11)$$

Q represents the activation energy for molecular relaxations, R is the universal gas constant, and T_r is the reference temperature. 140 ºC was chosen as the reference temperature. The curves show that over time CNF reinforced composites will exhibit much less creep compared to virgin TPU materials. This is consistent with the impeding effect of CNFs on molecular relaxation of the TPU’s polymer chains.

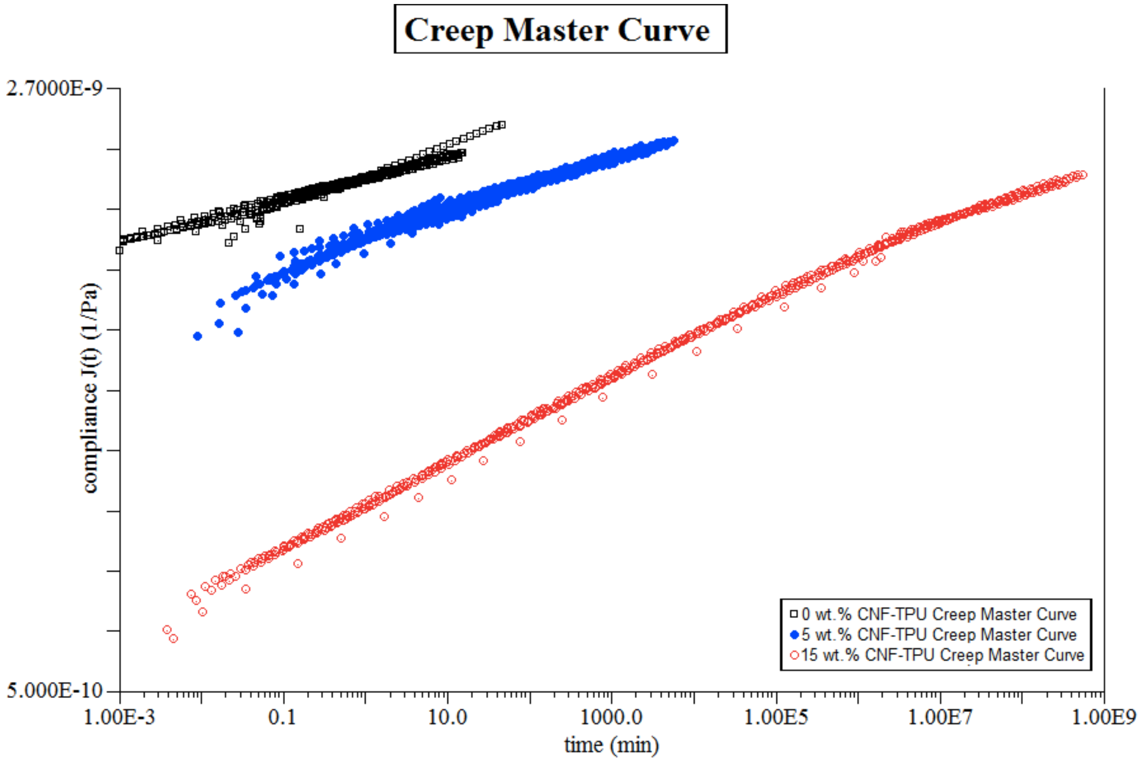

Figure 4.30: Creep Master Curve

4.9 Dynamic Modulus Testing

Rectangular test bars were made and tested on a dynamic mechanical analyzer (DMA) Model Q800 by TA Instruments. The tests measured the material storage modulus over a range of frequencies between 0.1 and 200 Hz. Tests were run at multiple temperatures to simulate aging and by utilizing time-temperature superposition a master curve was created. The temperatures ranged from 35 – 150 ºC with tests running at increments of 5 degrees.

Viscoelastic materials store and dissipate energy in two ways. By elastic deformation mechanisms they store energy and by viscous processes they dissipate energy as heat. The storage modulus is a measure of the stiffness of a viscoelastic material and indicates how much energy is stored as strain energy when a force is applied [50]. The loss modulus does the same for energy dissipated as the material is strained. These two responses are characterized by the following equations

$$\text{Storage Modulus: E'} = \frac{\sigma_0}{\varepsilon_0} \cos\delta \tag{12}$$

$$\text{Loss Modulus E''} = \frac{\sigma_0}{\varepsilon_0} Sin\delta \tag{13}$$

Where σ_0 and ε_0 are the amplitudes of stress and strain respectively and δ is the phase shift between them. Figure 4.31 displays the master curve shifted at 50 ºC of the dynamic storage modulus (E’) in Pascals as a function of frequency in Hertz (Hz). The storage modulus steadily increased with increasing CNF percentage after a large initial increase over the virgin material. The significant initial increase in E’ shown in the 5 wt.% CNF-TPU over the 0 wt.% CNF-TPU reflects the increase in stiffness from interconnected CNFs. CNF networks transferred the applied stresses, and by filling intermolecular spaces they pinned down polymer molecules dictating fiber-matrix and matrix-matrix interactions [41]. The storage modulus increases as molecules lost free volume to move [50]. These were the dominant mechanisms that increased the E’ in the composite material. At higher CNF loadings however, E’ increased because a mature 3-dimensinal network of fibers was established which reinforced the polymer matrix [51].

Analysis of the master curves revealed the logarithmic slope of E’ decreased slightly as the frequency increased along the curve. The greater slope at the beginning of the curve was due to the material storage modulus being primarily influenced by CNFs. Further down the master curve the slope decreased due to shorter frequencies interacting with TPU’s elastic matrix [52]. Figure 4.32 displays the loss modulus (E”) as function of frequency (Hz). Tan delta is the ratio of viscous modulus (E”) to elastic modulus (E’). Since the storage modulus was noticeably greater than the loss modulus the tan delta value was fraction therefore the material had elastically dominated behavior, i.e. solid like.

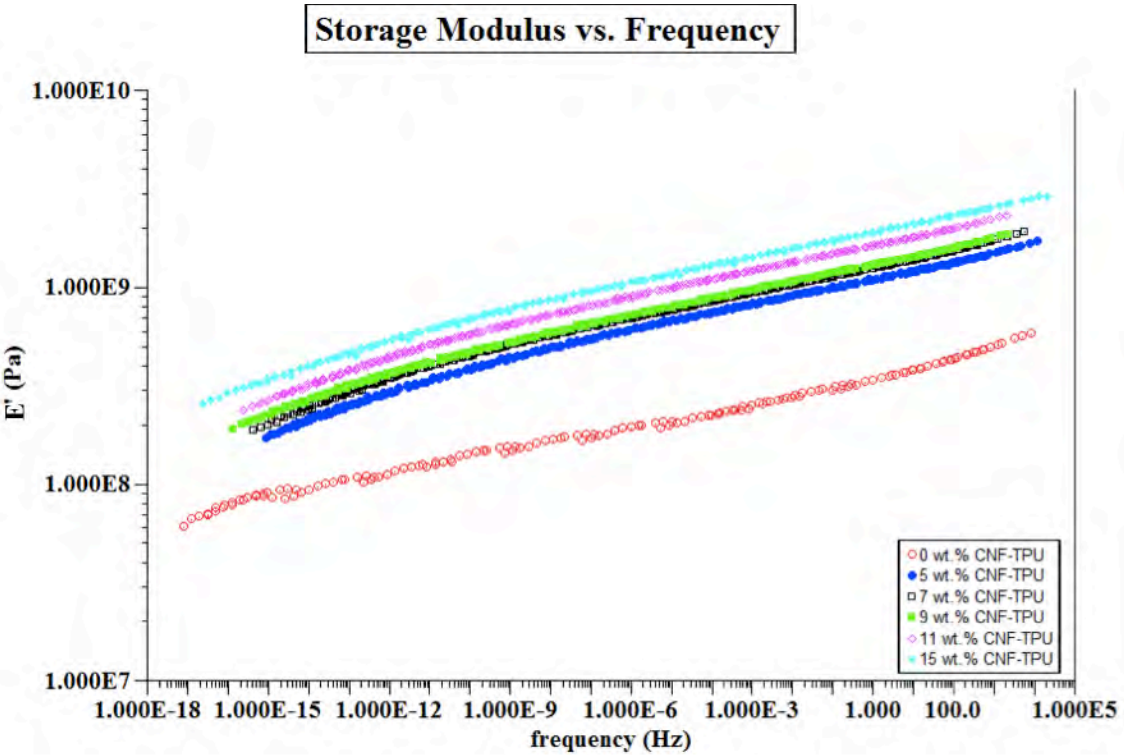

Figure 4.31: Storage Modulus vs. Frequency Modulus Master Curve 50 ºC shifting

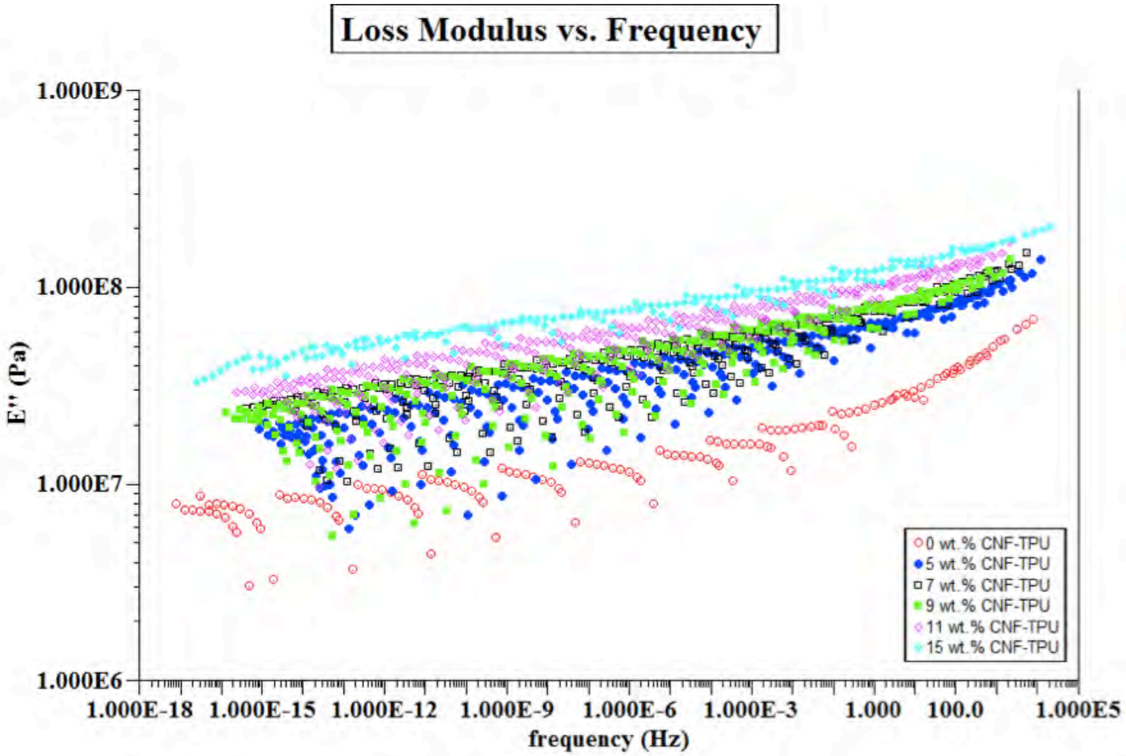

Figure 4.32: Loss Modulus vs. Frequency Master Curve 50 ºC shifting

4.10 Hysteresis Test

Hysteretic heating is a common phenomenon in thermoplastic polyurethane elastomers. This process occurs when an elastomer is subjected to rapid, repeating load cycles. TPU polymers are commonly subjected to these types of cyclic stresses in transportation applications. To understand the role of cyclic loading on internal heat generation and the effect of nanofibers on this process, a hysteresis test was performed on two pucks of 0 and 15 wt.% CNF-TPU. Pucks were 0.5” in height with diameters of 2.5”, Figure 4.33. The tests were performed on an MTS model 810 Servohydraulic Test System with a k class thermocouple inserted inside each puck to measure temperatures, Figures 4.34, 4.35. One set of tests was run with cyclic loads of 500 to 5,500 pounds of force on each puck at frequencies of 2, 4, 10, 20, 30, and 40 Hz. Higher frequencies were not run because the machine could not be maintain the oscillation range. Another set of test was run with a narrower loading range of 3,000 to 5,000 pounds of force at frequencies of 2, 4, 10, 20, 30, 40, 50, and 100 Hz. Both sets of tests were run until the pucks reached steady state temperatures.

a. 15 wt.% CNF-TPU

b. 0 wt.% CNF-TPU

Figure 4.33: Pucks used for hysteresis test

Figure 4.34: Hysteresis Test Set Up

Figure 4.35: Puck with Thermocouple

Figure 4.36 displays temperature fluctuations with respect to time as cyclic loads of 500 to 5,500 pounds of force were applied. Temperatures increased over time until a steady state was achieved. Figure 4.37 displays the final steady state temperatures for the 500 to 5,500 pound range with respect to frequency for 0 and 15 wt.% CNF-TPU. The steady state temperatures for 0 wt.% CNF-TPU increased more dramatically as frequency increased compared to 15 wt.% CNF-TPU. This occurred because under stress polymer chain conformations become distorted. When loads were removed the chains only gradually regain their original conformations as their motions are restricted by surrounding molecules. This friction with neighboring chains leads to energy loss in the form of heat [53]. During hysteresis the intermolecular hydrogen bonding between TPU's hard segments become disrupted. The degree of disruption was dependent on the microphase morphology, hard segment type, domain ductility, and the extent of mixing between hard and soft segments [44].

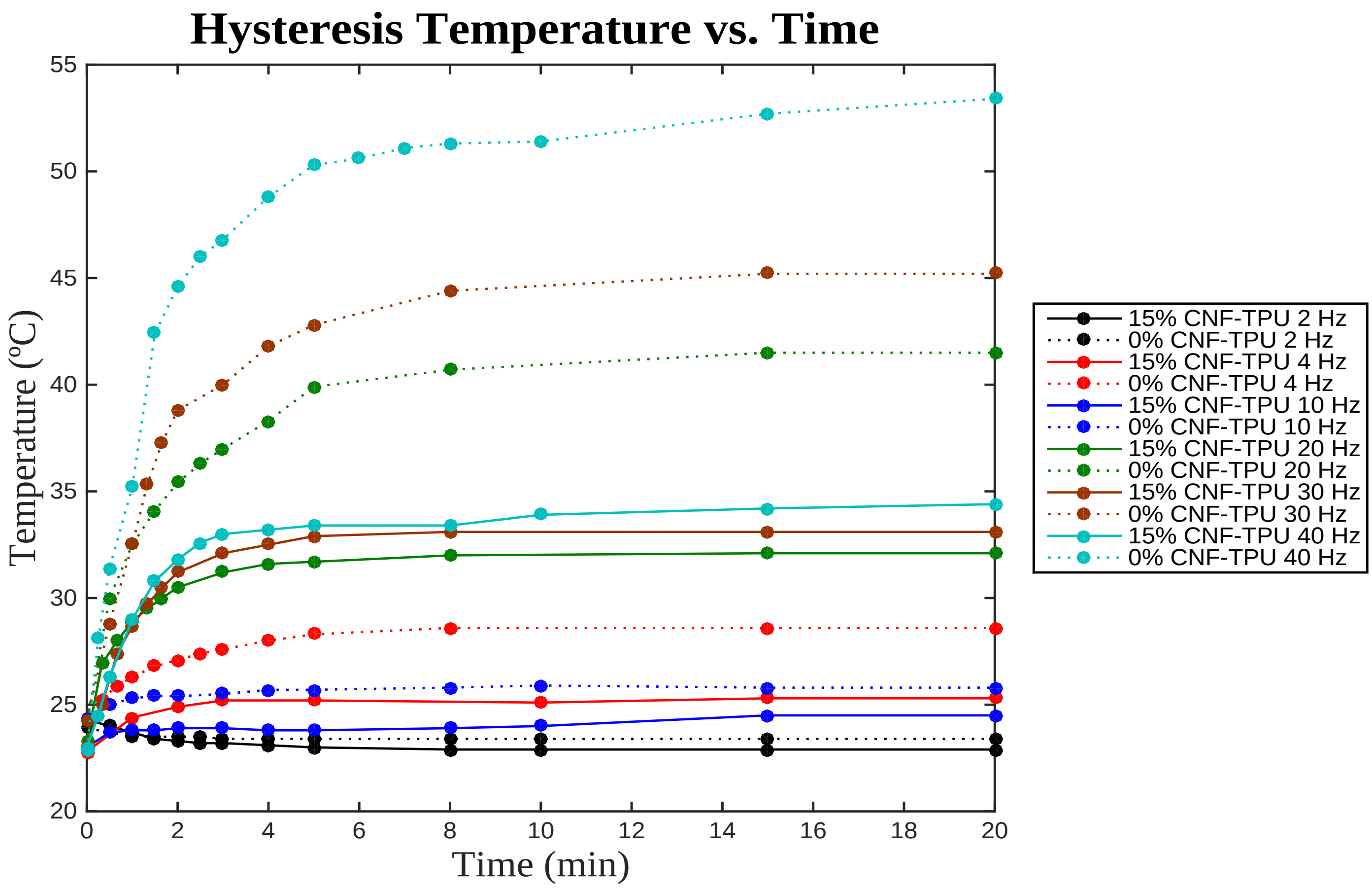

Figure 4.36: Temperature vs. Time for 0 and 15 wt.% CNF-TPU

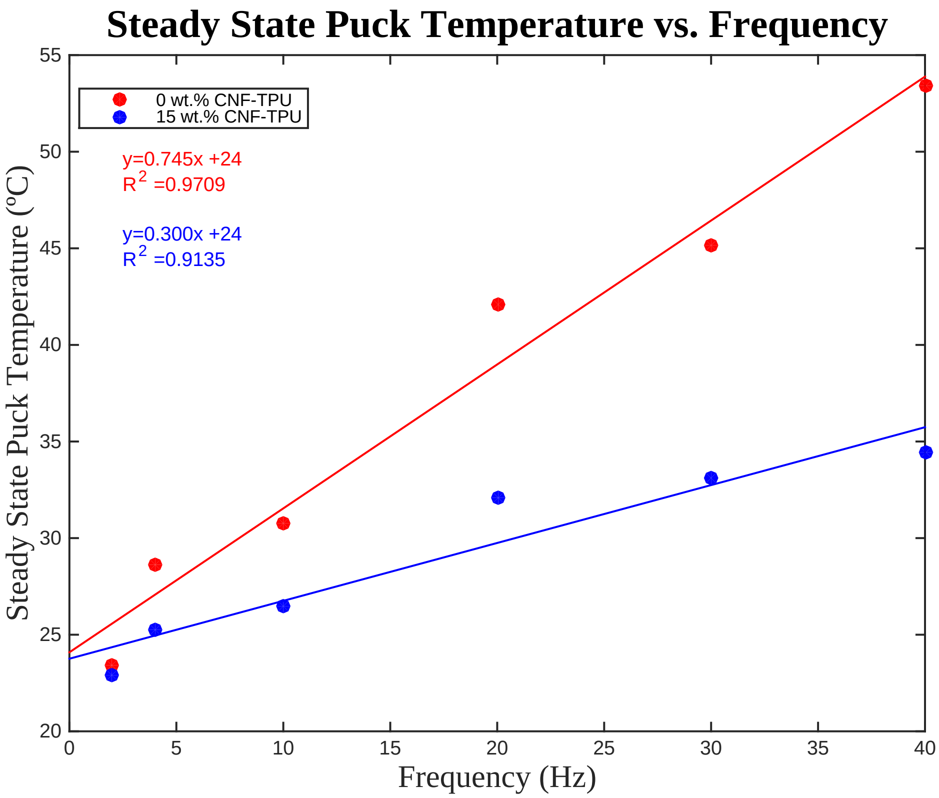

Figure 4.37: Steady State Temperature vs. Frequency

The 15 wt.% CNF-TPU puck did not experience as much hysteretic heating compared to the virgin puck. This occurred because CNFs not only constrained the molecules by occupying intermolecular space and pinning down polymer chains, but they also increased the overall heat transfer coefficient of the material [53]. Pinning down polymers chains inhibited molecules from slipping past each other and as a result the hydrogen bonding network remained more intact and little sliding energy was dissipated. Furthermore, a higher overall material heat transfer coefficient allowed heat to dissipate through the puck to the adjacent metal plates. As discussed in the heat transfer section, the heat transfer coefficients of 0 and 15 wt.% CNF-TPU were measured to be 0.206 and 0.508 W/m·K respectively.

Figure 4.38 displays the steady state temperatures for the 500 to 5,500 and 3000 to 5000 pound force tests. The illustration clearly shows that samples tested under the narrower oscillation range did not experience as much hysteretic heating. This proves that the amount of force applied to the samples was not a primary contributor to hysteresis but rather the oscillation range.

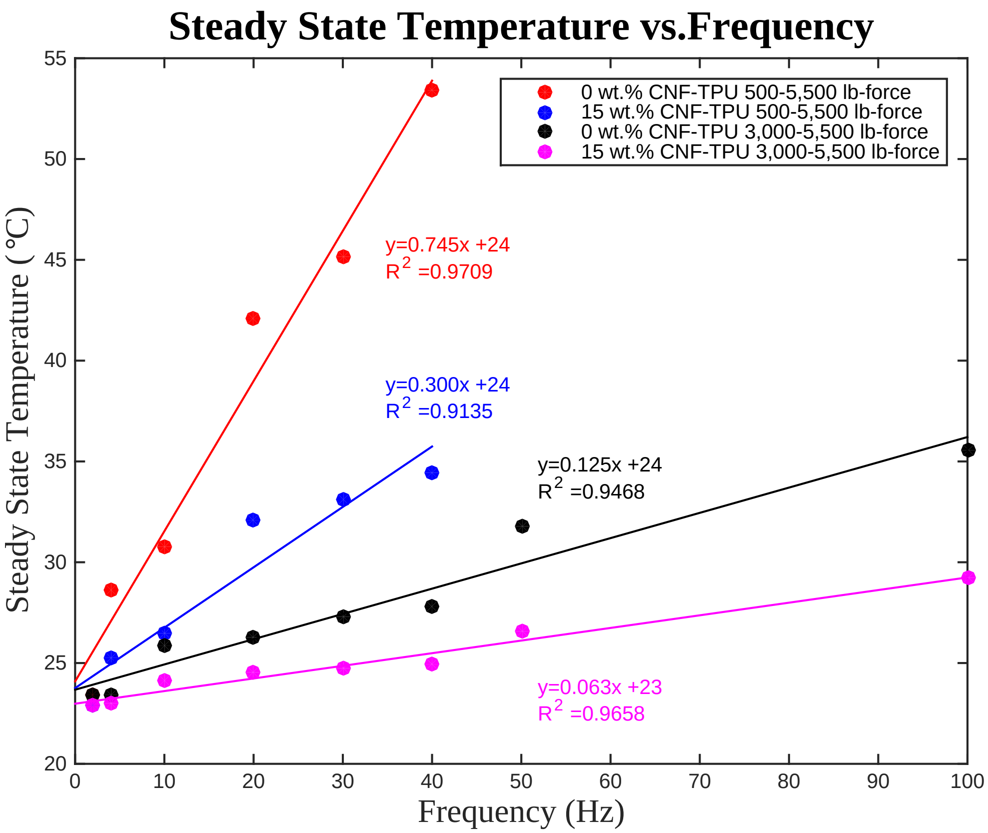

Figure 4.38: Steady State Temperatures vs. Frequency of both test sets

CHAPTER V

FUTURE WORK AND CONCLUSION

The principal objective of this research was to create a CNF-TPU composite material and study its mechanical, thermal, and electrical properties to determine its likely utility in severe service. The results showed that CNFs are choice additives for enhancing electrical and thermal properties, but they are limited as some properties were enhanced while others were diminished. Of primary concern was the decrease in toughness measured via both impact and tensile test which came with the increased hardness and strength. CNFs hold great promise for reinforcing polymers, and may be the key to creating the "perfect" material, a strong material with high elasticity. Although this research did not unlock the secrets to creating such a material, it did present a reinforced polymer with unique characteristics for new applications. The research performed was novel to the area of composites but was incomplete because every result presented a new set of questions to answer. Temperature effects, alternative-mixing methods, scale up procedures, and field implementation, would be some useful studies to conduct if this research were continued.

Temperature tends to inversely affect conductivity. In metal, increasing temperature will increase resistivity due to increased scattering effect. In polymers percolation is assisted by higher temperatures and it is possible that this effect will partially offset increases in resistivity induced by higher temperature. Characterizing current flow through CNF-TPU composites at different temperatures is vital to determining appropriate applications. Temperature affects mechanical properties as well. At higher temperatures polymers become more viscous and lose strength. The TGA analysis revealed that CNFs delayed TPU's decomposition onset and melting point to higher temperatures. Based on these findings it would be interesting to see if CNFs could improve the mechanical properties of TPU composites under stress or strain at higher temperatures.

Sources in the literature indicated that manipulating fiber alignment optimizes thermal, electrical, and mechanical properties. Controlling fiber alignment is usually accomplished by applying an electric field during the curing process of in-situ or solvent/solute polymerization in thermoset urethanes. It is also possible to orient fibers via shear flow or elongation in thermoplastic TPU. These methods cannot be applied to injection molded parts, however they do offer CNF orientation control. Researching an alternative production method that provides fiber orientation control may produce a superior product.

Developing the ideal composite material for a specific application is meaningless if it cannot be scaled up and mass-produced. Mass production of CNF composites is an interesting and vital area of research especially since current production methods are largely limited to melt mixing processes. Researching alternative avenues to scale up CNF composites is another worthy engineering thesis and the findings of this thesis could provide a springboard for determining these avenues. An industry sized branbury mixer can match the laboratory process outlined in this thesis to produce a scale up compound. Testing a scaled up composite product is a perfect continuation of this.

The scenarios described above are not an exhaustive list of future studies that may be developed from this thesis research, but any one of them are worthy of future study. It seems likely that a CNF elastomer composite will be used in an multi cycle, severe duty industry application in the near future. Reinforcing polymers with CNFs will continue to open new opportunities and create new jobs for many people.

REFERENCES

[1] "A Comparison of Carbon Nanotubes and Carbon Nanofibers." *Pyrograf Products Inc.* Applied Sciences, n.d. Web. 13 Nov. 2014.

[2] Cooper CA, Ravich D, Lips D, Mayer JJ, Wagner HD. Distribution and alignment of carbon nanotubes and nanofibrils in a polymer matrix. Compos Sci Technol 2002;62(7–8):1105–12.

[3] Mukhopadhyay K, Porwal D, Lal D, Ram K, Narayan Mathur G. Synthesis of coiled/straight carbon nanofibers by catalytic chemical vapor deposition. Carbon 2004;42(15):3254–6.

[4] Kuriger RJ, Alam MK. Extrusion conditions and properties of vapor grown carbon fiber reinforced polypropylene. Polym Compos 2001;22(5):604–12.

[5] Lee BO, Woo WJ, Kim MS. EMI shielding effectiveness of carbon nanofiber filled poly(vinyl alcohol) coating materials. Macromol Mater Eng 2001;286(2):114–8.

[6] Mohammed, H., and U. Sundararaj. "A Review of Vapor Grown Carbon Nanofiber/polymer Conductive Composites." *Journal of Carbon* 47 (2009): 2-22. Print.

[7] R. Suarez. Design and Optimization of a Railroad Conductive Suspension Element Pad Composed of Thermoplastic Polyurethane and Carbon Black. Master’s Thesis, University of Texas-Pan American, 2013

[8] Feng J, Chan CH. Electrical properties of carbon black-filled polypropylene/ultra-high molecular weight polyethylene composites. In: Rupprecht L, editor. Conductive polymers

and plastics in industrial applications. William Andrew Publishing/Plastics Design Library; 1999.

[9] Krause B, Pötschke P, Häußler L. Composites Science and Technology 2009;69(10):1505e15.

[10] Endo M, Kim YA, Hayashi T, Nishimura K, Matusita T, Miyashita K, et al. Vapor-grown carbon fibers (VGCFs) – basic properties and their battery applications. Carbon 2001;39(9):1287–97.

[11] Fissell, William, Aaron Fleischman, and David Humes. "Development of Continuous Implantable Renal Replacement: Past and Future." *Translational Research* (2007): n. pag. Print.

[12] Moniruzzaman M, Winey KI. Polymer nanocomposites containing carbon nanotubes. Macromolecules 2006;39(16):5194–205.

[13] VanHattum FWJ, Serp P, Figueiredo JL, Bernardo CA. The effect of morphology on the properties of vapour grown carbon fibres. Carbon 1997;35(6):860–3.

[14] Strumpler R, Glatz-Reichenbach J. Conducting polymer composites. J Electroceram 1999;3(4):329–46.

[15] L. Saenz. Calibration and Optimization of a Load Sensor Embedded in a Railroad Bearing Adapter. Master Thesis, University of Texas-Pan American, 2013

[16] Bar H, Narkis M, Boiteux G. The electrical behavior of thermosetting polymer composites containing metal plated ceramic filler. Polym Compos 2005;26(1):12–9.

[17] Chekanov Y, Ohnogi R, Asai S, Sumita M. Electrical properties of epoxy resin filled with carbon fibers. J Mater Sci 1999;34(22):5589–92.

[18] Prasse T, Cavaille JY, Bauhofer W. Electric anisotropy of carbon nanofibre/epoxy resin composites due to electric field induced alignment. Compos Sci Technol 2003;63(13):1835–41.

[19] Chen YM, Ting JM. Ultra high thermal conductivity polymer composites. Carbon 2002;40(3):359–62.

[20] Agari Y, Ueda A, Nagai S. Thermal conductivities of composites in several types of dispersion systems. J Appl Polym Sci 1991;42(6):1665–9.

[21] Gordeyev SA, Macedo FJ, Ferreira JA, van Hattum FWJ, Bernardo CA. Transport properties of polymer-vapour grown carbon fibre composites. Physica B 2000;279(1–3):33–6.

[22] Biercuk MJ, Llaguno MC, Radosavljevic M, Hyun JK, Johnson AT, Fischer JE. Carbon nanotube composites for thermal management. Appl Phys Lett 2002;80(15):2767–9.

[23] Andrews R, Jacques D, Minot M, Rantell T. Fabrication of carbon multiwall nanotube/polymer composites by shear mixing. Macromol Mater Eng 2002;287(6):395–403.

[24] Miyasaka K, Watanabe K, Jojima E, Aida H, Sumita M, Ishikawa K. Electrical conductivity of carbon polymer composites as a function of carbon content. J Mater Sci 1982;17(6):1610–6.

[25] BASF. *Elastollan 1195A* [Elastollan TPU Technical Data Sheet].

[26] Cui, Yanbin, Caihong Liu, and Xun Yu. "The Experimental Exploration of Carbon Nanofiber and Carbon Nanotube Additives on Thermal Behavior of Phase Change Materials." *Solar Energy Materials and Solar Cells* 95 (2011): 1208-2112. *Science Direct*. Web. 13 Nov. 2014.

[27] "Gaskets, Washers, Lathe Cut Washers, Metal Stampings." *Gaskets, Washers, Lathe Cut Washers, Metal Stampings*. N.p., n.d. Web. 13 Nov. 2014.

[28] Ozcelik, Babur, Emel Kuram, and Mustafa Topal. "Investigation the Effects of Obstacle Geometries and Injection Molding Parameters on Weld Line Strength Using Experimental and Finite Element Methods in Plastic Injection Molding."*International Communications in Heat and Mass Transfer* 39 (2012): n. pag. Print.

[29] Melcher, R., and W. Johnson. "Mode I Fracture Toughness of an Adhesively Bonded Composite–composite Joint in a Cryogenic Environment." *Composites Science and Technology* 67 (2007): n. pag. *Science Direct*. Web.

[30] Bergman, T. L., and Frank P. Incropera. *Fundamentals of Heat and Mass Transfer*. Hoboken, NJ: Wiley, 2011. Print.

[31] Choi YK, Sugimoto KI, Song SM, Endo M. Mechanical and thermal properties of vapor-grown carbon nanofiber and polycarbonate composite sheets. Mater Lett 2005;59(27):3514–20.

[32] Nielsen, Kresten. "The Radiation Degradation of a Nanotube-polyimide Nanocomposite." *Polymer Degradation and Stability* 93 (2008): 169-75. *Science Direct*. Web. 16 Nov. 2014.

[33] Frick, Achim, and Arif Rochman. "Characterization of TPU-elastomers by Thermal Analysis (DSC)." *Polymer Testing* 23 (2004): 413-17. Print.

[34] N.R. Legge, G. Hodlen, H.E. Schroeder. Thermoplastic Elastomers. Hanser Publishers, Munich, 1987. p. 16.

[35] Chen YM, Ting JM. Ultra high thermal conductivity polymer composites. Carbon 2002;40(3):359–62.

[36] Agari Y, Ueda A, Nagai S. Thermal conductivities of composites in several types of dispersion systems. J Appl Polym Sci 1991;42(6):1665–9.

[37] Moniruzzaman M, Winey KI. Polymer nanocomposites containing carbon nanotubes. Macromolecules 2006;39(16):5194–205.

[38] Huxtable ST, Cahill DG, Shenogin S, Xue L, Ozisik R, Barone P, et al. Interfacial heat flow in carbon nanotube suspensions. Nat Mater 2003;2(11):731–4.

[39] Bar H, Narkis M, Boiteux G. The electrical behavior of thermosetting polymer composites containing metal plated ceramic filler. Polym Compos 2005;26(1):12–9.

[40] J.L. Zeng, Z. Cao, D.W. Yang, L.X. Sun, L. Zhang, Thermal conductivity enhancement of Ag nanowires on an organic phase change material, Journal of Thermal Analysis and Calorimetry 101 (2010) 385–389.

[41] Barick, Aruna, and Deba Tripathy. "Effect of Nanofiber on Material Properties of Vapor-grown Carbon Nanofiber Reinforced Thermoplastic Polyurethane (TPU/CNF) Nanocomposites Prepared by Melt Compounding." *Composites* 41 (2010): 1471-482. *No Records.* Web. 16 Nov. 2014.

[42] Sonnenschein, Mark, and Steven Guillaudeu. "Comparison of Adipate and Succinate Polyesters in Thermoplastic Polyurethanes." *Polymer* 51 (2010): 3685-692. Web. 16 Nov. 2014.

[43] Nachman, Malgorzata, and Konrad Kwiatkowski. "The Effect of Thermal Annealing on the Abrasion Resistance of a Segmented Block Copolymer Urethane Elastomers." *Wear* 306 (2013): 113-18. *Science Direct*. Web. 16 Nov. 2014.

[44] Yilgor, Emel. "Hydrogen Bonding and Polyurethane Morphology. I. Quantum Mechanical Calculations of Hydrogen Bond Energies and Vibrational Spectroscopy of Model Compounds." *Polymer* 43 (2002): 6551-559. *Science Direct*. Web. 16 Nov. 2014.

[45] D.C. Evans, J.K. Lancaster. “Treatise on materials science and technology” in: D. Scott (Ed.), Wear, 13Academic Press (1979), pp. 85–139

[46] I.M. Hutchings. “Tribology: Friction and Wear of Engineering Materials” Edward Arnold, London (1992)

[47] Beck, R., and R. Truss. "Effect of Chemical Structure on the Wear Behavior of Polyurethane-urea Elastomers." *Wear* (n.d.): 145-52. *Science Direct*. Web. 16 Nov. 2014.

[48] Yao, Zhen, Defeng Wu, and Chong Chen. "Creep Behavior of Polyurethane Nanocomposites with Carbon Nanotubes." *Composites* 50 (2013): 65-72. Web. 16 Nov. 2014.

[49] Tang, Long, and Xu Wang. "Creep and Recovery of Polystyrene Composites Filled with Graphene Additives." *Composites Science and Technology* 91 (2014): 63-70.*No Records.* Web. 16 Nov. 2014.

[50] Kemei, S. "Storage Moduli, Loss Moduli and Damping Factor of GaAs and Ga1xMnxAs Thin Films Using DMA 2980." *Materials Science in Semiconductor Processing* 20 (2014): 23-26. Web.

[51] Lozano K, Yang S, Zeng Q. Rheological analysis of vapor-grown carbon nanofiber-reinforced polyethylene composites. J Appl Polym Sci 2004;93(1):155–62.

[52] Vidhate S, Shaito A, Chung J, D’Souza NA. Crystallization, mechanical, and rheological behavior of polyvinylidene fluoride/carbon nanofiber composites. J Appl Polym Sci 2009;112(1):254–60.

[53] Madkour, Tarek, and Fatma Hagag. "Molecular-level Modeling and Experimental Investigation into the High Performance Nature and Low Hysteresis of Thermoplastic Polyurethane/ Multi-walled Carbon Nanotube Nanocomposites."*Polymer* 53 (2012): 5788-797. *Science Direct*. Web. 16 Nov. 2014.

APPENDIX

MATERIAL SAFETY AND DATA SHEETS

Elastollan® TPU
Technical Data Sheet

BASF
The Chemical Company

Elastollan® 1195A
Polyether-based Grade

Elastollan® 1195A is specifically formulated for extruded profile, sheet and film applications. It exhibits excellent abrasion resistance, toughness, transparency, very good low temperature flexibility, hydrolytic stability and fungus resistance. It has excellent damping characteristics and outstanding resistance to tear propagation. Elastollan® 1195A is rated UL-94 HB in vertical flame test for wall thicknesses of 0.75 and 3.0 mm. Elastollan® 1195A also conforms to the FDA food contact regulations as described in book 21, section 177.2600 for wet food contact applications. Elastollan® 1195A also has NSF Standard 61 "Water Contact Material" certification. Elastollan® 1195A is supplied uncolored and in diced or pelletized form.

Typical Properties of Elastollan®	ASTM Test Method	Units	Typical Values
All the physical properties reported here are measured on injection molded samples. Properties of sheet or film samples of this product are also available upon request.			
Specific Gravity	ASTM D 792	g/cm^3	1.14
Shore Hardness	ASTM D 2240	Shore A or D	95A
Taber Abrasion	ASTM D 1044	mg loss	55
DIN Abrasion	DIN 53516	mm^3 loss	25
E-Modulus	ASTM D 412	psi	7500
Flexural Modulus	ASTM D 790	psi	7600
Tensile Strength	ASTM D 412	psi	5700
Tensile Stress at 100% Elongation	ASTM D 412	psi	2500
Tensile Stress at 300% Elongation	ASTM D 412	psi	5200
Ultimate Elongation	ASTM D 412	%	430
Tear Strength	ASTM D 624, Die C	lb/in	800
Compression Set **22h at 70ºC** **22h at 23 ºC**	ASTM D 395 "B"	% of original deflection	 45 30
Glass Transition temperature*	BASF Analytical Method	°C	-28
Vicat Softening Temperature	ASTM D 1525	°C	127
DMA Softening Temperature	BASF Analytical Method	°C	89

*Measured with Dynamic Mechanical Analysis (DMA). DMA profile is available upon request.
Above values are shown as typical values and should not be used as specifications.

Elastollan® TPU Technical Data Sheet

The Chemical Company

Elastollan® 1195A

Polyether-based Grade

MELT FLOW INDEX (MFI): Elastollan® 1195A is available in various MFI ranges. Depending on the process and application, different melt flow index can be used. Physical properties of all the materials are same. “ASTM D 1238, B” MFI test method is used for generation of data.

Elastollan® Name	MFI Conditions	MFI, g/10min
1195A10	210 °C, 10 kg	35-65
1195A10 Film	210 °C, 10 kg	40-60
1195A10LC	210 °C, 10 kg	35-65
1195A10R	210 °C, 3.8 kg	5-20
1195A50	210 °C, 10 kg	10-30
1195A55	205 °C, 8.7 kg	6-12

DRYING: Elastollan® materials are hydroscopic, i.e. dry Elastollan® will rapidly absorb moisture when exposed to atmosphere. Polyether-based Elastollan® grades absorb moisture more rapidly than polyester-based Elastollan® grades. As with all TPU products, Elastollan® 1195A must be dried before processing. The drying step is required to maintain a low moisture content until the product enters the processing equipment. The water content must be less than 0.03% before and during processing.

Drying diagram for Elastollan

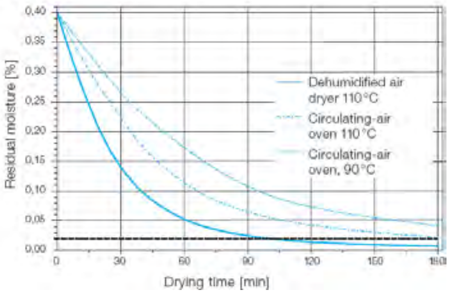

Elastollan® Hardness	Drying Time	Drying Temperature	
		Circulating air	Dehumidified Air
78A to 90A	2 to 3 h	100 to 110 °C	80 to 90 °C
> 90A	2 to 3 h	110 to 120 °C	90 to 120 °C

STORAGE: Elastollan® 1195A can be stored for up to one year in its original container. Containers should be stored in a cool and dry area. Containers should be tightly closed after use. Granulates should be exposed to the surrounding air only for as long as absolutely essential; it is therefore important to cover the feed hopper of the processing machine. Drying is recommended if the container has been opened several times. In order to prevent condensation, materials stored in cool conditions should be brought to room temperature before opening the container.

Moisture absorption
Polyether-TPU
Hardness 80 Shore A – 64 Shore D

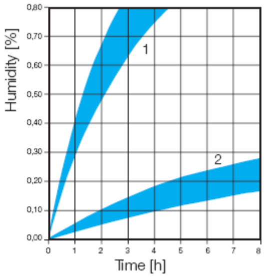

1 – Standard atmosphere 40 °C/92% rel. hum.
2 – Standard atmosphere 23 °C/50% rel. hum.

PROCESSING RECOMENDATIONS: Single screw extruder with a compression ratio of 1:2 to 1:3, preferably 1: 2.5, are recommended for processing Elastollan®. BASF experience shows that three section screws with an L/D ratio of 25 to 30 are most suitable. Three section screws should have continued constant pitch of 1D. The radial clearance between screw and barrel should be 0.1 to 0.2 mm. For processing Elastollan®, multizone screws, e.g. barrier screws, have also proven suitable. Short screws with high compression ratio are unsuitable for Elastollan®. Use of breaker plates and screen packs is recommended. Depending on the screw diameter and type of die, breaker plates should have holes of 1.5 to 5 mm in diameter. Since thermoplastic polyurethanes are shear sensitive, excessively high screw speeds may lead to reduction in product properties.

Screw configuration (diagrammatic view)

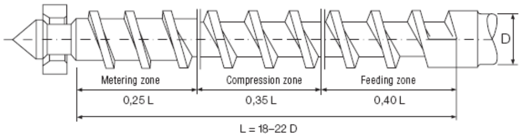

Elastollan® TPU
Technical Data Sheet

TYPICAL PROCESSING CONDITIONS: Elastollan® 1195A can be used for injection molding or extrusion conditions. Typical processing conditions are listed in the table below. We recommend you to call our technical service helpdesk for more information or troubleshooting.

INJECTION MOLDING		
Recommended barrel temperatures in ºC		
Elastollan® Hardness	Barrel Temperature	Nozzle
60A- 80A	170-210	200-210
85A- 95A	190-220	210-225
98A-74D	210-230	220-240

EXTRUSION				
Recommended barrel temperatures in ºC				
Elastollan® Hardness	Cylinder	Adapter	Die Head	Nozzle
60A to 70A	140-175	160-175	165-170	160-165
75A to 85A	160-200	175-200	175-205	170-205
90A to 98A	170-210	200-220	195-215	190-210

VISCOSITY CURVE:

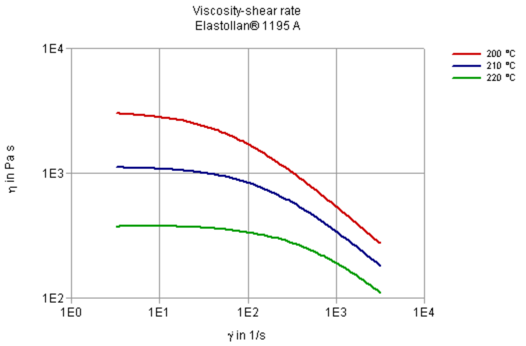

SHRINKAGE: This graph can be used for estimated shrinkage values of Elastollan® products in relation to the wall thickness. Please remember that depending on the molding conditions and part design these values can change. We recommend you to call technical service group for further information.

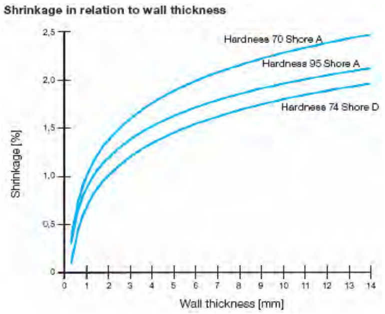

CHALLENGE US: Please contact us for more information on Elastollan® products.

You can reach our technical team at 1-800-892-3111 or tpu_helpdesk@basf.com. You can find more information at www.basf.com/elastollan. Our mailing address is BASF Corporation, 1609 Biddle Avenue, Wyandotte, Michigan 48192

For Further information, the following detailed brochures are available upon request:

- Elastollan® Material Properties
- Elastollan® Product Range
- Elastollan® Processing Recommendations
- Elastollan® Electrical Properties
- Elastollan® Chemical Resistance

DISPOSAL: Elastollan® materials are fully reacted and present no hazard to the environment. Waste can therefore be disposed at public waste disposal sites. The official regulations on waste disposal should be observed. For further information, please see BASF material safety data sheets.

CAUTION: Contact with product dusts from regrinding operations may cause temporary irritation of the eyes and the respiratory tract. Use with local exhaust. Under hot melt processing conditions (170-230°C), wear personal protective equipment to prevent thermal burns.

FIRST AID: Eyes-Flush eyes with flowing water at least 15 minutes. If irritation develops, consult a physician. *Skin*-Skin contact with hot melt may cause thermal burns. Call a physician immediately. *Inhalation*-If vapors generated from the hot melt process are inhaled, move to fresh air. Aid in breathing. If breathing difficulties develop, see a physician immediately.
In case of fire: Use water fog, foam, CO_2, or dry chemical extinguishing media. Firefighters should be equipped with self-contained breathing apparatus and turnout gear.

Pyrograf Products, Inc.

Material Safety Data Sheet
Revision Date: 6/14/11
Version 8

Section 1-Product and Company Information

Product Name	Pyrograf III® Carbon Nanofiber, LHT Grade
Product Number	N/A
Company	Pyrograf Products, Inc.
Street Address	154 West Xenia Ave. PO Box 579
City, State, Zip	Cedarville, OH 45314-0579
Technical Phone	(937)-766-4868
Fax	(937)-766-4878

Section 2-Composition/Information on Ingredients

Substance/Name	**Carcinogen**
Carbon Fiber (>98 wt %)	Unknown
Iron (<1.4 wt %)	No
Sulfur (<0.8 wt %)	No
Mineral content (<1 wt % from H_2O)	No

Section 3-Hazards Identification

Emergency Overview

Irritant if inhaled or exposed to skin or eyes

Health: 1 Flammability: 0 Reactivity: 0

Section 4-First Aid Measures

Dermal Exposure

In case of skin contact, wash with soap and water.

Inhalation Exposure

If inhaled, remove to fresh air.

Eye Exposure

In case of contact with eyes, flush with copious amounts of water for at least 15 minutes. Assure adequate flushing by separating the eyelids with fingers.

Section 5-Fire Fighting Measures

Flammable Hazards: No
Explosion Hazards: No
Extinguishing Media
ABC fire extinguisher or large quantities of water may be used to extinguish incipient stage fires.

Section 6-Accidental Release Measures

Procedures to be followed in Case of Leak or Spill
In case of leak or spill, gently sweep spillage into a closed container, follow-up with a vacuum cleaner. Dispose of spilled or residual material by hazardous waste incineration.

Section 7-Handling and Storage

Handling:
User Exposure
Do not inhale. Do not get into eyes or on skin.

Storage
Store in tightly closed container.

Special Requirements
None

Section 8-Exposure Controls/PPE

Personal Protective Equipment:

Respiratory
NIOSH certified air-purifying, tight-fitting full-face respirator equipped with N-100, P-100, or R-100 filter with an APF of 50 or greater

Hand
Molded Nitrile Gloves impervious to nanomaterials (passed ASTM standard F739)

Body
Full body protective clothing impervious to nanomaterials (passed ASTM standard F739)

Section 9-Physical/Chemical Properties

Appearance

Physical State	**Color**
Solid (fluffy agglomerates)	Black

Property	**Value**
pH	N/A
BP/BP Range	N/A
Vapor Pressure	N/A
Vapor Density	N/A
Specific Gravity	2.0
Volatile %	N/A
Evaporation Rate	N/A
Weight % Solid	>99%
Particle Diameter	~0.2 microns
Apparent Density	2 to 20 lbs/ft^3
Nanofiber Density*	1.55 to 1.70 g/cc
Flammability	N/A
Flash Point	N/A
Solubility	N/A
Odor	None

*The nanofiber density includes the volume of the hollow core of the nanofiber. The density of the nanofiber wall is 2.0 to 2.1 g/cc

Section 10-Stability and Reactivity

Stability	**Hazardous Decomposition Products**
Stable	None
Materials to Avoid	**Hazardous Polymerization**
Strong Oxidizers	Will not occur

Section 11-Toxicological Information

Routes of Exposure:
Skin Contact
Causes irritation

Inhalation
May cause lung damage or disease

Eye Contact
Causes irritation

Section 12-Ecological Information

Unknown

Section 13-Disposal Considerations

Appropriate Method of Disposal of Substance or Preparation
May be placed in an industrial hazardous waste incineration process according to applicable federal, state and local environmental regulations.

Section 14-Transport Information

Land transport (DOT): not regulated

Sea Transport (IMDG): not regulated

Air Transport (ICAO/IATA): not regulated

Section 15-Regulations

US Toxic Substances Control Act – product is listed on the TSCA chemical inventory

The TSCA Section 5(e) Consent Order issued for this product has set provisions for the end user when this product is used in a commercial application. It is important that Pyrograf Products, Inc. be notified prior to placing this product into a commercial application, as information may be needed to determine the extent of regulatory oversight. This product is subject to an Order issued under Section 5(e) of TSCA, to the TSCA Section 12(b) export notice requirement, and to the TSCA Section 8(b) chemical inventory.

Section 16-Other information

All carbon nanofibers are solid particles. Carbon nanofibers and their associated dust/shards may cause temporary irritation of the skin, eye, nasal passages, throat, upper respiratory tract, or gastrointestinal tract.

All forms of Pyrograf-III carbon nanofiber meet the definition of a respirable fiber (i.e. containing a length greater than 5 microns, a largest cross-sectional width less than 3 microns, and a length to cross-sectional width ratio greater than 3:1). Respirable fibers, dusts and shards may cause lung damage or disease.

During operations involving moving or mechanically working with this product, airborne fibers, shards, and dust may be generated. Any recipients of this product should assess their workplaces, processes, and material/products to determine if handling, processing, and/or incorporating Pyrograf-III carbon nanofibers in anyway allows for these fibers to become airborne in an open atmosphere. If so, recipients should take necessary precautions to protect people who may be exposed to Pyrograf-III carbon nanofibers.

Note: This MSDS is based upon data, information and other resources available at the time of the revision date listed. The information contained within this MSDS is considered accurate, to the extent known by Pyrograf Products, Inc. Pyrograf Products, Inc. assumes no legal responsibility for reliance or use of the information in this MSDS.

BIOGRAPHICAL SKETCH

Daniel Thomas Basaldua was born on December 20, 1989 in Weslaco, Texas to Mr. and Mrs. Thomas and Nancy Basaldua. Daniel graduated from Edinburg High School in 2008. He continued his education at The University of Texas Pan-American and graduated in the spring of 2012 with a Bachelor of Science Degree in Chemistry. While working on his undergraduate degree Daniel started his own business with Ambit Energy and financed his college education. Upon the completion of his undergraduate degree Daniel continued his education by pursuing a Master's Degree in Mechanical Engineering. He joined the University Transportation Center for Railway Safety where he researched nano reinforced composites for 2 years. He graduated with a Master of Science Degree in Mechanical Engineering in December of 2014. Daniel can be reached at Daniel.Basaldua@gmail.com